2013

Effect of Aviation Fuel Type and Fuel Injection Conditions on the Spray Characteristics of Pressure Swirl and Hybrid Air Blast Fuel Injectors

Rick Thomas Feddema
Purdue University

Graduate School ETD Form 9
(Revised 12/07)

PURDUE UNIVERSITY
GRADUATE SCHOOL
Thesis/Dissertation Acceptance

This is to certify that the thesis/dissertation prepared

By Rick T. Feddema

Entitled
Effect of Aviation Fuel Type and Fuel Injection Conditions on the Spray Characteristics of Pressure Swirl and Hybrid Air Blast Fuel Injectors

For the degree of Master of Science in Mechanical Engineering

Is approved by the final examining committee:

Paul E. Sojka
Chair

Robert P. Lucht

Timothee L. Pourpoint

To the best of my knowledge and as understood by the student in the *Research Integrity and Copyright Disclaimer (Graduate School Form 20)*, this thesis/dissertation adheres to the provisions of Purdue University's "Policy on Integrity in Research" and the use of copyrighted material.

Approved by Major Professor(s): Paul E. Sojka

Approved by: David C. Anderson 12/02/2013
Head of the Graduate Program Date

EFFECT OF AVIATION FUEL TYPE AND FUEL INJECTION CONDITIONS ON THE SPRAY CHARACTERISTICS OF PRESSURE SWIRL AND HYBRID AIR BLAST FUEL INJECTORS

A Thesis

Submitted to the Faculty

of

Purdue University

by

Rick Feddema

In Partial Fulfillment of the

Requirements for the Degree

of

Master of Science in Mechanical Engineering

December 2013

Purdue University

West Lafayette, Indiana

To Mattie Hensley and my family and friends for their encouragement

ACKNOWLEDGEMENTS

Thanks to my advisor Professor Paul Sojka for his guidance. Thank you to the project sponsors Air Force Research Laboratory, and engineers at Rolls Royce, Honeywell, GE Aviation and Williams for their support. Thank you to Scott Meyer, Joey Rideout and the other graduate students, faculty and staff for their excellent work at Maurice Zucrow Laboratories.

TABLE OF CONTENTS

Page

Page

Page

LIST OF TABLES

LIST OF FIGURES

Figure Page

Figure Page

Figure Page

LIST OF ABBREVIATIONS

Roman

ALR	Air Liquid Ratio
D_{10}	Sauter Mean Diameter
FAR	Fuel Air Ratio
HPL	High Pressure Laboratory
P3	Ambient Pressure
PDF	Probability Density Function
T3	Ambient Temperature
T fuel	Fuel Injection Temperature
W3	Mass flow rate of air
Wf	Mass flow rate of fuel
X_{10}	10% Drop Size Percentile
X_{50}	50% Drop Size Percentile
X_{90}	90% Drop Size Percentile

Greek

Δp	Fuel injection pressure
$\Delta p/p$	Pressure drop across experiment air box divided by ambient pressure

ABSTRACT

Feddema, Rick T. M.S.M.E., Purdue University, December 2013. Effect of Aviation Fuel Type and Fuel Injection Conditions on the Spray Characteristics of Pressure Swirl and Hybrid Air Blast Fuel Injectors. Major Professor: Dr. Paul E. Sojka, School of Mechanical Engineering

Spray performance of pressure swirl and hybrid air blast fuel injectors are central to combustion stability, combustor heat management, and pollutant formation in aviation gas turbine engines. Next generation aviation gas turbine engines will optimize spray atomization characteristics of the fuel injector in order to achieve engine efficiency and emissions requirements.

Fuel injector spray atomization performance is affected by the type of fuel injector, fuel liquid properties, fuel injection pressure, fuel injection temperature, and ambient pressure. Performance of pressure swirl atomizer and hybrid air blast nozzle type fuel injectors are compared in this study. Aviation jet fuels, JP-8, Jet A, JP-5, and JP-10 and their effect on fuel injector performance is investigated. Fuel injector set conditions involving fuel injector pressure, fuel temperature and ambient pressure are varied in order to compare each fuel type.

One objective of this thesis is to contribute spray patternation measurements to the body of existing drop size data in the literature. Fuel droplet size tends to increase with decreasing fuel injection pressure, decreasing fuel injection temperature and increasing ambient injection pressure. The differences between fuel types at particular set conditions occur due to differences in liquid properties between fuels. Liquid viscosity and surface tension are identified to be fuel-specific properties that affect the drop size of the fuel.

An open aspect of current research that this paper addresses is how much the type of aviation jet fuel affects spray atomization characteristics. Conventional aviation fuel specifications are becoming more important with new interest in alternative fuels. Optical patternation data and line of sight laser diffraction data show that there is significant difference between jet fuels. Particularly at low fuel injection pressures (0.345 MPa) and cold temperatures (-40 C), the patternation data shows that the total surface area in the spray at 38.1 mm from the pressure swirl injector for the JP-10 fuel type is one-sixth the amount of the JP-8.

Finally, this study compares the atomizer performance of a pressure swirl nozzle to a hybrid air blast nozzle. The total surface area for both the hybrid air blast nozzle and the pressure swirl nozzle show a similar decline in atomization performance at low fuel injection pressures and cold temperatures. However, the optical patternator radial profile data and the line of sight laser diffraction data show that the droplet size and spray distribution data are less affected by injection conditions and fuel type in the hybrid air

blast nozzle, than they are in the pressure swirl nozzle. One explanation is that the aerodynamic forces associated with the swirler on the hybrid air blast nozzle control the distribution droplets in the spray. This is in contrast to the pressure swirl nozzle droplet distribution that is controlled by internal geometry and droplet ballistics.

CHAPTER 1. INTRODUCTION

1.1 Overview

Fuel injectors are an important topic of research for the development of next generation aviation gas turbine engines. Enhanced fuel injector spray characteristics drive improvements in combustion stability, thermal management of the combustor, and a reduction in emissions. These advancements affect the performance and ultimate efficiency of the engine through increased pressure ratio, turbine inlet temperature, and a reduction in emissions.

Modern aviation gas turbine engine designs rely on computer models that predict the performance of engine components at various operational conditions. Models for fuel injector performance rely on experimental data for modeling and injector design validation. Experimental measurements of local drop size, velocity, and spray distribution are central to understanding the behavior of an injector at set conditions. The properties of the spray depend on fuel properties, fuel injector geometry, fuel injection temperature, fuel injection pressure, ambient pressure, and the gas entraining the spray.

The Air Force Research Laboratory sponsored a testing program at Maurice Zucrow Laboratories, Purdue University that funded the research for this thesis. Aircraft engine companies used the data collected at the various fuel injector set conditions in fuel injector modeling efforts. Engineers at Rolls Royce, Honeywell Aerospace, and GE Aviation acted as project consultants to provide fuel injector set conditions in a test matrix and to provide feedback on the design of the experiment.

1.2 Research Objectives

The focus of the testing program for this thesis is to report and provide reasoning for the differences in spray atomization characteristics between types of jet fuel. Jet fuels JP-8, Jet A, JP-5, and JP-10 were compared to one another at various set conditions. The set conditions for the experiments are summarized in a test matrix provided in Table 3.1 and Table 3.2. The set conditions in the test matrix varied the type of fuel injector, injection pressure, fuel injection temperature, and ambient pressure.

Two different experimental set ups were designed and assembled at Maurice Zucrow Laboratories to test the performance of two types of fuel injectors: a pressure swirl atomizer and a hybrid air blast nozzle. The first experiment involves testing both fuel injectors at various atmospheric set conditions and measuring spray properties using an En'Urga SETScan OP-600 optical patternator. The optical patternator provides spatially resolved droplet surface area to volume measurements that describe atomization quality and radial profile of the spray. The second experiment involves testing both fuel injectors at super atmospheric set conditions and measuring spray properties using a

Sympatec HELOS particle analyzer. The Sympatec HELOS particle analyzer provides a drop size probability density function that can determine characteristic diameters for drops in the spray.

One objective of this thesis is to verify and contribute to trends that are observed in the literature for comparing fuels and various set conditions. Work by Goldsworthy *et al.* (2011) suggests that differences between spray characteristics of fuels at various set conditions depend on the properties of the fuel. Wang *et al.* (1988) describes that drop size tends to increase with decreasing fuel injection temperature, and decreasing fuel injection pressure. De Corso *et al.* (1960) and Guildenbecher *et al.* (2008) suggest that spray cone angle tends to decrease and drop size tends to increase with increasing ambient pressure. The influence of the fuel injector set conditions on spray characteristics depends on the properties of the fuel type. Park *et al.* (2004) identifies that viscosity and surface tension affect spray atomization quality at cold temperatures.

One objective is to determine whether the difference in spray properties between aviation jet fuels is significant at the set conditions. Measurements taken at atmospheric conditions by the En'Urga OP-600 Optical Patternator can be compared to determine the dependence of fuel type on spray atomization quality.

Measurements taken at super atmospheric conditions by the Sympatec HELOS laser diffraction device show the dependence of characteristic diameter on fuel type.

Another objective of the thesis is to investigate the differences between fuel types on different types of fuel injectors. Pressure swirl atomizer and hybrid air blast nozzle type fuel injectors are tested in this experiment. The pressure swirl atomizer uses internal geometry to create a swirling liquid sheet at the exit of the atomizer. The breakup of the liquid sheet determines drop distribution and drop diameter. The hybrid air blast nozzle is a pressure swirl nozzle coupled with a swirler that entrains surrounding gas into the spray. The additional aerodynamic forces of the hybrid air blast nozzle will alter the significance of fuel type on the spray atomization characteristics when compared to the pressure swirl nozzle.

CHAPTER 2. LITERATURE REVIEW

2.1 Introduction

Current development of next generation gas turbine engines is driven by advancements in performance that are related to fuel injection. Improved fuel turndown or specific fuel consumption motivates designs for turbine engines with higher pressure ratios and turbine inlet temperatures. While performance improvements are realized with increased pressure ratio, the environment in a combustor and the ultimate efficiency of the engine are limited by material properties in the engine, combustion stability, and the overall design for thermal management of the engine and fuel injector (Benjamin, 2000).

Fuel injector design can improve combustion stability and heat distribution inside the combustor. Fuel atomization quality determines the direction and distance downstream of the fuel injector where combustion takes place. Fuel injectors that spray with more uniform drop concentration can reduce the effects of "hot spots" in the combustion chamber that lead to premature wear on the combustor wall, fuel injectors, or other parts in the engine (Benjamin, 2000). Variations in fuel drop concentration also affect combustion stability because the more uniformly the fuel burns, the smaller the pressure oscillations inside the combustor (Jasuja, 2006). Drop distribution and concentration are driven by a

number of fuel specific properties that will be investigated throughout this literature review.

Design of gas turbine engines and fuel injectors is also driven by the desire to decrease emissions. Reduction in emissions is motivated by environmental concerns and increasingly stringent emissions regulations. Smoke, unburned hydrocarbons, nitrogen oxides, and carbon monoxide are all products of combustion that can be reduced by improving fuel injector design (Benjamin, 2000).

Spray quality and local downstream air-to-fuel ratio affect the products of combustion. Improving how well the fuel is mixed with the surrounding air reduces the emissions that are produced. Sprays that have smaller characteristic diameter drops will burn with fewer emissions than sprays of larger drop diameters. Sprays that have increased air entrainment from the fuel injector swirler or flow through the combustor will make a leaner burning flame that also reduces emissions (Jasuja, 2006). Swirler type and fuel properties that play an important role in atomization quality will be discussed in this chapter.

Fuel injector performance is central to the current development challenges in next generation gas turbine engines. Therefore, it is important to investigate and understand the factors that influence fuel injector atomization characteristics. Spray parameters that are of interest are drop size, drop distribution, and spray cone angle. Factors that influence the atomization characteristics of the spray are the fuel injector type, the type of

fuel sprayed, the temperature of fuel sprayed, the ambient pressure of the fuel, and the viscosity and surface tension of the fuel. These factors are presented in the following sections along with the literature review of each.

2.2 Fuel Injectors

There are two different types of fuel injector used in the experiments for this thesis. One is a solid cone pressure swirl atomizer. The other is a hybrid air blast nozzle with pilot and main fuel lines and an air swirler to entrain the spray.

2.2.1 Pressure Swirl Atomizer

The pressure swirl atomizer is a common type of fuel injector with simple geometry. Fuel enters the injector through ports that are perpendicular to the spray axis of the nozzle. The ports provide a swirling component to the fuel velocity inside the injector. The swirling fuel flows through a contraction and exits via the injector tip where it creates a conical swirling sheet. As the sheet expands, the sheet thickness decreases until the sheet breaks into ligaments and drops. The spray has a radial component of velocity because of how the fuel was swirling in the injector (Rizk, 1985).

The size of the drops produced by the atomizer is related to the sheet thickness produced on the outlet of the fuel injector. A thicker sheet will yield larger drops in the spray (Rizk, 1985). The droplet size of the fuel spray is also affected by fuel properties and ambient pressure. Pressure swirl atomizers were used in most aircraft gas turbine engines until

the mid 1960's. Newer model engines no longer use pressure swirl atomizers because ambient pressure above 15 bar shows reduced performance and increased emissions (Jasuja, 2006).

2.2.2 Hybrid Air Blast Nozzle

The hybrid air blast nozzle is one of several current fuel injector concepts that are used in aircraft gas turbine engines. The concept for the hybrid air blast fuel injector was proposed by Lefebvre in the early 1970's (Jasuja, 2006). The hybrid air blast fuel injector uses a low flow pressure swirl atomizer as a pilot and a main that is a high flow air blast unit. At low fuel flows, all fuel is supplied through the pilot. Normal operation supplies fuel to both circuits. The primary spray angle is low enough so its drops do not wet the secondary fuel pre filmer surface on the swirler interior. The secondary fuel is discharged from a number of passages on the dome air swirler. The swirler entrains the fuel droplets to create an improved spray distribution with smaller drop sizes (Benjamin, 2000).

The design goal for a hybrid air blast nozzle is to mix the injected fuel with the air from the swirler as rapidly as possible. The hybrid air blast nozzle provides better thermal management, reduces emissions and improves fuel distribution in the spray (Jasuga, 2006).

2.3 Aviation Jet Fuel

The type of aviation fuel used in gas turbine engines depends on the application. Petroleum based aviation fuels vary by the type and number of different hydrocarbons present in the fuel. The differences in liquid properties of the fuel play a significant role in fuel injection and are investigated in this thesis. Fuels with higher viscosity do not atomize as well as fuels with lower viscosity (Dorfner *et al*, 1995). Fuels with higher volatility affect the internal pressure of the fuel spray and atomization characteristics (Moon *et al.*, 2007). Different fuels are affected by changes in temperature. As temperature decreases, viscosity increases, surface tension increases, and the volatility is reduced (Park *et al.*, 2004). The test matrix employed in this thesis varies fuel type and collects data on how the spray properties change with temperature, injection pressure and ambient pressure.

As the aviation industry moves to non-petroleum based jet fuels, it will become more important to understand the spray characteristics of common types of petroleum based aviation fuels in order to copy or improve their spray properties (Rizk, 2004). The data collected here can be used to assist modeling efforts of the fuel injector or combustor outlined in Rizk (1997), or Chong *et al.* (2005).

2.3.1 Types of Jet Fuels Tested

There are four different types of aviation fuels used in this thesis. Jet A, JP-8, JP-5 and JP-10 are the aviation fuels tested. Jet A, JP-8 and JP-5 are all gas turbine fuels that are blends of many different hydrocarbons. JP-10 is used in air breathing missile engines.

The types of hydrocarbons present in typical gas turbine fuels are paraffins, cycloparaffins, aromatics and olefins. These fuels are typically made up of a specific hydrocarbon(s) for specific performance characteristics (Frame, 1981). Fuel property data for the various fuels tested can be found in Coordinating Research Council (1983, 2004) "Handbook of Aviation Fuel Properties," or Frame (1981). Charts of particular interest for this thesis are the viscosity versus temperature plots and the surface tension versus temperature plots. The viscosity plots in Frame (1981) show the viscosity of JP-8, Jet A, and JP-5 to be the same at a given temperature. However, viscosity measurements were also made as a part of this project with the Air Force Research Laboratory. The results are presented in the, "Atomization Section of the Final Report of Rules and Tools Phase 2 Project." In contrast to the literature, the JP-8, Jet A, and JP-5 were measured to have different viscosities. The relative viscosities of JP-8, Jet A, JP-5 and JP-10 are included in the discussion below.

JP-8 is a military specified type of gas turbine aviation fuel. It is the primary fuel used by the US Army and Air Force. It is a kerosene fuel that is widely available. The composition of the fuel is similar to Jet A. The viscosity of the JP-8 fuel is lower compared to JP-5 or JP-10.

Jet A is the most common commercial grade aviation fuel used in gas turbine engines. Like JP-8, Jet A is a kerosene based fuel with a naptha mixture. The viscosity of Jet A is slightly greater than that of the JP-8 at cold temperatures.

JP-5 is a high flash point fuel that is used by the US Navy. The high flash point of JP-5 ensures that it is more stable for use on air craft carriers. The viscosity of the fuel is greater than that for Jet A and JP-8 at low temperatures.

JP-10 is used as a missile fuel in air breathing missile engines. Missile fuels are composed of pure hydrocarbons or a mixture of a specific number of hydrocarbons. JP-10 meets the -53.8 C (-65 F) Air Force operational requirement and is composied of exo-tetryhydrodi (cyclopentadiene) (Frame, 1981).

2.4 Effect of Temperature

A literature search into the effect of temperature on the spray characteristics of pressure swirl fuel injectors reinforced the known fact that temperature affects the viscosity of the fluid. Wang *et al*. (1988), Park *et al*. (2004), Park *et al*. (2006) observe Sauter mean diameter (D_{32}) increasing with decreasing temperature. They also comment that the spray cone angle for fuels at colder temperature is reduced and attribute this to changing fuel properties and condensation freezing to the fuel injector tip. The stability of the spray and its dependence on the temperature and viscosity of the fuel is discussed.

How sprays are affected at high temperature was investigated by Moon *et al*. (2006). They report that the spray D_{32} tends to decrease with increasing temperature. They also showed that the pressure inside the spray cone increases and ultimately disrupts the spray at higher temperatures.

2.4.1 Wang and Lefebvre (1988)

Wang and Lefebvre (1988) investigated how the spray characteristics of JP-4 and diesel oil sprayed using a pressure swirl nozzle tends to change with fuel temperature and ambient pressure. Three different hollow cone spray pressure swirl atomizers were used. The experimental apparatus consisted of a cylindrical pressure vessel 120 cm long and 75 cm in diameter. A Malvern particle size analyzer recorded mean drop sizes and drop size distributions. The Malvern optics plane of measurement was 15 cm downstream of the fuel injector. The temperature of the fuel sprayed varied from -20 to +50 C. Fuel injection pressure varied from 0.1 to 2 MPa, and ambient pressure varied between 0.1 and 10 MPa.

The results show plots for D_{32} as a function of temperature, fuel injection pressure, and ambient pressure. D_{32} was also shown to decrease with increasing temperature. Increasing fuel injection pressure initially reduced D_{32}, but leveled out above a fuel injection pressure particular to each nozzle. Increasing ambient pressure initially increased D_{32} and followed by a leveling out and subsequent decrease above an ambient pressure.

Wang and Lefebvre (1988) explain that the change in D_{32} with fuel injection temperature depends on the changing viscosity and surface tension in the liquid. The viscosity of Diesel oil changes from 1.85×10^{-3} kg/m s at 40 C to 4.44×10^{-3} kg/m s at 0 C. The viscosity of JP-4 changes from 0.580×10^{-3} kg/m s at 50 C to 1.531×10^{-3} kg/m s at -20 C. The Diesel oil is much more viscous than the JP-4, and this is reflected in how D_{32}

changes for the fuels with changing temperature; the slope of the Diesel oil D_{32} line as a function of temperature was -0.96, which is larger than the slope of the JP-4 D_{32} line as a function of temperature at -0.25. Because of the changing viscosities, D_{32} for the Diesel fuel is larger and changes with larger slope than the JP-4.

2.4.2 Park *et al.* (2004)

Park *et al*. (2004) investigated the effect of injection pressure, liquid temperature and viscosity on the spray characteristics of a dual-orifice type pressure swirl nozzle. Two different kerosene-based aviation fuels were sprayed, Fuel A and Fuel B. A Malvern particle sizer measured the downstream D_{32} of the drops. The spray cone angle was measured 3 cm downstream by capturing high resolution images of the spray. A 1-D patternator using 30 collection bins was also used to measure the volumetric distribution of the spray.

The viscosity and surface tension of Fuel A and Fuel B were recorded as a function of temperature. Fuel B was more viscous than Fuel A and both fuel viscosities increased exponentially with decreasing temperature. Fuel surface tensions increased linearly and slowly with decreasing temperature. Fuel line pressure and temperature were controlled and monitored.

Park *et al*. showed that stabile injection is a function of injection pressure, kinematic viscosity and surface tension. At low injection pressure, the kinematic viscosity and surface tension affect the spray shape and drop size. The 1-D patternator showed a

disruption of the volumetric distribution of the hollow cone spray at cold temperature. The Malvern particle analyzer showed that drop size increases with increasing viscosity. Park *et al*. also observed fluctuations in the atomizer and an icing phenomenon where the ice would partially obscure the fuel injector tip at cooled fuel conditions. Tests at higher injection pressure were shown to decrease the effect of the kinematic viscosity and surface tension on the spray shape and drop size.

2.4.3 Park *et al.* (2007)

Park and Kim's paper (2007) is a continuation of Park *et al*. (2004) and examines how spray drop sizes and instabilities in the spray are influenced by changing temperature of two kerosene type fuels. Similar to earlier work, the fuel temperature was varied from -30 to 120 C. Fuel B was more viscous than Fuel A and the fuel surface tension was greater for Fuel B than for Fuel A. The fuel injector used was a pressure swirl injector, and the drop size distribution and characteristic diameters were measured with a Malvern particle analyzer. Spray angle was captured using a CCD Camera whose measurement plane was centered 3cm downstream of the atomizer tip.

The spray performance was categorized into three categories: external unstable (T<260 K), internal/external unstable (260 -280 K), and stable (T>280). As the fuel temperature decreases, the spray becomes more unstable due to increased viscosity effects. Transition from the stable to the internal/external unstable spray regime is described by unsteady pulsation and collapse of the air core in the atomizer spray. When the temperature is

further reduced, the spray is characterized as unstable. The air core is completely disrupted and there is no longer a hollow cone.

The results between the two fuels at cold temperature illustrated their effect on the stability of the spray. Fuel A was shown to atomize stably across all temperature conditions. Fuel B did not atomize stably at the lower temperature due to the increase in its viscosity.

The Sauter mean diameter of the spray increased with decreasing temperature. D_{32} is strongly influenced by kinematic viscosity in low temperature range. Surface tension plays a more important role at higher injection temperatures. In addition, the spray cone angle was shown to decrease with decreasing temperature and eruption of the air core.

2.4.4 Moon *et al.* (2006)

Moon *et al.* (2006) investigated internal and near nozzle effects of changing the fuel temperature for a pressure swirl nozzle. The fuel spray was pulsed as in a spray ignition engine. The fuel used was gasoline and the temperature was varied from 298 to 358 K. Phase Doppler Anemometry (PDA) was used to measure local drop size and velocity in the spray. High resolution pictures were taken for spray angle and flow visualization. Static pressure measurements along the centerline of the spray were also taken with a pressure transducer.

The authors founds that as injector temperature increased, the spray width decreased and main spray penetration increased. The spray was shown to collapse at high temperatures due to the spray film breakup at the nozzle exit. The PDA data showed that the D_{32} decreased by 27.4% from 298 to 358 K while D_{10} only decreased by 11.6%. The drop size probability density function shows that the number of large droplets was reduced with increasing fuel temperature. The breakup was attributed to the expansion of locally formed bubbles of fuel vapor and reduced viscosity. The formation of fuel vapor bubbles was shown by measuring the static pressure in the spray cone. It was shown that pressure inside the spray increases with increasing fuel temperature.

2.5 Effect of Ambient Pressure

A literature review on the effect of ambient pressure on a pressure spray nozzle showed that the spray cone angle decreases and the drop size tends to increase with increasing pressure. De Corso *et al*. (1960) and Guildenbecher *et al*. (2008) performed experiments to determine and verify empirical correlations for the effect of ambient pressure on spray characteristics. They discuss how the ambient pressure affects spray cone angle and Sauter mean diameter of a pressure swirl nozzle.

2.5.1 De Corso *et al.* (1960)

De Corso investigated how changing the ambient pressure affects the drop size produced by a pressure swirl injector. The experimental set up used a pressure chamber with a fuel injector and optical ports to take spray measurements. Ambient pressure varied from sub atmospheric conditions to 100 psi. Injection delta p was either 25 or 100 psi. Drop sizes

were measured by sequential magnified photographic technique. The overall magnification of the pictures was 182/1. The drop sizes were tabulated and the data was presented as a t test.

When the pressure in the vessel was increased from 10 to 100 psi, several trends were noted. The results show that the fuel flow distribution shifts to smaller droplets in the inside areas of the spray. However, the overall trend of drop size distribution shows increasing Sauter mean diameter from 10 to 100 psi. Drop coalescence dominates at pressures above 10 psi, thus increasing drop sizes. A result of drop coalescence is that the Spray angle is shown to decrease with increasing pressure. Droplet velocity is also shown to be at maximum when the spray angle is a minimum.

The results from the experiments were explained in terms of ambient air entrainment and how it affects spray properties. Air flow at higher ambient pressure is dense and will entrain more spray droplets. The result is a smaller spray cone angle, more fine droplets in the center of the spray and drop coalescence resulting in larger D32.

2.5.2 Guildenbecher *et al.* (2008)

Guildenbecher measured how spray cone angle changed with changing ambient pressure. The pressure swirl injector with interchangeable swirl insert was used in the experiment to spray a synthetic lubricant with properties similar to Diesel fuel. The experiment involved a pressure vessel capable of pressures up to 10.2 MPa with 5.72 cm diameter optical windows for measuring spray characteristics. Shadowgraph back lighting and

optics allowed the image of the spray to be captured by digital camera. The image was used to measure spray cone angle of the spray.

At increased pressure, the spray cone angle contracts to a certain ambient injection pressure. Air entrainment becomes more important as pressure increases. Consequently, the difference between the upstream and downstream cone angle was found to decrease with increasing pressure. Guildenbecher found that at an ambient pressure above 1.5 MPa to 3.5 MPa, the spray cone angle measured does not further decrease with increasing ambient pressure.

Injection Δp was found to have very little influence on spray cone angle with varying ambient injection pressure. However the swirl number on the interchangeable swirl insert has an influence on spray cone angle. Swirl inserts with a larger swirl number were shown to have an effect on the spray cone angle at high pressure above 1.4 MPa.

2.6 Effect of Surface Tension and Viscosity

Research from Dorfner *et al.* (1995), Shanshan *et al.* (2012), Goldsworthy *et al.*(2011) and Li *et al.* (2012) investigate the effect of surface tension and viscosity on spray atomization characteristics. Dorfner *et al.* (1995) and Shanshan *et. al* (2012) investigated the effects of viscosity and surface tension by measuring spray characteristics of water glycerine mixtures of varying concentration. They found that the Sauter mean diameter of the spray increased with increasing viscosity of the liquid. Dorfner *et al.* (1995) varied the surface tension independently of the viscosity and showed that the Sauter mean

diameter also increased with increasing surface tension. Goldsworthy *et al.* (2011) tested two fuels of different viscosity and showed that the spray characteristics changed . Li *et al.* (2012) studied air entrainment effects and how changing viscosity alters the spray characteristics. It was shown that the air entrainment reduces the effect of viscosity on the spray.

2.6.1 Dorfner *et al.* (1995)

Dorfner *et al*. (1995) investigated the characteristics of a pressure swirl atomizer sprays and how they changed with surface tension and viscosity. They used phase doppler anamometry to measure drop sizes and reported the characteristic diameter of the spray. Two pressure swirl fuel injectors were used. Ethanol-water mixtures were mixed with surfactant TMA to independently change surface tension. The viscosity of the ethanol-water mixtures was changed by adding glycerine or sucrose. Measurements showed surface tension between $30 \times 10^{-3}$and 70×10^{-3} N/m, and viscosity between 2.5×10^{-3} and 40×10^{-3} Pa s. The ethanol-water mixture was sprayed at constant flow rate.

The results of the Phase Doppler Anemometry measurements at various local points in the spray were weighted to calculate representative drop size distributions for a cross section. The drop size distribution shifted to larger droplet diameters with increasing surface tension. The increasing size distribution caused the number and Sauter mean diameters to increase with surface tension. Increasing the viscosity of the spray increased both mean diameters. The size distributions show that the larger droplets in the spray are especially affected by increasing viscosity.

The Sauter mean diameter of the spray was not shown to be independently proportional to a constant power of surface tension or viscosity. Varying viscosity while holding surface tension constant yielded a constant power law curve. However, the surface tension exponent tended to vary considerably across the test space. This is in agreement with how the changing viscosity and surface tension affected drop size distributions.

2.6.2 Goldsworthy *et al.* (2011)

Goldsworthy *et al*. (2011) investigated the difference in spray characteristics between diesel fuel and 75% canola oil. The primary difference is the viscosity of the fluids - diesel at 0.0022 kg/m s and 75% canola at 0.042 kg/m s. A solid cone fuel injector with fuel injector pressure of 110 MPa was used to spray the fuels in a chamber that was pressurized to 2 MPa. Particle Image Velocimetry (PIV) was used to determine droplet velocities. Shadowgraphy using a 27:1 magnification was used to measure droplet sizes.

At larger drop sizes in more viscous sprays, the droplet velocity was shown to be higher, but overall spray penetration and cone angle were not observed to change. Comparing viscosities of fuels show that the 75% canola is 20 times higher than the viscosity of the diesel fuel. The Sauter mean diameter of the 75% canola is 1.5 times compared to the diesel fuel. Computer analysis of the magnified images from the shadowgraphy showed that the D_{10} particle size for the diesel Fuel was 16 um while the D_{10} for the 75% canola was 24.5 um. The Sauter mean diameter for the diesel fuel was 26.2 um while for the 75% canola it was 38.9 um.

2.6.3 Shanshan *et al.* (2012)

Shanshan *et al*. (2012) investigated the effects of liquid viscosity on the spray characteristics and instabilities during transient operation of a pressure swirl nozzle. Water-glycerol mixtures were used to test a range of viscosities from 0.937 to 251.84 mPa-s. Variation of the surface tension in the liquid mixtures was less than 10%. The temperature of the mixtures remained at room temperature (23 C). The experiment involved a piston dispensing mechanism and trigger that was used to start the spray and signal when to start the high speed 40 kHz camera.

From the high speed digital images, Shanshan *et al.*calculated the frequencies of the waves on the surface of the spray cone. They found that the frequency is the same for all locations in the spray and that the frequency of the oscillations decreases as the spray develops with time. Fluid viscosity plays a role in the transient spray cone angle and drop break up. The image analysis showed there was less drop break up for the higher viscosity solutions. For more viscous liquids, the spray cone angle was reduced.

2.6.4 Li *et al.* (2012)

Li *et al*. (2012) studied the influence of viscosity on atomization in an internal mixing twin fluid atomizer. Glycerin and water mixtures were used to change the liquid viscosity while maintaining similar surface tensions. The liquid viscosities tested were 1.3, 30 and 120 mPa s. The injection pressure and gas to liquid mass ratio were also varied independently.

Results showed that D_{32}decreases with increasing gas to liquid mass ratio. At low injection pressure and low gas liquid ratio, $D_{32}$was shown to behave independently of viscosity. However, at high gas liquid ratio, it was shown that D_{32} increases with increasing viscosity. At low injection pressure (0.1 MPa) D_{32} was affected less by viscosity than at higher injection pressure (0.5 MPa) where the D_{32} increased by 27% due to changes in viscosity.

2.7 Summary

The literature has sufficient description of trends that are produced from varying fuel temperature [Wang *et al*. (1988), Park *et al*. (2004), Park *et al*. (2006)]. More work is needed to describe how aviation industry types of fuel will behave at cold temperatures.

Optical patternation of cold fuel sprays is not employed in any of these studies. The benefit of optical patternation is that the results will show the local regions of high and low concentration with changing temperature. Comparison of a pressure swirl to air blast nozzle is also not investigated in the literature.

The effect of increasing ambient air pressure on the spray cone angle and D_{32} has been investigated [De Corso *et al.* (1960), Guildenbecher *et al*. (2008)]. However, the tests have not been conducted with a variety of aviation jet fuels. In addition, the effects of ambient pressure on a hybrid air blast nozzle when compared to that of a pressure swirl nozzle have not been reported with different jet fuels.

Studies show that the fluid viscosity plays a role in the droplet size of the spray and spray cone angle of the fuel injector [Dorfner *et al.* (1995), Goldsworthy *et al.* (2011), Shanshan *et al.* (2012), Li *et al.* (2012)]. However, no significant studies compare how different aviation fuels behave when sprayed. Substantial D_{32} data has been collected for liquids of different viscosity, but very little optical patternator data has been collected for aviation fuels. The advantage of looking at optical patternator data and changing viscosity is that the data can show where the local concentrations of droplets increase with increasing viscosity.

In summary, a review of how fuel injector spray atomization characteristics change with type of fuel injector, fuel type, fuel injection pressure, fuel injection temperature, and ambient pressure demonstrated that there is still a need for further investigation. This thesis addresses the following open aspects about fuel injector atomization characteristics.

- Contribute spray patternation measurements to the body of existing drop size data in the literature.
- Discuss the influence of fuel type, ambient pressure and fuel injection temperature and fuel injection pressure on spray atomization quality.
- Compare the performance of a pressure swirl atomizer to a hybrid air blast nozzle at similar set conditions.

CHAPTER 3. EXPERIMENTAL APPARATUS AND UNCERTAINTY

The test matrix that was proposed by the Air Force Research Lab and the Atomization Committee tests two different injectors across a variety of set conditions. The test matrix for the pressure swirl nozzle and the test matrix for the hybrid air blast nozzle vary with fuel type, fuel injection temperature, fuel injection pressure, and ambient pressure.

The experiments at atmospheric pressure were conducted at Zucrow Lab 1 (ZL1), Maurice Zucrow Laboratories, Purdue University. The experimental setup is composed of several sub-systems, each of which is described in this section. They are the fuel cart, air box assembly, fuel collection system and optical patternator.

The experiments at super atmospheric pressures were conducted in a high-pressure/high-temperature vessel at the High Pressure Lab (HPL), Maurice Zucrow Laboratories, Purdue University. The subsystems for the experiment are the fuel cart, pressure vessel, fuel injector assembly, nitrogen co flow system, exhaust system, data acquisition/control system, and Sympatec optical system.

The test procedure and data collected for atmospheric testing in ZL1 and the super atmospheric testing in HPL was documented. The procedural checklists for both tests are found in the Appendix. The data of interest for describing the effect of fuel temperature, ambient pressure, and pressure of the working fluids in the injector are collected by the optical techniques in the experimental set up. A description of the data collected and the uncertainties associated with these measurements will be described in this chapter.

3.1 Fuel Injector and Test Matrix Description

The two fuel injectors provided by the Rules and Tools Atomization Committee are the pressure swirl atomizer and the hybrid air blast nozzle. The nozzles were tested according to a test matrix that outlines what the set conditions are for the fuel injector at each condition. The test matrix for each of the nozzles is shown in Table 3.1 and Table 3.2. The data collected will be used in modeling efforts at Rolls Royce and other engine companies to understand atomization and its effect on the performance of the engine as a whole. The descriptions of the nozzles and test matrices are in the following sections.

3.1.1 Pressure Swirl Nozzle

The pressure swirl atomizer was provided to the project because the spray from the fuel injector at a particular set condition was tested and well understood. The flow number, which is equal to the fuel flow rate divided by the square root of the pressure drop across the injector, for the pressure swirl atomizer that was tested is 0.6. The Stoddard Solvent test condition 14 on the atmospheric test stand and test condition 16 on the super atmospheric test stand were used to check against previously acquired Patternator and

Sympatec data. This ensured that the data collected from the optical devices at Purdue could be checked for agreement with previous work.

The pressure swirl nozzle also provided important insight into how the spray from the fuel injector changed with changing fuel type, fuel temperature, injector pressure, and ambient pressure. The results section shows that the data from the pressure swirl atomizer was consistent and showed strong trends for all of the changing parameters.

3.1.2 Pressure Swirl Atomizer Test Matrix

The pressure swirl atomizer test matrix is shown in Table 3.1. Four jet fuels were tested at every point on the test matrix. The fuels are JP-8, Jet A, JP-5, and JP-10. The pressure swirl atomizer test matrix is divided into two sections: atmospheric testing, and super atmospheric testing. Atmospheric testing is described in set condition points 9 through 14. The parameters that varied across the atmospheric testing set conditions are the fuel injection pressure at 0.345 MPa or 0.689 MPa (50 or 100 psig) and the fuel temperature at the point of injection at -40, -17.8, and 15.6 C (-40, 0, and 60 F). Super atmospheric testing is described in set condition points 15 through 26. The parameters that varied across the atmospheric testing set conditions are the fuel injection pressure at 0.345 or 0.689 MPa (50 or 100 psig) the ambient pressure at 0.206, 0.345, 0.689, 1.379, and 1.723 MPa (20, 50, 100, 200, and 250 psi) and the ambient temperature at 15.6 and -17.8 C (60, and 0 F).

3.1.3 Hybrid Air Blast Nozzle

The hybrid air blast nozzle was developed for the Rules and Tools project with the eventual intent of integrating a type of hybrid air blast nozzle into a next generation gas turbine engine. The hybrid air blast nozzle consists of concentric pilot and main fuel injection atomizers. The pilot atomizer sprays a solid cone and the main fuel atomizer sprays a hollow cone. The flow number for the pilot atomizer is 1.5 and the main flow number for the main atomizer is 36.5.

The hybrid air blast nozzle is composed of the pilot and main pressure swirl atomizer inserted into a nitrogen swirler so that nitrogen will entrain the droplets from the pilot and main fuel lines. The pressure drop across the swirler is set by the pressure drop across the swirler divided by the ambient pressure of the swirler ($\Delta p/p$).

3.1.4 Hybrid Air Blast Nozzle Test Matrix

The hybrid air blast nozzle test matrix is shown in Table 3.2. Four fuels were tested for every point on the test matrix. The fuels are JP-8, Jet A, JP-5, and JP-10. The hybrid air blast nozzle test matrix is divided into two sections: atmospheric testing, and super atmospheric testing. Atmospheric testing is described in set condition points 9 through 14. The parameters that varied across the atmospheric testing set conditions are the fuel injection pressure at 0.358 or 0.806 MPa (52 or 117psig) and the fuel temperature at the point of injection at -40, -17.8, 15.6 C (-40F, 0F, 60F). Super atmospheric testing is described in set condition points 15 through 36. The parameters that varied across the super atmospheric testing set conditions are the ambient pressure at 0.206, 0.345, 0.689,

1.379, and 1.723 MPa (20, 50, 100, 200, and 250 psi), and the percent of the flow coming from the pilot versus main fuel injector corresponding to the ambient pressure. Held constant for the super atmospheric testing is the fuel air ratio tested (0.006), and the temperature of the fuel at 15.6 C (60F).

3.2 Fuel Cart

The fuel cart system is designed to control the injection pressure and temperature of the aviation fuel at the atmospheric testing in ZL1 and super atmospheric testing at HPL. The system is designed to be mobile so that it may be moved between the two facilities. The fuel cart is equipped with a pump and recirculation loop for providing the upstream pressure. There are two lines with pneumatic valves and needle valves for controlling flow rate and fuel injection pressure. The fuel cart has a chiller with heat exchangers and jacketed fuel line to cool the fuel to the specified fuel injection temperature. There are thermocouples, pressure transducers, flow meters and data acquisition electronics to monitor the operation and fuel properties before injection. The plumbing and instrumentation diagram for the cart is shown in Figure 3.1. The instrumentation and controls list for the fuel cart is shown in Table 3.3. Each of these components are discussed in the following sections

3.2.1 Fuel Recirculation Loop

The fuel intake line pumps fuel out of the dedicated fuel can for each type of fuel, passes through a 3 micron water absorbing Norman Filter and into the intake side of the pump. The pump is a CIG Lip Seal and Weep Hole Design IMO Pump. The pump is equipped

with an external drain that is plumbed to the fuel can and a high pressure outlet for the fuel lines. The fuel in the high pressure outlet passes through a pulsation dampener and a diaphragm bypass pressure regulating valve. The pulsation dampener has an internal diaphragm that when pressurized to half the set pressure of the line, reduces pressure oscillations caused by the pump. The Hydra-Cell C62 bypass pressure regulating valve has an internal spring that adjusts the allowable upstream pressure in the fuel lines. When the pressure exceeds the set pressure, the valve opens and allows fuel to return to the fuel can. The 5 gallon volume of the fuel can used at ZL1 required there to be a heat exchanger on the return line to the fuel can in order to expel excess heat from the pump. This heat exchanger consists of a stainless steel coil of tube in a vessel of water that is continuously exchanged. No heat exchanger on the recirculation loop is necessary at HPL because the 55 gallon drum of fuel has enough volume that the temperature of the fuel doesn't increase as quickly.

3.2.2 Fuel Cart Panel Valves and Instrumentation

The pilot fuel line is teed off from the fuel pressure control valve on the recirculation loop of the fuel cart. The fuel passes through a 10 micron fuel filter, pneumatic valve, coriolis flow meter, needle valve, two heat exchangers and is jacketed up to the air box. The pneumatic valve is controlled by a 24 VDC signal and 0.413 to 0.827 MPa (60 to 120 psi) pilot pressure line that allows for rapid on, off control of the pilot line. The Micro Motion coriolis flow meter measures the mass flow rate of the fuel in the pilot line with accuracy to +/- 0.030% full scale deflection. The needle valve coupled with ETI Systems electronic valve actuator provides flow adjustment to +/- 0.045 kg/hr (0.1 lb/hr)

of the pilot line. The main line uses a pneumatic valve and coriolis flow meter that is identical to the pilot line. The main line has a needle valve with a larger control volume and provides control for the maximum flow rate required for super atmospheric testing 45.04 kg/hr (99.3 lb/hr).

3.2.3 Chiller, Heat Exchanger, and Jacketed Fuel Line

The chiller responsible for cooling the fuel is a SP Scientific ULT chiller, capable of chilling the heat exchanger fluid to -80 C. The heat exchanger fluid used to cool the fuel is Duratherm XLT. The fluid properties allow the chiller to operate over its entire functional temperature range. From the outlet of the chiller, the heat exchanger fluid divides into 3 flow paths. Two of the flow paths go to the heat exchangers, one of the flow paths connect to the jacketed fuel line. The amount of flow to the heat exchangers is controlled by cryogenic valves mounted on the fuel cart. The tubing connections to the heat exchangers running in parallel and back to the chiller are all made with 0.5 inch tygon tubing.

The benefit of connecting the heat exchangers and jacketed fuel line in parallel is that the fuel enters each of the heat transfer elements at the coolest possible temperature. This allows increased heat transfer and allows the fuel in the heat exchangers and jacketed fuel lines to rapidly cool to the fuel injector test set temperature.

The two Exergy, LLC heat exchangers are coiled 3/8 inch diameter stainless steel tubes jacked in 3/4 inch diameter stainless steel tubes. The jacketed fuel line consists of a

flexible, 0.25 inch stainless steel Swagelok flexible line jacketed in a 0.75 inch diameter tygon tube. The heat exchangers and jacketed fuel line allows the pilot line to be chilled as cold as -40 C (-40 F). The main line is not temperature conditioned.

3.2.4 Fuel Cart Instrumentation

The fuel cart is equipped with thermocouples, pressure transducers, and flow meters to measure fuel properties before fuel injection. All of the thermocouples are 1/16 inch diameter type K Chromega and Alomega with temperature measurement ranges from -200 C to 1250 C (-328 to 2282 F). The GE UNIK 5000 premium accuracy pressure transducers used are all 0 to 20 V excitation, and 0 to 10 V output. The accuracy of the pressure transducer is 0.04% full scale deflection and the input range used depends of the location on the fuel cart.

There is a pressure and temperature transducer between the recirculation loop and the pneumatic valves on the fuel cart panel. The pressure transducer is a 0 to 13.78 MPa (0 to 2000 psi) transducer to monitor pressure on the outlet side of the pump. The thermocouple measures the temperature on the outlet side of the pump. These transducers are used to monitor pump health and ensure that the pump is operating normally. During operation the outlet pressure of the pump oscillates no more than +/- 0.068 MPa (10 psi) and the temperature of the fuel does not increase above 37.7 C (100 F).

The thermocouples that are used to measure the temperature of the heat exchanger fluid and the intermediate temperature readings of the fuel monitor how the working fluids are interacting in the fuel cart. For the heat exchanger fluid, there are thermocouples on the outlet of the chiller and on the return port from both heat exchangers. The thermocouples on the heat exchangers ensure that the chiller is operating normally and achieving set point conditions. The heat exchanger fluid leaving the chiller typically needs to be 16 to 22 C cooler than the set point temperature of the fuel. There is also a thermocouple measuring fuel temperature downstream of both heat exchangers but upstream of the jacketed fuel line. This thermocouple ensures that the fuel is not being excessively cooled below the temperature set point for injection.

There is a thermocouple and pressure transducer that measure fuel properties directly before injection. The pressure transducer input range is 0 to 3.447 MPa (0 to 500 psi) and is mounted after the jacketed fuel line and before the air box. The thermocouple is mounted as close as possible to the fuel injector inside the air box. For the pressure swirl atomizer, the thermocouple is 76.2 mm (3 inches) above the injector. The thermocouple for the hybrid air blast nozzle is mounted 152.4 mm (6 inches) above the injector.

For the atmospheric lab in ZL1, the fuel cart is the only electronic data acquisition method, so the nitrogen properties for the swirl flow on the nitrogen line are also measured with the fuel cart. Upstream of the Venturi in the nitrogen line, the temperature and pressure are monitored. The input of the pressure transducer is 0 to 3.447 MPa (0 to 500 psi). The pressure of the air box is also measured. The input of the pressure

transducer in the air box is 0 to 0.206 MPa (0 to 30 psi). The range of the pressure transducer in the air box allows for an uncertainty in measurement of +/- 82 Pa (0.012 psi) when setting the $\Delta p/p$ in the atmospheric lab.

3.2.5 Fuel Cart System Electronics and Data Aquisition

The fuel cart electronics box houses National Instruments data acquisition and electronics that controls analog and digital signals to the valves and instrumentation. The LabVIEW program records measurements and feedback from the valves and instrumentation while the optical spray measurements are performed.

Inside the electronics box, there are two power supplies that control valve power and power to instrumentation. The power supply for valve power is used to provide 20VDC to the pneumatic valves and needle valves. This ensures that the power to the valves can be shut off in case of emergency and the valves will default closed. The other power supply is an Acopian Series B 20 V power supply that provides 20 VDC power to instrumentation. The power output is regulated to +/- 0.005% full scale deflection so that there is no uncertainty in the data associated with power fluctuation.

There is a NI USB X Series data acquisition box that is connected to circuits used to condition the signal for pressure transducers and thermocouples. The NI data acquisition has 32 analog inputs, 4 analog outputs, and 48 digital input/output channels. The fuel cart data acquisition is wired to record 8 thermocouples, 4 for pressure transducers, 2 for needle valves, 2 pneumatic valves and 2 flow meters.

3.3 Experimental Apparatus for Atmospheric Testing

The purpose of the testing at atmospheric pressure in ZL1 is to collect patternator data on how the spray changes with injection pressure and temperature. The piping and instrumentation diagram for the experiment is in Figure 3.2.

3.3.1 Fuel and Nitrogen Supply for Atmospheric Testing

The fuel supply is plumbed from the jacketed line on the fuel cart into the air box. At atmospheric testing conditions, only the pilot on the hybrid air blast nozzle is used, so a main fuel line is not required in the assembly. The flow rate of the fuel injectors is low enough (less than 100 ft/s) that the pressure of the fuel line can be measured upstream of the air box without introducing any error in the injection pressure measurements. The injection temperature measurement is recorded by a thermocouple that is closely coupled to the tube immediately upstream of the injector. For the pressure swirl atomizer, the thermocouple is 76.2 mm (3 inches) upstream of the injector. For the hybrid air blast nozzle, the thermocouple is 127 mm (5 inches) upstream of the injector.

High pressure nitrogen lines are plumbed from HPL to ZL1 to supply flowing nitrogen to the assembly. The nitrogen lines come off of a regulator panel in ZL1 that sets that pressure upstream of a Venturi. The upstream side of the Venturi is equipped with a pressure transducer and thermocouple to calculate flow rate of the nitrogen. The nitrogen enters through the side of the air box. The pressure in the air box is measured to set the $\Delta p/p$ of the swirler. The nitrogen exits through the swirler at the bottom of the air box. In the pressure swirl atomizer case, there is no nitrogen flowing.

3.3.2 Air Box Design

The design of the air box is primarily driven by the hybrid air blast nozzle because it requires instrumentation and plumbing for the pilot fuel line and a nitrogen pressure drop across the swirler. See Figures for assembly drawing of air box. The air box design has redundant straight thread ports drilled in the flange in the top of the assembly for an air box pressure transducer, pilot fuel line and pilot fuel line thermocouple. Nitrogen is supplied to the pressure swirl atomizer by a line through the side wall of the 3" NPT Sch 80 pipe. The 0.5 in tube supplying the nitrogen has a Venturi with upstream ports for pressure and temperature measurements. Although the $\Delta p/p$ is used to set the pressure drop across the swirler, the Venturi and upstream instrumentation allow the nitrogen flow rate through the air box to be calculated.

The hybrid air blast nozzle is attached to the air box by an air box plug that mates with the air box and the swirler assembly. An o-ring sealing surface on the air box prevents air from escaping between the air box and the air box plug.

The pressure swirl atomizer requires the ports for the fuel line and thermocouple line, but it requires a different air box plug. The pressure swirl atomizer air box plug accommodates the fuel injector shape and allows it to mate to the side wall of the air box pipe. See Figure 3.6 for drawings of the air box plug part and assembly.

3.3.3 Fuel Collection

After the fuel is sprayed, the fuel is collected with a custom designed duct and fan unit installed in ZL1. The spray is directed into a 16 inch diameter sheet metal tank with a conical bottom. The fuel will collect in the bottom and drain out of a 1 inch NPT fitting in the bottom and collect in a 5 gallon fire suppressant can. The air and remaining fuel will be pulled out of the tank through a 14 inch duct that is mated to the side wall of the tank. An exhaust fan draws the air in the duct out of the room. This air flow has minimal effect on spray characteristics, but prevents spray droplets from recirculating in the laboratory space.

3.3.4 En'Urga OP-600 SETScan Optical Patternator

The OP-600 SETScan Optical Patternator (En'Urga, Inc., USA) was used to collect data from the spray. The measurement plane of the Optical Patternator was centered and oriented perpendicular to the spray axis of the fuel injector. The measurement plane was located 38.1 mm (1.5 inch) downstream from the tip of the fuel injector.

The optical patternator was developed by En'Urga based on the principals of the Beer-Lambert Law that defines light extinction in terms of liquid properties. The OP-600 Patternator uses six Lasiris SNF laser line generators (Stockeryale, USA) with plano convex lenses to make collimated sheet beam with 256 pixels about 170 mm wide and 2 mm thick. Each of the six beam sheets are oriented in a circular pattern and where the beams cross creates a measurement area that is 18 cm in diameter.

On the side opposite each of the six laser line generators is a 256 element photo diode array detector. Each of the detectors measures the laser intensity allowing the devices to find the laser intensities for 1536 locations in the measurement zone. The radial resolution in the measurement plane for the optical patternator is 1.4 mm and the angular resolution is 15 degrees.

Prior to any measurement, a one second reference scan at 1000 Hz is taken with no droplets in the measurement plane. The reference scan accounts for the loss of laser transmittance intensity due to the ambient medium. The laser transmittance intensity data for the fuel spray is collected at 1000 Hz and the measurement duration for the ZL1 atmospheric tests were 5 seconds long.

The data from the measurements is processed using a deconvolution algorithm, Maximum Likelihood Estimation (MLE), to find the local absorbances for each of the measurement locations. This data is related to the local surface area per unit spray volume. A detailed description of the calculation can be found Lim *et al.* (2005).

3.4 Experimental Apparatus for Super Atmospheric Testing

The experiments at super atmospheric pressures were performed at the High Pressure Laboratory in the rocket test cell. The super atmospheric experiments were conducted at HPL because the facility has the capability of running experiments remotely from a control room away from the test cell and pressurized test hardware. This reduces the risk to

personnel when the test hardware is pressurized. The lab also has built-in nitrogen panel with a 41.36 MPa (6000 psi) source that is required for the experiment.

The test hardware that is integrated into the facility will also be described in this section. The experiment consists of the fuel cart connected to the fuel injector assembly that is installed in the pressure vessel. The plumbing and instrumentation diagram for the fuel injector assembly is shown in Figure 3.3. The exhaust system collects fuel droplets on the outlet of the pressure vessel. The Sympatec laser diffraction instrument is used to collect drop size data on the fuels sprayed. Experiment pressure, temperature and flow rate measurements are collected by the fuel cart and by the HPL facility instrumentation and data acquisition. The instrumentation and controls list is shown in Table 3.4

3.4.1 High Pressure Laboratory Nitrogen System

The High Pressure Lab facility nitrogen system provides nitrogen up stream pressure of up to 41.36 MPa (6000 psi). The nitrogen source for testing activities at the lab is stored in a large tube trailer. The high pressure nitrogen line is connected to a panel inside the facility where multiple Tescom pressure regulators (Model 44-4019V108-27) and Tescom ER 3000 control modules remotely control the downstream nitrogen pressure. The super atmospheric testing uses two of the facility nitrogen panel regulators (CR-FU-01 and CR-N2-01) to control the sweeping flow and the air box flow independently of one another. The ER 3000 for the sweeping flow in the pressure vessel is set to external feedback from a pressure transducer on the pressure vessel. This maintains a consistent set pressure in the

vessel regardless of what the other valves and nitrogen lines are operating at. The ER 3000 for air box flow is set on internal feedback so that the air box flow may be toggled until the correct $\Delta p/p$ is set between the air box and the pressure vessel. Although the pressure drop is set, the nitrogen flow rate in the air box flow is measured using a Venturi upstream of the fuel injector assembly.

3.4.2 Fuel Injector Assembly

The design of the fuel injector assembly was driven by the desire to use the same pressure vessel as Rachedi *et al.* (2007). The fuel injector assembly required a custom design for the fuel injection, nitrogen and air flow assemblies in the vessel. The concept for the fuel injector assembly consists of a vertically actuated air box that extends from the entrance of the pressure vessel down towards the optical windows. The sub-assemblies are the sweeping flow assembly, the air box assembly, and the vertical traverse assembly. Assembly drawings of the fuel injector assembly can be found in Figure 3.4.

The purpose of the sweeping flow assembly is to provide nitrogen flow along the outer wall of the pressure vessel to prevent fuel from spraying the optical windows during testing. The fuel injector sweeping flow assembly attaches to the pressure vessel by a Class 600 lower flange that has a concentric 8 inch, schedule 80 pipe and upper flange and provides sweeping nitrogen flow to the pressure vessel. The facility nitrogen regulator, CR-FU-01 supplies sweeping flow to the sub-assembly through a 2 inch diameter ports on opposite sides of the schedule 80 pipe. The sweeping flow is

introduced into the pressure vessel through the lower flange and enters through a hole pattern of 0.5 inch holes that provides flow straightening for the sweeping flow. The upper and lower flanges have a hole in the center of the parts so that the air box assembly may pass into the pressure vessel. The top flange has two piston O-ring groves that are used to seal against the air box in order to have an assembly that can be pressurized.

The air box is designed to secure the fuel injector to the fuel injector assembly and provide ports for air box nitrogen, fuel injector fuel lines, and instrumentation. The fuel cart is used to supply fuel to the fuel lines. The fuel lines enter through the top of the air box via Swagelock connections. The fuel lines pass through the air box and connect to the fuel injector at the bottom of the air box. The fuel injector is held to the bottom of the air box by the same air box plugs used in the atmospheric tests. In order to set the $\Delta p/p$ of the swirler for the hybrid air blast nozzle, the facility nitrogen regulator, CR-N2-01 supplies the air box with air box flow. A Venturi up stream of the air box is used to calculate the flow rate for the nitrogen in the air box flow. The nitrogen is plumbed into the air box through 1 inch Swagelock ports on the sides of the air box.

The air box is capable of traversing up and down relative to the sweeping flow assembly. The air box is constructed of a 3 inch, schedule 80 stainless steel pipe that is machined to fit through the O-ring seal in the top flange of the sweeping flow assembly. The top of the air box is designed so that it connects to the vertical traverse assembly by a shoulder screw.

The vertical traverse assembly consists of a ball screw whose end connections rigidly hold the air box in place during pressurization but also allow the injector to be vertically adjusted relative to the optical windows. The vertical traverse assembly is capable of moving the air box 254 mm (10 inches). The two parts that connect to the air box are the Ball Screw Holder and Ball Screw Collar. The Ball Screw Holder is connected to the ball screw by thrust bearings so that the ball screw may rotate independently from the rest of the assembly. The Ball Screw Collar is used to connect the air box to the tight tolerance rods that are structural and also used to prevent the air box from rotating relative to the sweeping flow assembly. The tight tolerance rods are connected to the sweeping flow assembly by a hole pattern on the top plate. The other end of the tight tolerance rods is connected to a top flange that is threaded for the ball screw to pass through.

3.4.3 Pressure Vessel

The pressure vessel was designed by Loren Crook as a part of Rachedi's *et al.* (2007). The high pressure and temperatures needed for Rachedi's experiments required a vessel capable of withstanding 600 psi (4.14 MPa) at 1200°F (648.9°C). The body of the pressure vessel is 12 NPS schedule 80, 316 stainless steel. The ends of the pressure vessel are reduced to 6 NPS and flanged with class 600, 316 stainless steel flanges. When the pressure vessel is assembled on the stand, it is 249 cm (98.1 inches) tall, has an inside diameter 29.85 cm (11.750 inches), and has a wall thickness of 1.27 cm (0.500 inches).

There are four optical ports welded to the middle of the pressure vessel. The height of the optical windows when assembled to the stand is 146.3 cm (57.6 inches) tall. Two of the optical ports are designed for a Schlieren system and are positioned on opposite sides of the pressure vessel. These ports are 114.3 mm (4.5 inches) in diameter. The other two optical ports are designed for LDA (Laser Doppler Anemometer), PDA (Phase Doppler Anemometer), and PIV (Particle Image Velocimetry) systems. They are 65.5 mm (2.5 inches) in diameter and located 60 degrees off center from the optical axis.

The optical windows and the flanges for the pressure vessel were redesigned for the current project. The 127 mm (5 inches) diameter optical windows are Schlieren polished and were designed to be 30.48 mm (1.2 inches) thick. The 76.2 mm (3 inches) diameter optical windows are also Schlieren polished and were designed to be 17.78 mm (0.7 inches) thick. The flanges are mounted to the optical windows using a Grafoil gasket seal between all mating surfaces. The bolt pattern on the 127 mm (5 inches) optical windows was torqued to 20 ft/lb. The bolt pattern on the 76.2 mm (3 inches) diameter optical windows was torqued to 10 ft/lb.

There are instrumentation ports in several locations on the pressure vessel. There are two ports for 1/8 Omega type-K thermocouples and one port for a Druck PMP-1260 pressure transducer. The pressure and temperature measurements are recorded for the tests. The pressure tranducer is used for external feedback to the nitrogen regulator CR-FU-01.

3.4.4 Exhaust System

The purpose of the exhaust system is to separate the majority of fuel droplets from the nitrogen flow, control the amount of nitrogen flowing through the system, and exhaust the fuel and nitrogen separately to ambient conditions. The exhaust system consists of an Eaton 31L gas/liquid separator, Robo Drain RD750 and back pressure control valve.

The Eaton 31L gas liquid separator is connected to the outlet of the pressure vessel by a 6 inch, 600 lb 316 SS flange connected to a 6 inch schedule 80 elbow and reduced to a 4 inch schedule 80 pipe with a 4 inch 150 lb flange. The vessel is rated for 2.41 MPa (350 psia) pressure and the allowable flow rate inside the air liquid separator is a function of the pressure inside the vessel. The fuel droplet and nitrogen mixture enters the gas liquid separator and is swirled around in the gas liquid separator so that the fuel droplets spin to the outside of the fuel air separator by centrifugal motion. The velocity of the flow is reduced and the liquid fuel droplets fall out of the gas stream. The nitrogen leaves the liquid air separator to be exhausted and the fuel droplets leave through an external drain to be collected as sprayed fuel.

The Robo Drain RD750 is connected to the outlet of the external drain on the Gas Liquid Separator. The Robo Drain allows for the fuel to be exhausted to a fuel drum without losing any upstream nitrogen pressure so that the set pressure in the pressure vessel is not affected by the fuel collection line. The Robo Drain works by filling a reservoir until a float mechanism reaches the capacity of the drain. Then the control air is activated and

purges the fuel from the tank until the float reaches the minimum drain level. This cycle repeats and exhausts fuel but never lets nitrogen escape through outlet of the drain.

The back pressure control valve is connected to the outlet side of the gas/liquid separator via a 4 inch schedule 40 pipe. The back pressure control valve is an ABZ 028 valve with electronic actuator that is controlled remotely during test operation. The valve controls the amount of nitrogen flow out of the pressure vessel to ambient pressure.

3.4.5 Sympatec HELOS Laser Diffraction System

The Sympatec HELOS central unit is a device for determining particle size distributions of sprays using a laser diffraction technique. The unit is mounted so that the transmitter and receiver are positioned in front of the 114.3 mm (4.5 inches) optical windows on opposite sides of the pressure vessel. The unit consists of a laser source and focusing lens, a measurement zone and the optical system used to convert the laser light into an image that can be recorder by a photo detector. The intensity of the light is converted into an electronic signal that is processed by the provided WINDOX software. The results are reported as probability density functions. Characteristic drop diameters are calculated from the probability density functions.

Operation of the Sympatec HELOS involves specifying a lens, reference measurement duration, and measurement duration, and method determining probability density function. Selecting the correct lens is important because lenses of different focal lengths provide resolution to different ranges of drop sizes. The R6 lens used has a line of sight

working distance of less than or equal to 566 mm. The drop size measurement range is 9 to 1750 µm. The reference measurement used for collecting data in this thesis is 10 seconds in duration. The measurement duration is 5 seconds.

3.4.6 HPL Assembly Instrumentation and Control

In order to control the facility nitrogen system and facility instrumentation, the HPL LabVIEW control and data acquisition was implemented in addition to the fuel cart data acquisition. The instrumentation and controls that were on the HPL LabVIEW VI are shown in Table 3.4.

On the sweeping flow circuit there is a pneumatic valve PV-N2-08 upstream of the regulator that serves as an isolation valve for the experiment. The regulator controlling the set pressure in the pressure vessel and sweeping flow in the vessel is CR-FU-01. This control regulator is set in external feedback mode with pressure feedback coming from PT-INJ-01. The amount of nitrogen flow through the sweeping flow circuit is controlled by the back pressure butterfly control valve. The additional instrumentation of the sweeping flow line is a GE UNIK 5000 (6.895 MPa) 1000 psi input pressure transducer and type K thermocouple on the 2 inch diameter pipe upsteam of the fuel injector assembly. The pressure and temperature measurements can be used as a check to estimate the flow through the sweeping flow assembly.

The air box circuit is controlled by regulator CR-N2-02 set in internal feedback mode. This allows the test operator to set the $\Delta p/p$ of the air box by increasing the regulator

pressure above that of the pressure vessel pressure. The test operator feedback for the Δp/p is calculated from pressure transducers PT-ARBX-01 and PT-INJ-01. Both pressure transducers are 3.447 MPa (500 psi) input GE-UNIK 5000. Since the difference between the two measurements is small and the sampling rate is 50 Hz when setting the Δp/p, the LabVIEW control is set to real time average the 50 most recent measurements and display the output for the Δp/p of the front panel of the VI. This allows the test operator to have sufficient control authority to set the Δp/p accurately.

The other measurements controlled by the facility on the air box nitrogen circuit are a pressure and temperature transducer and Venturi on the upstream side of the air box. This allows the nitrogen flow rate to be calculated from the data collected when the Δp/p is set.

3.4.7 Experiment Data Acquisition

Operation of the super atmospheric experiment at the High Pressure Lab requires additional data acquisition from that which is provided on the fuel cart VI. The facility data acquisition is run by a separate LabVIEW VI. The instrumentation and controls for the facility is summarized in Table 3.4.

3.5 Experimental Uncertainty

Experimental uncertainties affect the spray characteristics results. There are measurement uncertainties in the fuel cart data acquisition, OP-600 Optical Patternator

scans, high pressure facility data acquisition, and uncertainty in Sympatec HELOS measurements.

3.5.1 Fuel Cart and Data Acquisition Uncertainty

The experimental uncertainties that develop with operation of the fuel cart have to do with the uncertainty associated with each of the temperature, pressure and flow rate transducers used to measure fuel properties. The measurement statistics from the fuel cart that are reported for each test are the average and standard deviation of the measurement. All of the fuel, nitrogen, and heat exchanger fluid property data for atmospheric testing in ZL1 was collected by the fuel cart data acquisition. The super atmospheric testing also involved the fuel cart data acquisition. The following sections breakdown the uncertainties in pressure, temperature and flow rate measurements for the fuel cart in the atmospheric and super atmospheric experiments.

The pressure transducers on the fuel cart are GE UNIK 5000 pressure transducers and are summarized in a Table 3.3. All of the pressure transducers on the fuel cart are the premium accuracy models with +/- 0.04% full scale deflection. Measurements of pressure data for ambient conditions provide zero offset data that is used to set all of the pressure transducer measurements to similar atmospheric conditions. The calculation for the corrected pressure transducer data is the measurement value minus the zero offset plus the recorded barometric pressure for the lab.

The error from the pressure measurement accuracy is small compared to the standard deviation of the typical pressure transducer measurement of the fuel line pressure during testing. The standard deviation for each test is averaged and presented in Table 3.3 for all of the pressure transducers. The IMO Pump used to pressurize the fuel recirculation loop is responsible for the pressure oscillations that are recorded in the pressure transducer data. The pulsation dampener and bypass pressure regulating valve are designed into the fuel cart to provide some dampening of pressure oscillations. However, PT-FU-01, the pressure transducer that measures the pressure on the pump recirculation loop records a standard deviation of 3.08 psi. The pressure oscillations are reduced further as the fuel passes through the needle valve toward the injection point. The standard deviation reported by PT-FU-02 and PT-FU-03, the pressure transducers that record the injection pressure is 0.63 psi.

The pressure transducer measuring Venturi and air box pressure in the ZL1 atmospheric testing are used to calculate the flow rate and $\Delta p/p$ for the hybrid air blast fuel injector and swirler. The standard deviations for the Venturi and air box pressure are 0.44 psi and 0.08psi. The uncertainty for these measurements is related to the pressure fluctuations associated with the upstream Tescom pressure regulator in ZL1.

The Emerson Micro Motion flow meters measure the flow rate of the pilot and main fuel lines on the fuel cart. The flow meters were calibrated by Micro Motion before they were sent to Purdue for integration on the fuel cart. The calibration stand uncertainty is +/-

0.030% and the percent error of the flow meter relative to the stand was 0.017% maximum. The standard deviation for the flow meter measurements is 0.065 lb/hr and is greater than the predicted error from uncertainty analysis. Similar to the fuel pressure transducers, the variation in flow rate is associated with the pressure oscillations from the IMO pump on the fuel recirculation loop.

The thermocouples on the fuel cart operate using a Universal DIN Rail Transmitter (TXDIN1600 Series). The Universal DIN Rail Transmitter accepts the input from the Type K thermocouples and outputs a 4 to 20mA signal. The standard deviation of the temperature measurements in the experiment vary from temperature transducer to temperature transducer. This occurs because the experiment is not completely at steady state. Particularly at cold (-40 F) set conditions, the fuel is exchanging heat with the surroundings and fluctuating during the measurement. The typical uncertainty in temperature standard deviation for each thermocouple on the fuel cart is shown in Table 3.3. The important standard deviation measurement to note is TC-FC-01 which shows a standard deviation of 1.88 psi for a 10 second temperature measurement at -40 C (-40 F).

3.5.2 Patternator Uncertainty

The uncertainty in Patternator measurement occurs from fuel injection conditions and optical noise. A minimum of 3 Patternator scans was taken at each of the fuel set conditions during atmospheric testing at ZL1. Each of the individual measurements is shown in Chapter 4. The uncertainty for these measurements is evaluated by finding the

standard deviation of the 3 to 5 measurements at similar set conditions. One standard deviation from the average is shown on plots in the results section.

The uncertainty in Patternator measurement from fuel injector conditions occurs because the set point of the fuel injector changed very slightly each time the injection conditions were set. The Optical Patternator is sensitive to changes in the injection pressure and temperature of the fuel spray. The injection pressure is controlled by the needle valve on the fuel cart and one standard deviation for the set point was 0.63 psi. The standard deviation of the fuel injection temperature is 1.88 F.

The optics in the Patternator is sensitive to how the Patternator reference is collected. During testing, a patternator reference was collected every two Patternator Scans. The reference must be collected often because the noises in the optical measurements tend to increase with time between references. The reference is taken when there is no spray passing through the optical system. However, fine particulates or small atomized droplets that pass through the measurement plane during the reference measurement propagate uncertainty into the actual patternator scan. These uncertainties are quantified by looking at the signal-to-noise ratio of the patternator. If the signal-to-noise ratio was above 400, the uncertainty due to the patternator reference was considered acceptable.

During testing, visual inspection of the fuel injector provided feedback on spray patternation measurements. Figure 3.7 and Figure 3.8 show images of the pressure swirl atomizer and hybrid air blast nozzle during an optical patternator measurement. Areas of

high spray density are more illuminated by the measurement plane than areas of lower spray density. The optical patternator results for the pressure swirl nozzle show a high density of droplets in the center of the spray. The optical patternator results for the hybrid air blast nozzle show a high density of droplets in an annular ring. At colder fuel injection temperatures, visual inspection of the spray confirmed that the density and symmetry of the spray was decreasing. Figure 3.9 illustrates this with the pressure swirl nozzle, spraying JP-8 at -40 C. The areas of spray density in these images show trends that are in agreement with the results presented in Chapter 4 for the radial profiles of the pressure swirl atomizer and hybrid air blast nozzle sprays.

Results from the optical patternator testing were verified by comparing the results to results obtained by engineers at Honeywell Aerospace. For the set condition of the pressure swirl nozzle at 0.345 MPa (100 psi) fuel injection pressure and 15.6 C (60 F) fuel injection temperature, the total surface area and spray cone angle measurements were compared to existing data. The total surface area varied from the Honeywell results by 9.2% error and the full spray cone angle measurements showed 5.8% error.

3.5.3 HPL Super Atmospheric Uncertainty

The super atmospheric testing at the High Pressure Laboratory required the use of the facility data acquisition system in addition to the fuel cart data acquisition for pressure and temperature measurements on the experiment. A summary of the pressure transducers and thermocouples that are recorded by the facility data acquisition are shown in Table 3.4.

The four pressure transducers that are used on the super atmospheric experiment as a part of the facility data acquisition are PT-N2-01, PT-N2-02, PT-INJ-01, and PT-ARBX-01. The pressure transducers are GE UNIK 5000 with accuracy +/- 0.030% full scale deflection. The average standard deviation of the pressure measurements for the facility data acquisition is summarized in Table 3.4. The larger standard deviation of the pressure measurements is caused by fluctuations in pressure by the nitrogen regulators CR-FU-01 and CR-N2-02.

The sweeping flow regulator CR-FU-01 and the air box flow regulator CR-N2-02 cause fluctuations in the pressure transducer measurements because they are controlled by Tescom ER 3000 devices. The Tescom ER 3000 proportional-integral-derivative controller (PID) can set the downstream pressure of the system in internal or external feedback mode. CR-FU-01 is controlled by external feedback with pressure vessel transducer PT-INJ-01. CR-N2-02 is controlled by external feedback from a pressure transducer (PT-03) just downstream from the regulator. Since the control regulators cannot exactly match the feedback from the transducers, the downstream pressure varies about the set point.

The oscillations in pressure values play into the calculation of the $\Delta p/p$ of the air box. PT-INJ-01 and PT-ARBX-01 are used to measure the $\Delta p/p$ of nitrogen in the air box. Since the $\Delta p/p$ is set to 0.06 or less and pressure transducer measurement uncertainty is 0.030% on a 0 to 3.447 MPa (0 to 500 psi) input transducer, an average of the last 50 measurements at 50 Hz is used to find the $\Delta p/p$.

3.5.4 Sympatec HELOS Uncertainty

The uncertainty in Sympatec measurement occurs from fuel injection conditions, recirculation effects, and optical noise. A minimum of 2 Sympatec measurements were taken at each of the fuel set conditions during super atmospheric testing at HPL. Each of the individual measurements is shown in Chapter 4 figures. The uncertainty for these measurements is evaluated by calculating the standard deviation. The standard deviations are plotted in uncertainty bars in the Chapter 4 figures.

The uncertainty in Sympatec measurement is partially due to fuel injection conditions. Sympatec measurements are sensitive to changes in injection pressure and temperature of the fuel. Recirculation effects also affect the uncertainty of the Sympatec measurements. The pressure vessel's sweeping flow generally keeps stray fuel droplets clear of the optical windows. However, if the flow by the sweeping flow air is not great enough, droplets can recirculate through the measurement space and cause inconsistency between measurements.

Optical noise is another factor in Sympatec uncertainty. A reference for the system is taken before any testing procedure with the super atmospheric experiment. However, changing conditions in ambient lighting, condensation or fuel droplets collecting on the optical windows will affect the measurement results.

During testing, visual inspection of the fuel injector provided feedback on laser diffraction measurements of the spray. Figure 3.10 and 3.11 show images of the spray of

the pressure swirl atomizer at 0.172 and 1.72 MPa (25 and 250 psi) ambient pressure and 0.689 MPa (100 psi) fuel injection pressure. The images show how the spray cone angle visually decreases with increasing pressure. The higher droplet density due to the decreased spray cone angle promotes drop coalescence and increasing characteristic drop size. These observations agree with the trend of increasing drop characteristic diameter with increasing ambient pressure shown in the Chapter 4 results.

Results from the laser diffraction device were verified by comparing the results to results obtained by engineers at Honeywell Aerospace. The Sauter mean diameters were compared for the set condition of the pressure swirl nozzle at 0.345 MPa (100 psi) fuel injection pressure, 15.6 C (60 F) fuel injection temperature, and 0.172 MPa (25 psi) ambient pressure. The Sauter mean diameter in the measurement was 33.5 μm, which showed 4.6% error when compared to the Honeywell results.

Table 3.1. Pressure Swirl Nozzle Test Matrix.

Pt	P3, psia	P3, kPa	T3, F	T3, K	T fuel, F	T fuel, K	Air dens, kg/m3	Wf, lb/hr	Pilot %	Wf pilot lb/hr	DP pilot, psid	Measure Techniques
ZL1 Atmospheric Testing												
9	14.7	101.4	60	288.9	-40	233.3	1.22	4.24	100	4.24	50	Optical Patternator
10	14.7	101.4	60	288.9	-40	233.3	1.22	6.00	100	6.00	100	Optical Patternator
11	14.7	101.4	60	288.9	0	255.6	1.22	4.24	100	4.24	50	Optical Patternator
12	14.7	101.4	60	288.9	0	255.6	1.22	6.00	100	6.00	100	Optical Patternator
13	14.7	101.4	60	288.9	60	288.9	1.22	4.24	100	4.24	50	Optical Patternator
14	14.7	101.4	60	288.9	60	288.9	1.22	6.00	100	6.00	100	Optical Patternator
HPL Superatmospheric Testing												
15	14.7	101.4	60	288.9	60	288.9	1.22	4.24	100	4.24	50	Sympatec HELOS
16	14.7	101.4	60	288.9	60	288.9	1.22	6.00	100	6.00	100	Sympatec HELOS
17	50	344.8	60	288.9	60	288.9	4.16	4.24	100	4.24	50	Sympatec HELOS
18	50	344.8	60	288.9	60	288.9	4.16	6.00	100	6.00	100	Sympatec HELOS
19	100	689.5	60	288.9	60	288.9	8.32	4.24	100	4.24	50	Sympatec HELOS
20	100	689.5	60	288.9	60	288.9	8.32	6.00	100	6.00	100	Sympatec HELOS
21	200	1379.0	60	288.9	60	288.9	16.63	4.24	100	4.24	50	Sympatec HELOS
22	200	1379.0	60	288.9	60	288.9	16.63	6.00	100	6.00	100	Sympatec HELOS
23	250	1723.8	60	288.9	60	288.9	20.79	4.24	100	4.24	50	Sympatec HELOS
24	250	1723.8	60	288.9	60	288.9	20.79	6.00	100	6.00	100	Sympatec HELOS
25	14.7	101.4	60	288.9	0	255.6	1.22	4.24	100	4.24	50	Sympatec HELOS
26	14.7	101.4	60	288.9	0	255.6	1.22	6.00	100	6.00	100	Sympatec HELOS

Table 3.2. Hybrid Air Blast Nozzle Test Matrix.

Pt	P3, psia	P3, kPa	T3, F	T3, K	T fuel, F	T fuel, K	Air dens, kg/m3	FAR comb	ALR nozzle	Liner W3, lb/s	Liner W3, kg/s	Wf, lb/hr	Pilot %
Atmospheric													
9	14.7	101.4	60	288.9	-40	233.3	1.22	0.01	23.3	0.30	0.14	10.82	100
10	14.7	101.4	60	288.9	-40	233.3	1.22	0.015	15.5	0.30	0.14	16.22	100
11	14.7	101.4	60	288.9	0	255.6	1.22	0.01	23.3	0.30	0.14	10.82	100
12	14.7	101.4	60	288.9	0	255.6	1.22	0.015	15.5	0.30	0.14	16.22	100
13	14.7	101.4	60	288.9	60	288.9	1.22	0.01	23.3	0.30	0.14	10.82	100
14	14.7	101.4	60	288.9	60	288.9	1.22	0.015	15.5	0.30	0.14	16.22	100
Superatmosphere													
15	14.7	101.4	60	288.9	60	288.9	1.22	0.006	38.8	0.30	0.14	6.49	100
18	50	344.8	60	288.9	60	288.9	4.16	0.006	38.8	1.02	0.46	22.07	50
24	100	689.5	60	288.9	60	288.9	8.32	0.006	38.8	2.04	0.93	44.15	20
30	200	1379.0	60	288.9	60	288.9	16.63	0.006	38.8	4.09	1.85	88.30	10
36	250	1723.8	60	288.9	60	288.9	20.79	0.006	38.8	5.11	2.32	110.37	10

Table 3.2. Continued.

Pt	Wf pilot lb/hr	DP pilot, psid	Wf main, lb/hr	DP main, psid	Dp/p, ratio	Air vel, m/s	Nozzle air flow, kg/s	Measurement Technique
Atmospheric								
9	10.82	52.00	0	0	0.02	57.59	0.032	Optical Patternator
10	16.22	116.99	0	0	0.02	57.59	0.032	Optical Patternator
11	10.82	52.00	0	0	0.02	57.59	0.032	Optical Patternator
12	16.22	116.99	0	0	0.02	57.59	0.032	Optical Patternator
13	10.82	52.00	0	0	0.02	57.59	0.032	Optical Patternator
14	16.22	116.99	0	0	0.02	57.59	0.032	Optical Patternator
Superatmosphere								
15	6.49	18.72	0.00	0.00	0.02	57.59	0.032	Sympatec HELOS
18	11.04	54.14	11.04	0.09	0.02	57.59	0.108	Sympatec HELOS
24	8.83	34.65	35.32	0.94	0.02	57.59	0.216	Sympatec HELOS
30	8.83	34.65	79.47	4.74	0.02	57.59	0.431	Sympatec HELOS
36	11.04	54.14	99.33	7.41	0.02	57.59	0.539	Sympatec HELOS

Table 3.3. Fuel Cart Instrumentation and Controls List.

Lab ID	Description	Fluid	Limits		Units	Manufacturer	Model (P/N)	Standard Deviation
			Low	High				
ZL1 - room 103 - Rules and Tools								
Analog Ins								
FM-FC-01	Flow Meter, Main Fuel line	Fuel	0	(100)	(lb/hr)	Micro Motion	-	(0.065)
FM-FC-02	Flow Meter, Pilot Fuel line	Fuel	0	(30)	(lb/hr)	Micro Motion	-	(0.065)
PT-FC-01	Pressure, Fuel line after dampening	Fuel	0	(2000)	MPa (psi)	GE	UNIK 5000	(3.08)
PT-FC-02	Pressure, Main Fuel line injector	Fuel/N2	0	(1000)	MPa (psi)	GE	UNIK 5000	(0.63)
PT-FC-03	Pressure, Pilot Fuel line injector	Fuel	0	(1000)	MPa (psi)	GE	UNIK 5000	(0.65)
PT-AirBox/P3	Pressure, airbox	N2	0	(30)	MPa (psi)	GE	UNIK 5000	(0.08)
TC-AirBox/P3	Temperature, airbox	N2	-200 (-328)	1250 (2282)	C (F)	OMEGA	Type K	(0.65)
TC-FC-01	Temperature, Fuel line	Fuel	-200 (-328)	1250 (2282)	C (F)	OMEGA	Type K	(1.88)
TC-FC-02	Temperature, Fuel line	Fuel	-200 (-328)	1250 (2282)	C (F)	OMEGA	Type K	(0.65)
TC-FC-03	Temperature, Fuel line after chilling	Fuel	-200 (-328)	1250 (2282)	C (F)	OMEGA	Type K	(0.65)
TC-FC-04	Temperature, Main Fuel line injector	Fuel/N2	-200 (-328)	1250 (2282)	C (F)	OMEGA	Type K	(0.34)
TC-FC-05	Temperature, Pilot Fuel line injector	Fuel	-200 (-328)	1250 (2282)	C (F)	OMEGA	Type K	(0.34)
TC-FC-06	Temperature, Heat exchanger fluid	Hxer Fluid	-200 (-328)	1250 (2282)	C (F)	OMEGA	Type K	(0.65)
TC-FC-07	Temperature, Heat exchanger fluid	Hxer Fluid	-200 (-328)	1250 (2282)	C (F)	OMEGA	Type K	(0.65)
CV-FC-01	Metering Valve, Main Fuel line	Fuel	0	100	% open	ETI Systems	-	-
CV-FC-02	Metering Valve, Pilot Fuel line	Fuel	0	100	% open	ETI Systems	-	-

Table 3.3. Continued.

Lab ID	Description	Fluid	Limits		Units	Manufacturer	Model (P/N)	Standard Deviation
			Low	High				
ZL1 - room 103 - Rules and Tools								
Analog Outs								
CV-FC-01	Metering Valve, Main Fuel line	Fuel	0	100	% open	ETI Systems	-	-
CV-FC-02	Metering Valve, Pilot Fuel line	Fuel	0	100	% open	ETI Syetems	-	-
Digital Ins								
PV-FC-01	Pneumatic Valve, Main Fuel Isolation	Fuel	-	-	open/closed	-	-	-
PV-FC-02	Pneumatic Valve, Pilot Fuel Isolation	Fuel	-	-	open/closed	-	-	-
Digital Outs								
PV-FC-01	Pneumatic Valve, Main Fuel Isolation	Fuel	-	-	open/closed	-	-	-
PV-FC-02	Pneumatic Valve, Pilot Fuel Isolation	Fuel	-	-	open/closed	-	-	-
CV-FC-01	Metering Valve, Main Fuel line	Fuel	0	100	% open	ETI Systems	-	-
CV-FC-02	Metering Valve, Pilot Fuel line	Fuel	0	100	% open	ETI Systems	-	-
Pump on/off	remote fuel pump power		-	-	open/closed	-	-	-

Table 3.4. High Pressure Laboratory Instrumentation and Controls List.

Lab ID	Description	Fluid	Limits		Units	Manufacturer	Model	Standard Deviation
			Low	High				
HPL - Rocket Cell - Rules and Tools								
Analog Ins								
PT-N2-01	Sweeping Flow Pressure	Fuel	0	(500)	MPa (psi)	GE	UNIK 5000	(2.83)
PT-N2-02	Air Box Pressure	Fuel	0	(1000)	MPa (psi)	GE	UNIK 5000	(1.24)
PT-INJ-01	Pressure, Fuel line after dampening	Fuel	0	(500)	MPa (psi)	GE	UNIK 5000	(2.63)
TC-N2-01	Temperature, Sweeping Flow		-200 (-328)	1250 (2282)	C (F)	OMEGA	Type K	(0.65)
TC-N2-02	Temperature, Air Box	Fuel	-200 (-328)	1250 (2282)	C (F)	OMEGA	Type K	(0.65)
TC-INJ-01	Temperature, Pressure Vessel	Fuel	-200 (-328)	1250 (2282)	C (F)	OMEGA	Type K	(0.65)
TC-INJ-02	Temperature, Pressure Vessel	Fuel	-200 (-328)	1250 (2282)	C (F)	OMEGA	Type K	(0.65)
Analog Outs								
CR-N2-02	Control Regulator, Sweeping Flow	N2	0	(6000)	MPa (psi)	Tescom	ER 3000	-
CR-FU-01	Control Regulator, Air Box	N2	0	(6000)	MPa (psi)	Tescom	ER3000	-
CV-BP-01	Back Pressure Control Valve		0	100	% open	ABZ	028	-
Digital Outs								
PV-N2-08	Pneumatic Valve, Main Fuel Isolation	Fuel	-	-	open/ closed	-	-	-
PV-N2-15	Pneumatic Valve, Pilot Fuel Isolation	Fuel	-	-	open/ closed	-	-	-

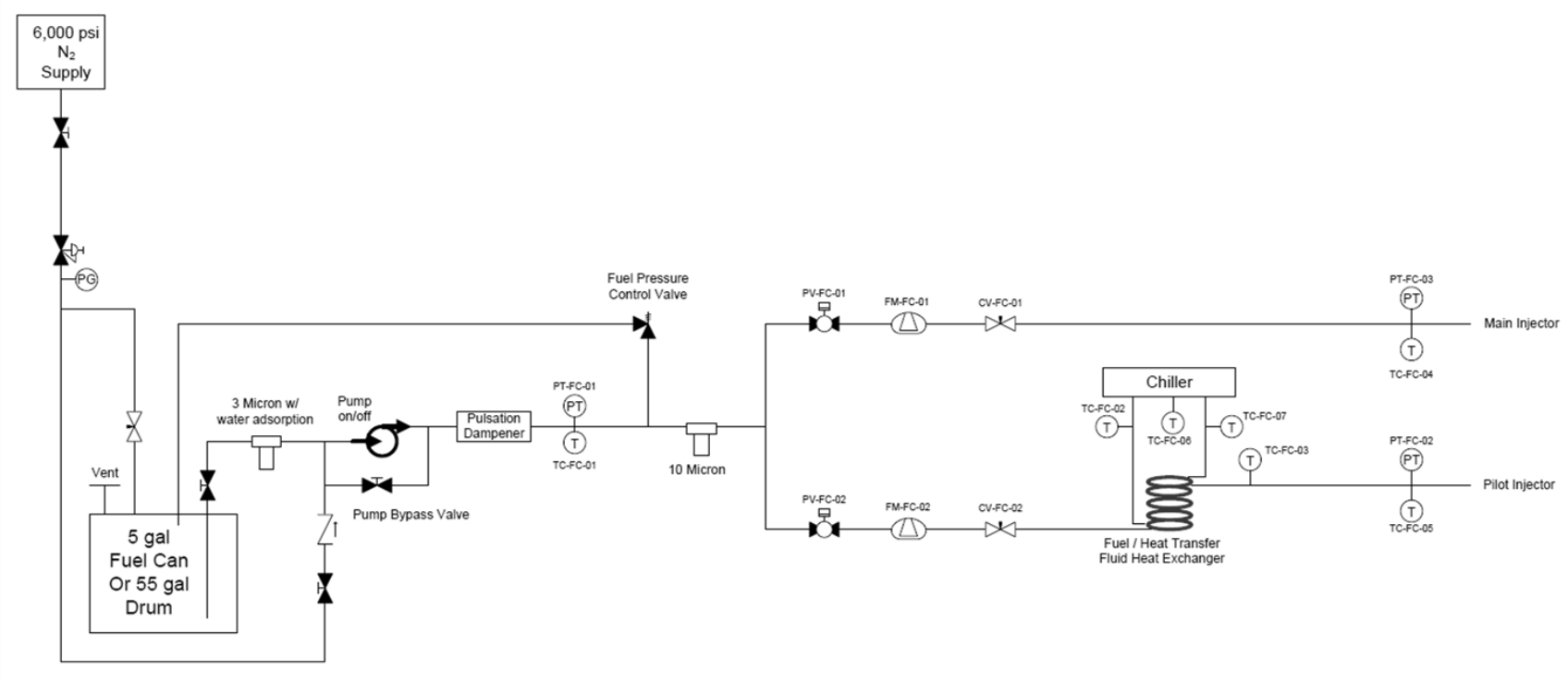

Figure 3.1. Fuel Cart Plumbing and Instrumentation Diagram.

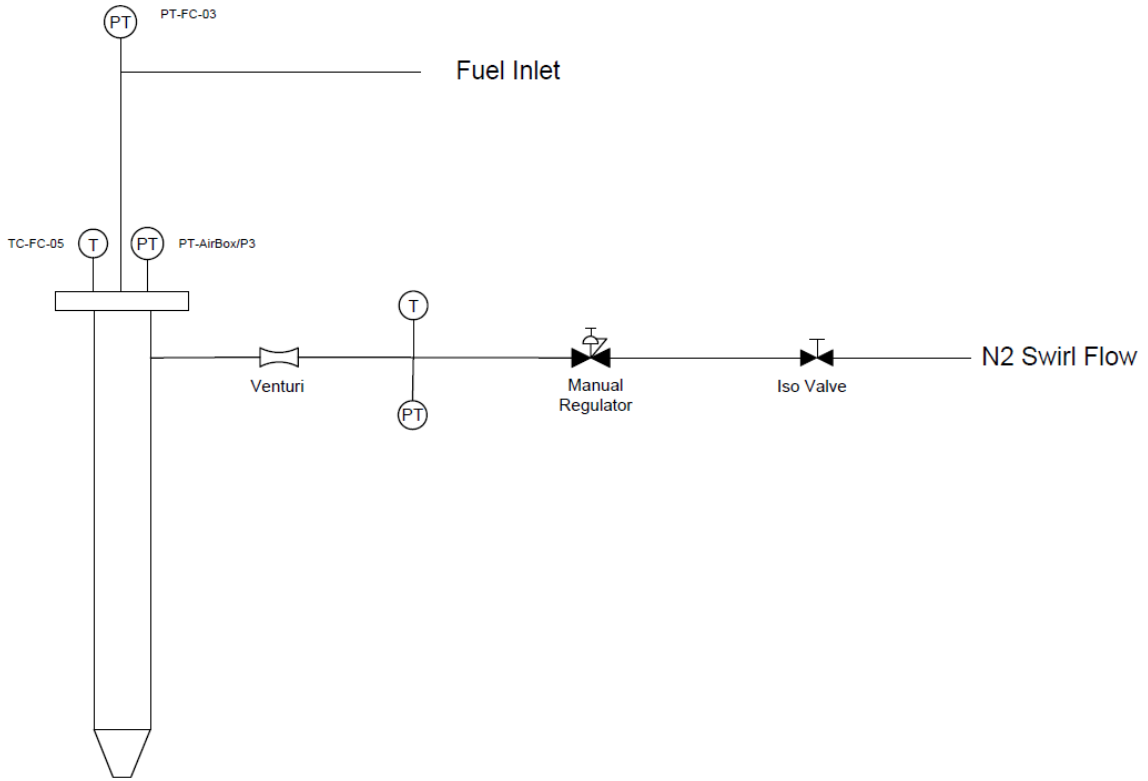

Figure 3.2. Atmospheric Air Box Plumbing and Instrumentation Diagram.

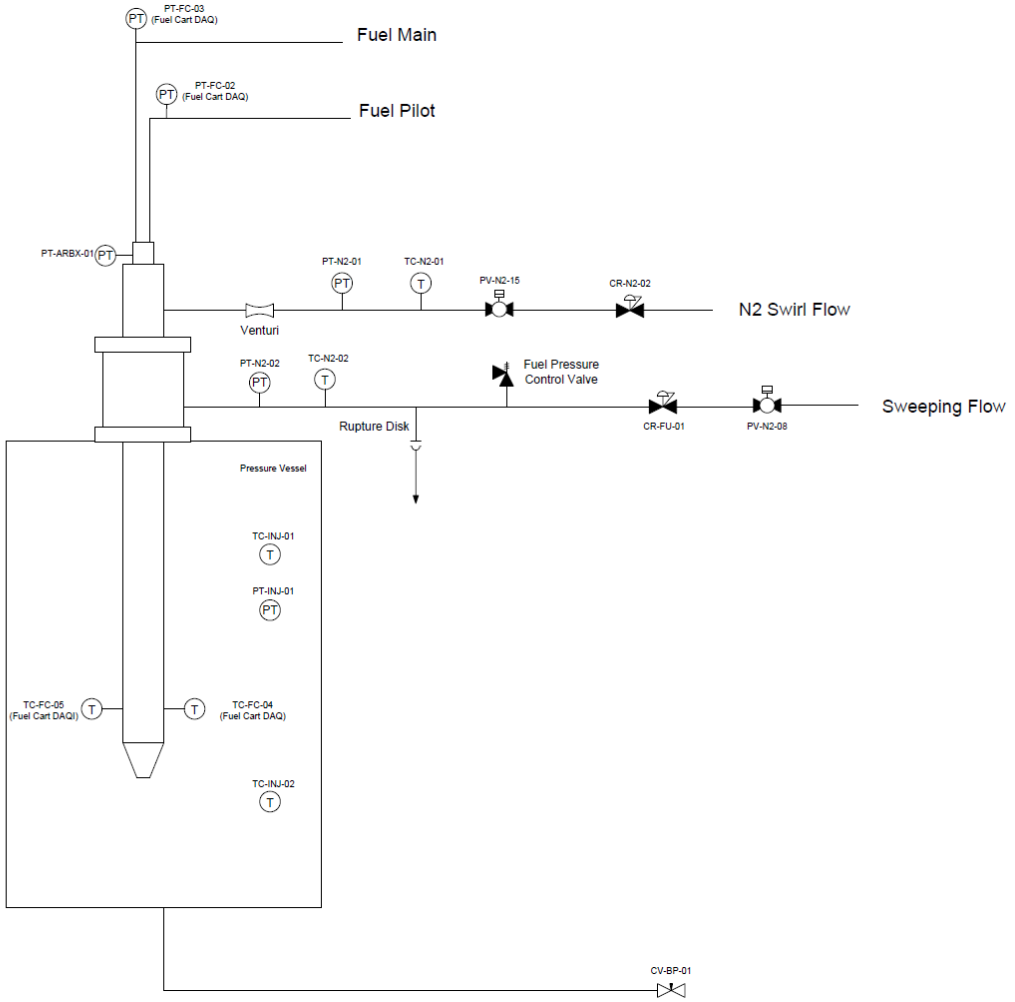

Figure 3.3. Super Atmospheric Fuel Injector Assembly Plumbing and Instrumentation Diagram.

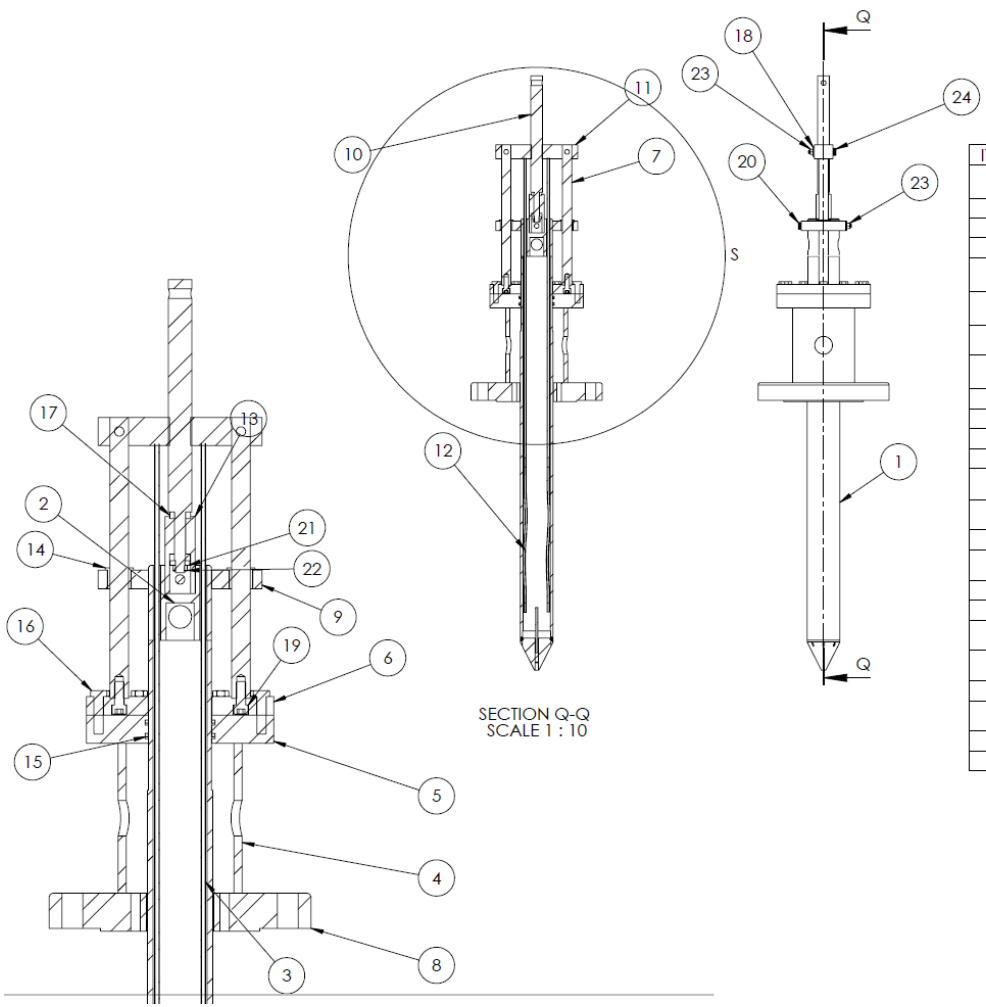

ITEM NO.	DESCRIPTION	QTY.
1	AIR BOX PIPE	1
2	AIR BOX INLET CAP	1
3	0.25IN FUEL LINES	2
4	MODIFIED 6IN DIAMETER PIPE	1
5	UPPER FLANGE WITH ORING SEAL	1
6	TOP FLANGE	1
7	MODIFIED TIGHT TOLERANCE ROD 8934K213	2
8	MODIFIED CLASS 600 6IN BLIND TEXAS FLANGE	1
9	BALL SCREW COLLAR	1
10	BALL SCREW 98804A040	1
11	TOP BRACKET	1
12	FLEXIBLE FUEL LINES	2
13	BALL SCREW HOLDER	1
14	BRONZE BUSHING SAE 841 (6338K437)	2
15	AS568A-2-340 SILICONE O-RING	2
16	SOCKET HEAD CAP SCREW 90128A846	12
17	SKF 81102 TN	2
18	WASHER 93852A104	3
19	SOCKET HEAD CAP SCREW 90128A842	2
20	91259A731 SHOULDER SCREW	1
21	CUSTOM WASHER	1
22	94945A225 NUT	1
23	90099A031 NUT	3
24	91259A720 SHOULDER SCREW	2

Figure 3.4. Fuel Injector Assembly with Pressure Vessel.

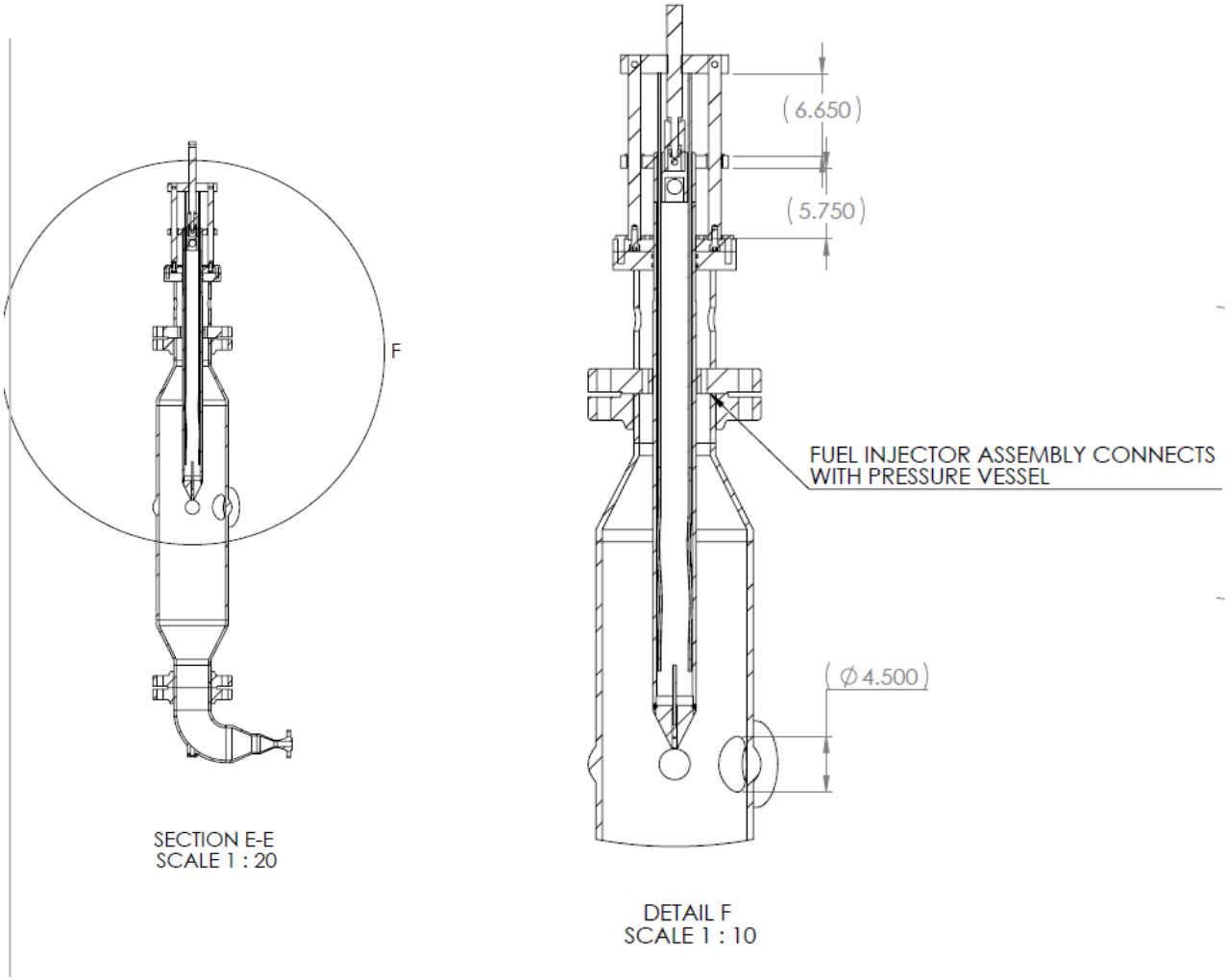

Figure 3.5. Pressure Vessel and Fuel Injector Assembly.

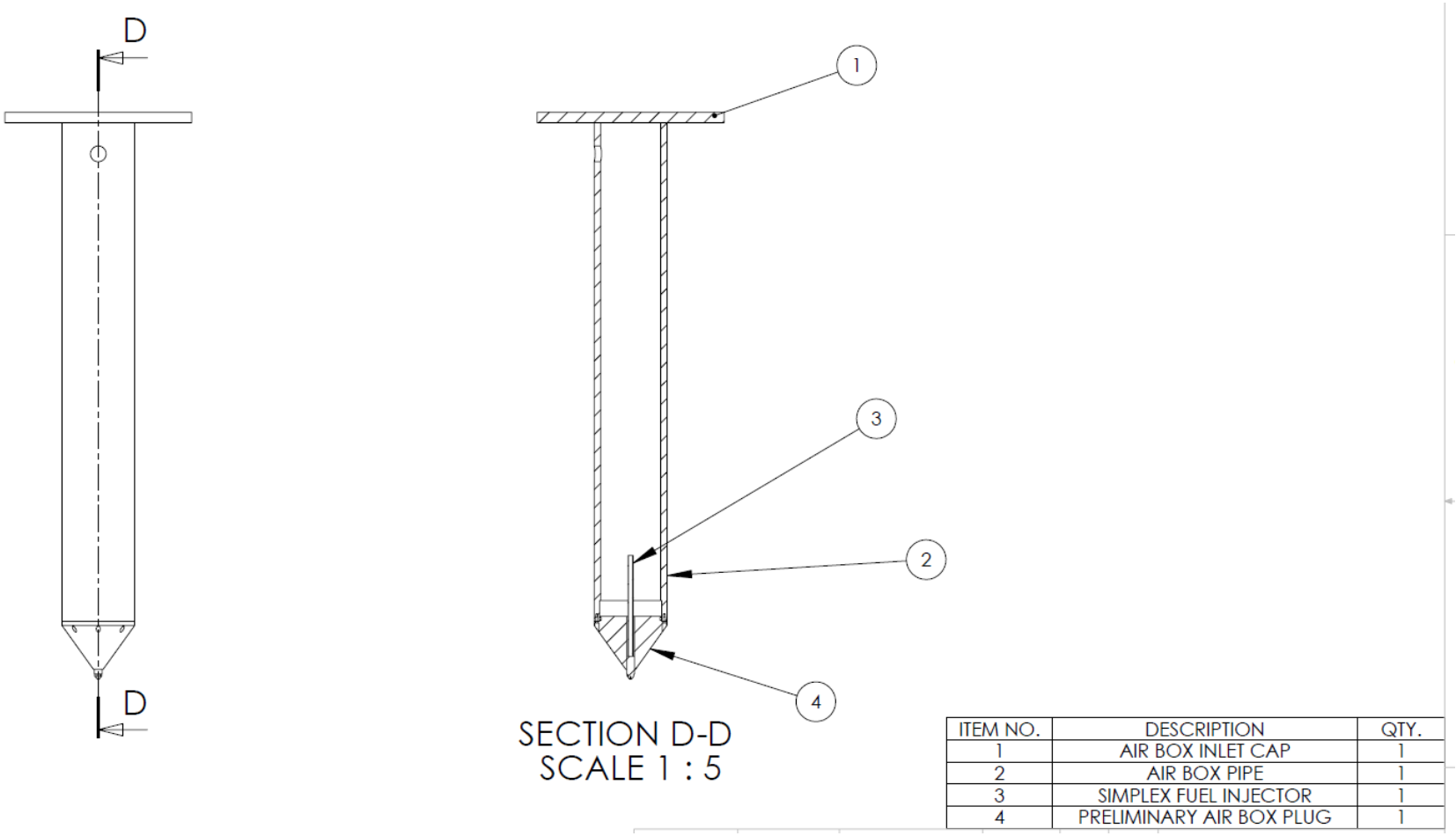

Figure 3.6. Atmospheric Air Box Assembly.

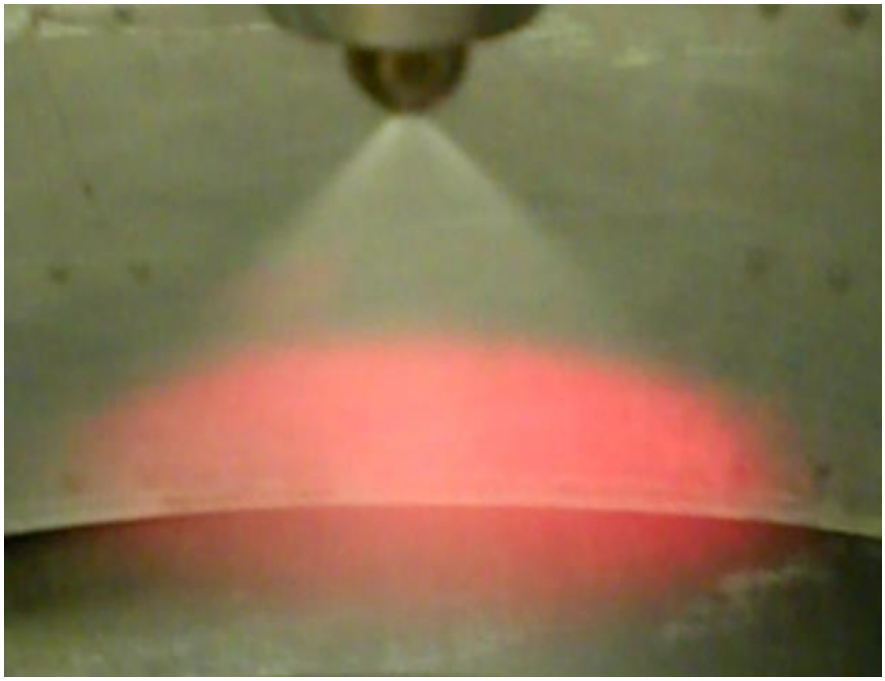

Figure 3.7. Spray Visualization of Optical Patternator Pressure Swirl Nozzle, JP-8, -40 C Fuel Injection Temperature.

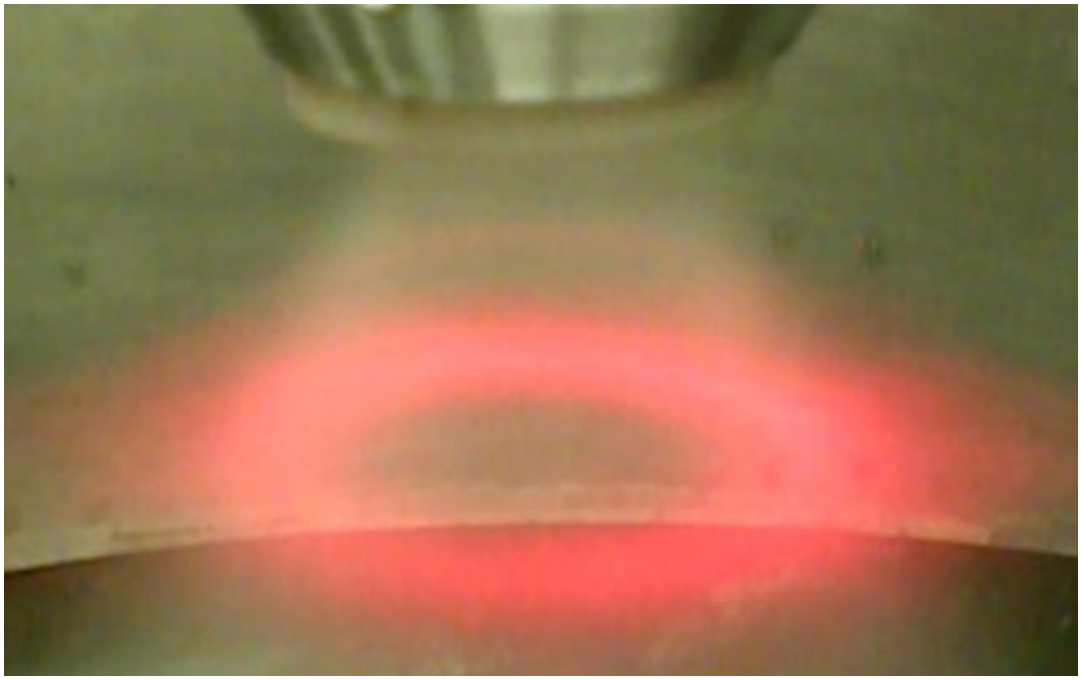

Figure 3.8. Spray Visualization of Hybrid Air Blast Nozzle.

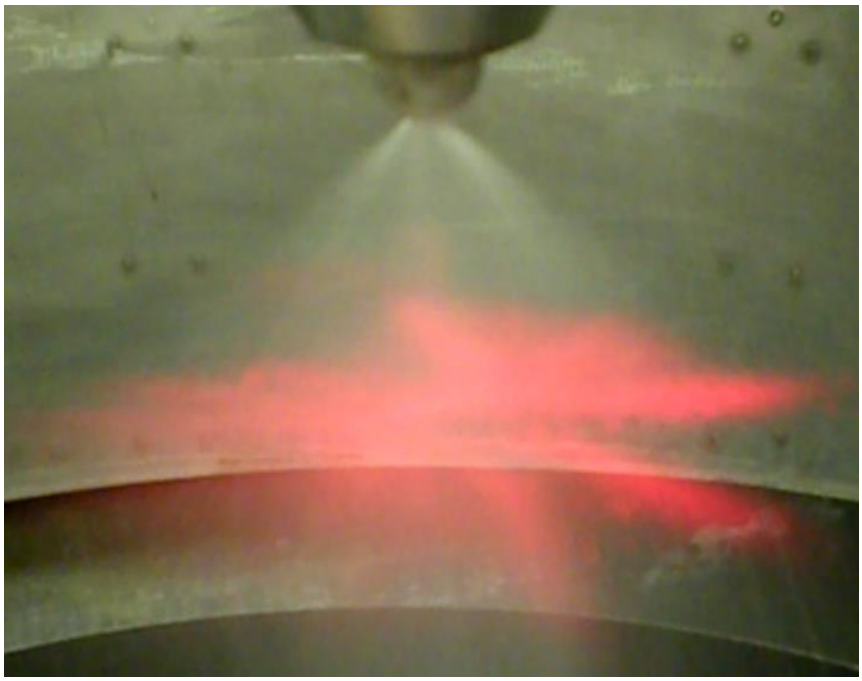

Figure 3.9. Spray Visualization of Optical Patternator Pressure Swirl Injector, JP-8, -40 C Fuel Injection Temperature.

Figure 3.10. Spray Visualization of Super Atmospheric Testing Pressure Swirl Injector, JP-8, 0.172 MPa (25 psi) Ambient Pressure.

Figure 3.11. Spray Visualization of Super Atmospheric Testing Pressure Swirl Injector, JP-8, 1.723 MPa (250 psi) Ambient Pressure.

CHAPTER 4. EXPERIMENTAL RESULTS AND DISCUSSION

4.1 Atmospheric Testing Overview

Atmospheric testing was conducted from 24 June 2013 to 30 July 2013 in ZL1, room 103, Maurice Zucrow Laboratories, Purdue University. Four different aviation jet fuels were tested: JP-8, Jet A, JP-5, and JP-10. Two nozzles were tested: a pressure swirl nozzle, and a hybrid air blast nozzle. Each nozzle was tested at two different fuel injection pressure conditions. The fuel injection temperature set conditions for atmospheric testing are 15.6, -17.8, and -40 C (60, 0, and -40 F). Three to five En'Urga OP-600 Optical Patternator scans were collected per set condition. Fuel cart data acquisition recorded system measurements including fuel injection pressure, fuel flow rate, and fuel injection temperature.

The optical patternator measurements were compared against different set conditions and types of jet fuel to determine trends in fuel injector performance. Patternator measurements that were collected include total surface area, patternation number, spray cone angle, and radial profiles. The results are compared to results and trends in the literature in the following sections.

4.2 Pressure Swirl Nozzle Patternator Results

Full pressure swirl nozzle patternator scan measurements are summarized in Figure 4.1 thru Figure 4.12. Atmospheric test matrix set conditions are summarized in Table 3.1. Corresponding uncertainty in the fuel cart set conditions are summarized in Table 3.3.

4.2.1 Total Surface Area Measurements

Total surface area measurements for the patternator sum the surface area of drops that are in the measurement plane at a time during the measurement. The total surface area describes the quality of atomization because greater total surface area indicates that there are many more drops or many smaller drops in the spray. Figure 4.1 and Figure 4.2 show measured surface area versus injection temperature for the four different jet fuels tested at the 0.345 MPa (50 psi) and the 0.689 MPa (100 psi) injection pressure case. Three to five measurements at each of the set conditions were averaged and plotted with error bars for one standard deviation.

The patternator total surface area plot for the 0.689 MPa (100 psi) injection pressure case in Figure 4.2 shows areas of higher concentration of droplets with greater total surface area measurements than the plots for the 0.345 MPa (50 psi) injection pressure cases in Figure 4.1. This is consistent with the expectation that the fuel flow rate is greater in nozzle at 0.689 MPa (100 psi) injection pressure and that there is increased atomization. Wang *et al*. (1988) also describes that increased injection pressure leads to improved atomization quality of sprays.

Each fuel type in Figure 4.1 and Figure 4.2 shows a trend of decreasing total surface area with decreasing temperature. This is consistent with Wang *et al*. (1988) who describes atomization quality to decrease with temperature. However, the differences in total surface measurements between fuel types increases with decreasing temperature. This may be attributed to fuel viscosity being a nonlinear function of temperature as discussed in Park *et al*. (2004).

The total surface area measurements depend on the type of jet fuel. The difference in total surface area measurements between types of jet fuel tends to increase as the temperature decreases. JP-8 has the greatest total surface area at any of the temperatures. Jet A has a slightly smaller total surface area measurement. JP-5 has a smaller surface area measurement at a given temperature. JP-10 has the smallest total surface area for a given temperature measurement. For the 0.345 MPa (50 psi) injection pressure case, the total surface area for JP-8 decreased 38%, Jet A decreased 45%, JP-5 decreased 54%, and JP-10 decreased 89% from injection temperature decreasing from 15.6 to -40 C (60 to -40 F). For the 0.689 MPa (100 psi) injection pressure case, the total surface area for JP-8 decreased 25%, Jet A decreased 46%, JP-5 decreased 38%, and JP-10 decreased 88% from injection temperature decreasing from 15.6 to -40 C (60 to -40 F). The differences between injector performances with fuel types may be attributed to fuel viscosity, similar to Goldsworthy *et al.* (2011).

4.2.2 Patternation Number

Patternation Number represents how symmetrical the spray is relative to the centerline of the fuel injector. The patternation number is obtained by integrating the local drop surface area per volume as shown in Lim *et al.* (2003). A spray with low patternation number is more symmetrical than a spray with high patternation number. Figure 4.3 and Figure 4.4 show each fuel type sprayed at 15.6, -17.8, -40 C (-40, 0 and, 60 F) injection temperature. The fuel injection pressure for Figure 4.3 is 0.345 MPa (50 psi) and the fuel injection pressure for Figure 4.4 is 0.689 MPa (100 psi).

In Figure 4.3 and Figure 4.4, the patternation number is shown to increase with decreasing injection temperature. At 15.6 C (60 F), the spray is symmetrical with areas of high concentration in the middle and lower concentration on the outsides. The symmetry of the spray tends to decrease with decreasing temperature; therefore, the patternation number increases. Consistent with the results, at -17.8 C (0 F), local drop concentrations were observed to be smaller with pockets of high drop concentration moving away from the center of the spray. At -40 C (-40 F), the area that the spray covers is diminished with local areas of asymmetrical, high drop concentration. Park *et al.* (2004), attributed similar behavior in their experiment to icing of the fuel injector, but steps in the testing procedure for the current study (Appendix) were taken to de-ice the injector before patternator measurements were made.

The effect of temperature on the patternation number depends on fuel type. Plots for JP-8, Jet A, JP-5, JP-10 are included in Figure 4.3 and 4.4. At 15.6 C (60 F) the patternator

plots for the different fuel types look similar in distribution of local concentration. However, the differences between fuel types become more apparent at colder temperatures. The patternation number for JP-8 and Jet A at -17.8 and -40 C (0 and -40 F) increases very little compared to the JP-5 and JP-10 fuel types. The JP-5 patternation number is significantly affected at a fuel temperature of -40 C (-40 F) for the 0.345 MPa (50 psi) fuel injection pressure case. The patternation number for JP-10 at -40 C (-40 F) increases significantly and represents a highly asymmetrical spray. Goldsworthy *et al.* (2011) shows that atomization quality depends on the viscosity of the liquid sprayed. This is consistent with the results because JP-8 and Jet A are the least viscous and JP-5 is more viscous and JP-10 is the most viscous.

4.2.3 Spray Cone Angle

The patternator spray cone angle measurement uses the known 38.1 mm (1.5 inch) distance from the tip of the injector and the spray concentration plot to calculate a spray cone angle. The spray cone angle calculated by the patternator is defined as the angle subtended by the spray that contains a fixed percentage of the planar surface area density. (Sivathanu *et al.* 2006) The value used for this study is 98% of the planar surface density. This value is comparable to visual results of sprays that are symmetrical. For sprays that are asymmetrical, the calculation for the spray cone angle can be greatly affected and provide a solution that is not physical.

Figure 4.5 and Figure 4.6 shows the spray cone angle measurement as a function of temperature for the different jet fuels. For JP-8, Jet A and JP-5 fuel types, the spray cone

angle at a given temperature is nearly constant and differences between spray angle are only slightly outside of the standard deviation of the measurement. The results are consistent with Goldsworthy *et al.* (2011) research that present the spray cone angle as a weak function of liquid properties.

The spray cone angle calculation for JP-10 at -40 C (-40 F) fuel injection temperature is not a physical solution because the spray was highly asymmetrical. For JP-10 at -40 C (-40 F) injection temperature, the injector was observed to spray in jets of high concentration that were slightly off center of the spray at the particular set conditions.

4.2.4 Radial Profile

The radial profiles are measurements of drop surface area divided by drop volume. The radial profile is plotted versus distance from calculated the center of the spray. For the pressure swirl atomizer nozzle, the radial profiles describe a high concentration of droplets at the center of the spray. The concentration of droplets decreases as the distance from the center of the spray increases.

Figure 4.7 and Figure 4.8 shows the radial profile of each fuel type at 15.6 C (60 F) injection temperature, and 0.345 MPa (50 psi) and 0.689 MPa (100 psi) injection pressure. The shapes of the plots for each of the fuel types look similar to one another at 15.6 C (60 F). However, the magnitude of the spray area divided by volume is different for different fuel types and depends of viscosity of the fuel. Greater localized spray area divided by volume means that there is more local concentration of small droplets. The

0.689 MPa (100 psi) injection pressure case in Figure 4.8 shows greater spray area/volume than the 0.345 MPa (50 psi) injection pressure case in Figure 4.7. The difference in spray area divided by volume is consistent with the observation of decreasing drop size with increasing injection pressure in Wang *et al.* (1988).

The radial profiles of each fuel type at -17.8 and -40 C (0 and -40 F) in Figure 4.9, 4.10, 4.11, and 4.12 show similar trends to the 15.5 C (60 F) fuel injection temperature cases. The 0.689 MPa (100 psi) injection pressure cases continue to have greater spray area divided by volume compared to the 0.345 MPa (50 psi) injection pressure. The influence of fuel type at the -17.8 and -40 C (0 and -40 F) fuel injection temperature cases is shown to behave similarly to the 15.6 C (60 F) cases. JP-8 continues to have the greatest spray area divided by volume and JP-10 has the smallest spray area divided by volume.

The radial profiles can also be used to show how the local spray surface area to volume changes with decreasing temperature for a specific fuel. JP-8 radial profiles from Figure 4.7 thru Figure 4.12 show the radial spray area to volume distribution becoming more concentrated towards the center of the spray with decreasing temperature. The magnitude of the spray area divided by volume tends to decrease with decreasing temperature. There are similar surface area to volume trends for Jet A, JP-5, and JP 10 fuel types with decreasing temperature at 0.345 MPa (50 psi) and 0.689 MPa (100 psi) fuel injection cases. Less viscous fuels like JP-8 or Jet A have smaller changes to their radial profile with decreasing temperature. More viscous fuels like the JP-5 and JP-10

have radial profiles that collapse and become asymmetrical at colder temperature similar to Park *et al*. (2004).

There is uncertainty in radial profiles for asymmetric sprays. Off axis areas of high concentration can skew the radial profile in a way that makes it look like what would be expected for a hollow cone spray. Figure 4.11, the plot of the radial profiles for fuel type at -40 C (-40 F) injection temperature and 0.345 MPa (50 psi) injection pressure is an example of this with a local spray area/volume maximum that is off center of the spray.

4.3 Hybrid Air Blast Nozzle Patternator Results

Full hybrid air blast patternator scan measurements are summarized in Figure 4.13 thru Figure 4.24. The test matrix for the hybrid air blast nozzle is shown in Table 3.1. The fuel cart uncertainty is summarized in Table 3.3

4.3.1 Total Surface Area Measurements

Total surface area measurements for the patternator sum the surface area of drops that are in the measurement plane at a time during the measurement. The total surface area measurements are plotted against temperature in order to demonstrate fuel injection temperature and pressure dependence on different types of jet fuels. Figure 4.13 and Figure 4.14 are plots of the total surface area measurement for different jet fuels versus temperature. The plot scale shows that the difference between total surface area measurements for a particular jet fuel is greater in the hybrid air blast nozzle compared to the pressure swirl nozzle. The primary reason for the increase in surface area is the

increased aerodynamic forces on the fuel droplets from the nitrogen flowing through the swirler.

The total surface area measurements depend on fuel injection pressure and temperature. Figure 4.14 shows that the total surface area for 0.806 MPa (117 psi) fuel injection pressure condition is greater than the total surface area in Figure 4.13 for the 0.358 MPa (52 psi) fuel injection pressure condition. In addition, the total surface area is shown to decrease with temperature. The decrease in total surface area with decreasing temperature is consistent with the results from the pressure swirl nozzle in addition to the paper in Park *et al.* (2004).

Total surface area measurements vary from fuel to fuel at a particular set condition as shown in Figure 4.13 and Figure 4.14. JP-8 shows very small change in total surface area with decreasing temperature. The total surface area for Jet A decreases more with temperature than the JP-8. The total surface area for the JP-5 decreases more than the JP-8 or Jet A. The JP-10 total surface area decreases the most with temperature. For the 0.358 MPa (52 psi) injection pressure case, the total surface area for JP-8 decreased 2%, Jet A decreased 52%, JP-5 decreased 59%, and JP-10 decreased 91% from injection temperature decreasing from 15.6 to -28.8 C (60 to -20 F). For the 0.806 MPa (117 psi) injection pressure case, the total surface area for JP-8 increased 10%, Jet A decreased 8%, JP-5 decreased 34%, and JP-10 decreased 72% from injection temperature decreasing from 15.6 to -28.8 C (60 to -20 F). These results are consistent with the results from the pressure swirl nozzle.

Similar to the pressure swirl nozzle, the different viscosities of the fuels contribute to the differences in spray performance. The JP-8 is the least viscous and the spray characteristics are least affected by changes in temperature. JP-10 is the most viscous and the spray characteristics are greatly affected by changes in temperature similarly to Goldsworthy *et al.* (2011).

4.3.2 Patternation Number

Patternation Number represents how symmetrical the spray is relative to the centerline of the fuel injector. A spray with low patternation number is more symmetrical than a spray with high patternation number. Figure 4.15 and Figure 4.16 show patternation number versus temperature for each fuel type sprayed at -28.8, -17.8, 15.6 C (-20, 0 and, 60 F) injection temperature. The fuel injection pressure for Figure 4.15 is 0.358 MPa (52 psi) and the fuel injection pressure for Figure 4.16 is 0.806 MPa (117 psi).

Patternation number increases with decreasing temperature. This implies that the local concentrations in the spray are more asymmetrical with decreasing temperature. The effect of temperature on patternation number is increased compared to the patternation number for the pressure swirl nozzle. One explanation for the increased patternation number is that the nitrogen flow through the swirler generates areas of off axis high concentration in the spray. This is consistent with the discussion of the radial profiles in Section 4.3.4.

The patternation number depends on the fuel type. In Figures 4.15 and 4.16, the patternation number for the JP-8 fuel type does not depend on temperature. In contrast, the Jet A, JP-5 and, Jet-10 patternation numbers increase with temperature. This implies that fuels with greater viscosity tend to generate asymmetrical areas of high concentration in the spray. This is consistent with trends of decreasing drop size with increasing viscosity shown in Park *et al.* (2004).

4.3.3 Spray Cone Angle

The patternator computes the full spray cone angle from the concentration plot and the distance of the injector from the measurement plane. The full spray cone angle versus temperature is shown for the various jet fuels in Figures 4.17 and 4.18. The spray cone angle increases very slightly with decreasing temperature. When compared to the pressure swirl nozzle, the additional stability of the spray cone angle can be attributed to the nitrogen swirler on the hybrid air blast nozzle. The nitrogen is the driving medium that controls the distribution pattern of the droplets.

The spray cone angle is a weak function of fuel type. Figures 4.17 and 4.18 do not show a clear dependence of spray cone angle on fuel type. This conclusion is consistent with Goldsworthy *et al.* (2011) who did not find significant changes to spray cone angle. In the case of a hybrid air blast nozzle, the aerodynamic forces of the nitrogen flow dominate the fluid property forces for determining the spray cone angle. This is consistent with the increased total surface area measurements in the hybrid air blast nozzle when compared to the pressure swirl nozzle.

4.3.4 Radial Profile

The radial profiles are spray surface area divided by volume measurements. The radial profile is plotted versus distance from the calculated center of the spray. Figure 4.19 and 4.20 shows radial profiles for four fuel types at 15.6 C (60 F). The plots are similar in shape with different scaling of amplitude based on atomization quality. Each plot shows an off center maximum of spray area divided by volume. This describes a hollow cone type spray with a greater concentration of drops spraying outward radially than down the centerline of the nozzle.

Fuel type has varying influence on the radial profile at the -17.8 and -28.8 C (0 and -20 F) injection temperature cases. Figures 4.21, 4.22, 4.23, 4.24 plot the radial profile of the four fuel types at specific temperatures and at 0.358 MPa (52 psi) or 0.806 MPa (117 psi) injection pressure. The shapes of the plots tend to be consistent with one another, but the dependence of fuel type is not as apparent as with the pressure swirl nozzle. The dominating aerodynamic forces reduce the differences in spray performance between types of jet fuel.

The dependence of the radial profile for the JP-8 and other fuel types versus changing temperature is illustrated by comparing Figures 4.19 thru 4.24. The shape of the radial profile for JP-8 is not a strong function of temperature. However, the magnitude of the spray area divided by volume for the JP-8 fuel does change depending on fuel injection pressure. The other, more viscous, fuel types have radial profiles that depend on fuel temperature. The magnitude of the Jet A, JP-5, and JP-10 radial profiles is shown to

decrease with decreasing injection temperature and decreasing injection pressure. In addition, the maximum value of the radial profile is shown to move toward the center of the spray with decreasing temperature. This is consistent with observations of the pressure swirl nozzle in Park *et al.* (2004).

4.4 Super Atmospheric Testing Overview

Super atmospheric testing was conducted from 1 August 2013 to 20 October 2013 at the High Pressure Laboratory, Maurice Zucrow Laboratories, Purdue University. The test matrix used for super atmospheric testing was proposed by the Rules and Tools Atomization Committee. Sympatec laser diffraction measurements was the experimental data that was collected for the Super Atmospheric testing. Set conditions for the nitrogen system conditions were monitored with the facility data acquisition. Fuel cart data acquisition was used to record fuel injector set conditions. In the following sections, the results for the Sympatec data are compared to the fuel injector set conditions and specific fuel properties. The results are compared to work done in the literature.

4.5 Pressure Swirl Nozzle Sympatec Results

JP-8 and JP-10 fuel types were tested at 15.6 C (60 F) fuel injection temperature with increasing ambient pressure up to 1.723 MPa (250 psi). Four different aviation jet fuels were tested: JP-8, Jet A, JP-5, JP-10 using the pressure swirl nozzle at 0.206 MPa (30 psi) ambient pressure conditions and at 15.6 and -17.8 C (60 and 0 F) fuel injection temperature. A complete table of set condition and Sympatec measurements can be found in Figure 4.25 thru Figure 4.40.

4.5.1 Distribution Range of Drop Sizes for Increasing Ambient Pressure

The Sympatec particle sizing device generated characteristic diameter data from the probability density function measurements (PDF). Characteristic diameter data are statistical representations of different aspects of the PDF. X_{10} is the diameter of the 10 percentile drop in the PDF plot. X_{10} describes the smaller droplets in the spray. X_{50} describes the drops on the 50 percentile in the spray. X_{90} describes the 90 percentile drops in the PDF plot. The X_{90} compared to the X_{10} gives a good description of the span of drop sizes in a spray.

JP-8 and JP-10 were sprayed at 0.345 and 0.689 MPa (50 and 100 psi) fuel injection pressure with increasing ambient pressure conditions from 0.172 to 1.723 MPa (25 to 250 psia). The plots for these fuel types show similar trends. Figure 4.25 and Figure 4.26 are plots of X_{10}, X_{50} and X_{90} diameters for the JP-8 fuel at 0.345 and 0.689 MPa (50 and 100 psi) injection conditions. Figure 4.27 and Figure 4.28 are plots of X_{10}, X_{50} and X_{90} diameters for the JP-10 fuel at 0.345 and 0.689 MPa (50 and 100 psi) injection conditions. In all cases, the X_{10} diameter is shown to be a weak function of ambient pressure. For example, the X_{10} showed a 17% increase for the JP-8 fuel and a 12% increase in the JP-10 fuel for 0.345 MPa (50 psi) injection pressure and ambient pressure increasing from 0.172 to 1.723 MPa (25 to 250 psi). By comparison, the X_{50} and X_{90} diameters show increasing diameter with increasing ambient pressure. For example, the X_{50} showed a 48% increase for the JP-8 fuel and a 10% increase in the JP-10 fuel for 0.345 MPa (50 psi) injection pressure and ambient pressure increasing from 0.172 to 1.723 MPa (25 to 250 psi). The X_{90} showed a 32% increase for the JP-8 fuel and a 10%

increase in the JP-10 fuel for 0.345 MPa (50 psi) injection pressure and ambient pressure increasing from 0.172 to 1.723 MPa (25 to 250 psi). These trends imply, especially for the JP-8 fuel type, that larger drop sizes tend to show more increase in diameter with increasing ambient pressure. The result is that the range of drop sizes tends to show slight increase with increasing ambient pressure. These results are supported by observations of drop coalescence with increasing pressure discussed in De Corso *et al.* (1960) and Guildenbecher *et al.* (2008).

The X_{10}, X_{50}, and X_{90} plots for JP-8 and JP-10 show trends in fuel injection pressure. Comparing the 0.345 MPa (50 psi) injection pressure cases in Figure 4.25 and 4.27 to the 0.689 MPa (100 psi) injection pressure cases in Figure 4.26 and 4.28, the drop size decreases with increasing injection pressure for the JP-8 and JP-10 fuel types. This is consistent with the patternator results for total surface area because higher total surface area implies improved atomization and smaller drop size distribution. Results in the literature also support this in Wang *et al.* (1988).

4.5.2 Sauter Mean Diameter for Increasing Ambient Pressure

Sauter mean diameter is a characteristic diameter that is calculated from the probability density function generated by the Sympatec device. The Sauter mean diameter compares a mean droplet volume to a mean droplet surface area. The result is a characteristic diameter that is commonly used in industry because it can be applied in governing equations that drive simulation efforts.

The Sauter mean diameter of drops in the spray for all fuel types depends on ambient pressure and fuel injection pressure. Figure 4.29 and Figure 4.30 shows the plot for D_{32} versus ambient pressure at 0.345 MPa (50 psi) injection pressure and 0.689 MPa (100 psi) injection pressure. The D_{32} is shown to increase slightly with increasing ambient pressure. For example, the change in D_{32} over the range of ambient pressures showed a 32% increase for the JP-8 fuel and a 10% increase in the JP-10 fuel for 0.345 MPa (50 psi) injection pressure and ambient pressure increasing from 0.172 to 1.723 MPa (25 to 250 psi). In addition, the 0.689 MPa (100 psi) injection pressure cases tend to have slightly smaller D_{32} than the 0.345 MPa (50 psi) pressure cases for the same set conditions. These results are consistent with the results for the X_{10}, X_{50}, and X_{90} diameters.

The D_{32} has a weak dependence on the fuel type. Figure 4.29 and Figure 4.30 show that for a given set condition, the D_{32} for the JP-10 fuel type is slightly greater than that for the JP-8. The difference between D_{32} with various fuel types at the same set condition can be explained by comparing the viscosity of the fuel types. The results of a more viscous fuel yielding a higher D_{32} is consistent the previous patternator results. Li *et al.* (2013) also describes the D_{32} to be a weak function of fuel viscosity at small axial distances.

4.5.3 Distribution Range of Drop Sizes for Chilled Fuel Conditions

Drop size distributions were measured for four different aviation jet fuels at 0.172 MPa (25 psi) ambient pressure conditions and at 15.6 and -17.8 C (60 and 0 F) fuel injection temperature. JP-8, Jet A, JP-5 and JP-10 fuel types were tested at 0.345 and 0.689 MPa (50 and 100 psi) injection conditions. The results for the X_{10}, X_{50}, and X_{90} diameters are discussed below.

The drop size distribution depends on the injection temperature. Figure 4.31, 4.32, 4.33, 4.34, 4.35, 4.36, 4.37, 4.38 shows X_{10}, X_{50} and X_{90} drop size diameters as a function of fuel injection temperature. The X_{10} drop size diameter changes the least from 15.6 to -17.8 C (60 to 0 F) fuel injection temperature. The X_{50} and X_{90} drop diameters show significant increases in drop size diameter with decreasing temperature. The results imply that the drop size distribution for all fuel types increase with decreasing temperature. When compared to the effect of ambient pressure on drop size distribution, it can be shown that drop size distribution is a stronger function of injection temperature. This is supported by Park *et al.* (2004) who described drop size to be a strong function of fuel viscosity at cold temperature.

The drop size distribution depends on fuel injection pressure. Figure 4.31, 4.33, 4.35, 4.37 represent the 0.345 MPa (50 psi) injection cases. Figure 4.32, 4.34, 4.36, 4.38 represent the 0.689 MPa (100 psi) injection cases. The X_{10}, X_{50} and X_{90} diameters are smaller for the 0.689 MPa (100 psi) injection cases compared to the 0.345 MPa (50 psi) injection case. This is consistent with the results for changes in injection pressure with

changing ambient pressure. In addition these results agree with the previously discussed results and Wang *et al.* (1988).

The drop size distribution depends on fuel type. The trend shows JP-10 with the largest drop sizes for a given set condition, followed by JP-5, Jet A and JP-8 with decreasing drop size. At colder fuel injection temperature, the differences in the drop size distributions become larger. The X_{10} showed a 12% increase for the JP-8 fuel, a 15% increase for the Jet A fuel, a 20% increase for the JP-5 fuel and a 21% increase in the JP-10 fuel for 0.345 MPa (50 psi) injection pressure and fuel injection temperature decreasing from 15.6 to -17.8 C (60 to 0 F). The X_{50} showed a 12% increase for the JP-8 fuel, a 20% increase for the Jet A fuel, a 17% increase for the JP-5 fuel and a 50% increase in the JP-10 fuel for 0.345 MPa (50 psi) injection pressure and fuel injection temperature decreasing from 15.6 to -17.8 C (60 to 0 F). The X_{90} showed a 29% increase for the JP-8 fuel, a 48% increase for the Jet A fuel, a 40% increase for the JP-5 fuel and a 58% increase in the JP-10 fuel for 0.345 MPa (50 psi) injection pressure and fuel injection temperature decreasing from 15.6 to -17.8 C (60 to 0 F). This is consistent with the effect of fuel injection temperature on the total surface area of the spray. The viscosity of the fuel type depends on temperature with more viscous fuels atomizing with larger droplet sizes.

4.5.4 Sauter Mean Diameter for Chilled Fuel Conditions

The Sauter mean diameter was also calculated from the drop size distributions for the four fuel types at 15.6 and -17.8 C (60 and 0 F) fuel injection temperatures. The plot of

D_{32} versus fuel injection temperature for the four fuel types is shown in Figure 4.39 and 4.40. The general trend for the graphs is increasing D_{32} with decreasing temperature. This is consistent with the results for the drop size distributions discussed previously.

The Sauter mean diameter was shown to increase with all fuel types. The results for the JP-8, Jet A, JP-5, and JP-10 are similar. The D_{32} showed a 20% increase for the JP-8 fuel, a 11% increase for the Jet A fuel, a 46% increase for the JP-5 fuel and a 30% increase in the JP-10 fuel for 0.345 MPa (50 psi) injection pressure and fuel injection temperature decreasing from 15.6 to -17.8 C (60 to 0 F).

4.6 Hybrid Air Blast Nozzle Sympatec Results

Two different aviation jet fuels were tested: JP-8, and JP-10 using the hybrid air blast nozzle. The hybrid air blast nozzle was tested at constant fuel air ratio and increasing ambient pressure.

4.6.1 Sauter Mean Diameter and Other Characteristic Diameters

The Sympatec particle sizing device generated characteristic diameter data from the probability density function measurements. Characteristic diameter data are statistical representations of different aspects of the PDF function. The D_{32}, X_{10}, X_{50}, X_{90} were recorded for the different set conditions. The D_{32} shows limited dependence on fuel type and no functional dependence on ambient pressure. The results from the X_{10}, X_{50} and X_{90} diameters do not show any significant trends in fuel type or ambient pressure.

The Sympatec measurements of the hybrid air blast nozzle showed no functional dependence on ambient pressure. Figure 4.41 is a plot of Sauter mean diameter versus ambient pressure. The D_{32} measurements at varying ambient pressure do not vary outside the standard deviation for either jet fuel type. The swirling nitrogen that entrains the fuel spray for the hybrid air blast nozzle may reduce the effects of the ambient pressure on drop size distribution.

The Sympatec measurements of the hybrid air blast nozzle showed limited dependence on fuel type. Figure 4.41 shows that the D_{32} for the JP-8 is slightly smaller than the JP-10. Fuel viscosity likely plays a slightly reduced role in determining the atomization characteristics for the hybrid air blast nozzle. The spray distribution depends less on fuel type compared to the pressure swirl atomizer because the swirling nitrogen flow drives droplet break up in the hybrid air blast nozzle. This is consistent with the trends observed in the patternator results and the pressure swirl atomizer results. In addition, Li *et al.* (2013) describes the D_{32} to be a weak function of fuel viscosity for measurements near the nozzle

4.7 Summary of Results

Experimental testing was conducted at Maurice Zucrow Laboratories in order to investigate the effect of jet fuel type on pressure swirl and hybrid air blast nozzles. Fuel injection temperature, fuel injection pressure, and ambient pressure set points were varied. The spray properties for experiments conducted at atmospheric pressure were measured by an En'Urga Op-600 Optical Patternator. Spray properties for experiments

conducted at super atmospheric pressure were measured by a Sympatec HELOS laser diffraction device.

At atmospheric testing conditions, the optical patternator collected total surface area measurements, patternation number measurements, spray angle measurements and radial profile measurements. The bullets below summarize the findings for these measurements in the pressure swirl nozzle and the hybrid air blast nozzle.

- Total surface area measurements decreased with decreasing fuel injection temperature and decreasing fuel injection pressure.
- Total surface area measurements depend on fuel type. For the pressure swirl nozzle at 0.345 MPa (50 psi) injection pressure, JP-8 showed a 38% decrease, Jet A showed a 45% decrease, JP-5 showed a 54% decrease and JP-10 showed a 89% decrease in total surface area from 15.6 to -40 C (60 to -40 F) injection temperature.
- Total surface area measurements were slightly greater for the hybrid air blast nozzle compared to the pressure swirl nozzle at similar conditions
- The fuel type effects on the spray of the hybrid air blast nozzle were similar to the pressure swirl nozzle. For the 0.358 MPa (52 psi) injection pressure case, the total surface area for JP-8 decreased 2%, Jet A decreased 52%, JP-5 decreased 59%, and JP-10 decreased 91% from injection temperature decreasing from 15.6 to -28.8 C (60 to -20 F).
- Patternation number results showed decreasing symmetry in the spray with decreasing fuel injection temperature and decreasing fuel injection pressure.

- The spray angle measurements were independent of fuel type for both fuel injector types. There was a slight increase in spray angle with decreasing temperature for both fuel injectors. Some error in the spray angle measurements occurred at cold injection temperature, resulting in artificially high spray cone angle measurements.
- The radial profile measurements showed decreasing local surface area divided by volume measurements for decreasing fuel injection temperature and decreasing fuel injection pressure.
- The radial profile for the pressure swirl nozzle showed areas of high concentration in the center of the spray. The local surface area to volume of droplets in the spray decreased with decreasing temperature. The difference between fuel types was consistent with the viscosities of the fuel.
- The radial profile for the hybrid air blast nozzle showed an annular ring of high concentration in the spray. The differences between fuel type was less significant compared to the pressure swirl nozzle.

At super atmospheric testing conditions, the Sympatec laser diffraction device collected X_{10}, X_{50}, X_{90}, and D_{32} characteristic diameters. The bullets below summarize the findings for these measurements in the pressure swirl nozzle and the hybrid air blast nozzle.

- The X_{10} measurements did not change significantly with ambient pressure or fuel injection pressure. The X_{10} measurements showed slight increase with decreasing

fuel injection temperature for the pressure swirl nozzle. The X_{10} measurements showed slight dependence on fuel type for decreasing fuel injection temperature.

- Especially for the JP-8 results, the X_{50} and X_{90} measurements were shown to increase with increasing ambient pressure and decreasing fuel injection pressure.
- The change in X_{50} and X_{90} measurements depended on the fuel type with changing ambient pressure. The X_{50} showed a 48% increase for the JP-8 fuel and a 10% increase in the JP-10 fuel for 0.345 MPa (50 psi) injection pressure and ambient pressure increasing from 0.172 to 1.723 MPa (25 to 250 psi). X_{90} showed a 32% increase for the JP-8 fuel and a 10% increase in the JP-10 fuel for 0.345 MPa (50 psi) injection pressure and ambient pressure increasing from 0.172 to 1.723 MPa (25 to 250 psi).
- The change in X_{50} and X_{90} measurements depended on fuel type for changing fuel injection temperature. The X_{50} showed a 12% increase for the JP-8 fuel, a 20% increase for the Jet A fuel, a 17% increase for the JP-5 fuel and a 50% increase in the JP-10 fuel for 0.345 MPa (50 psi) injection pressure and fuel injection temperature decreasing from 15.6 to -17.8 C (60 to 0 F). The X_{90} showed a 29% increase for the JP-8 fuel, a 48% increase for the Jet A fuel, a 40% increase for the JP-5 fuel and a 58% increase in the JP-10 fuel for 0.345 MPa (50 psi) injection pressure and fuel injection temperature decreasing from 15.6 to -17.8 C (60 to 0 F).
- The D_{32} for the pressure swirl nozzle was shown to increase slightly with increasing ambient pressure and decreasing fuel injection temperature.
- The D_{32} also depends on fuel type with the most viscous fuel having the greatest D_{32} and the least viscous fuel having the smallest D_{32}.

- The hybrid air blast nozzle did not show significant trends in X_{10}, X_{50}, X_{90}, and D_{32} measurements with ambient pressure or fuel type. One explanation for this is the swirling nitrogen resulted in aerodynamic forces that dominated forces from the set conditions.

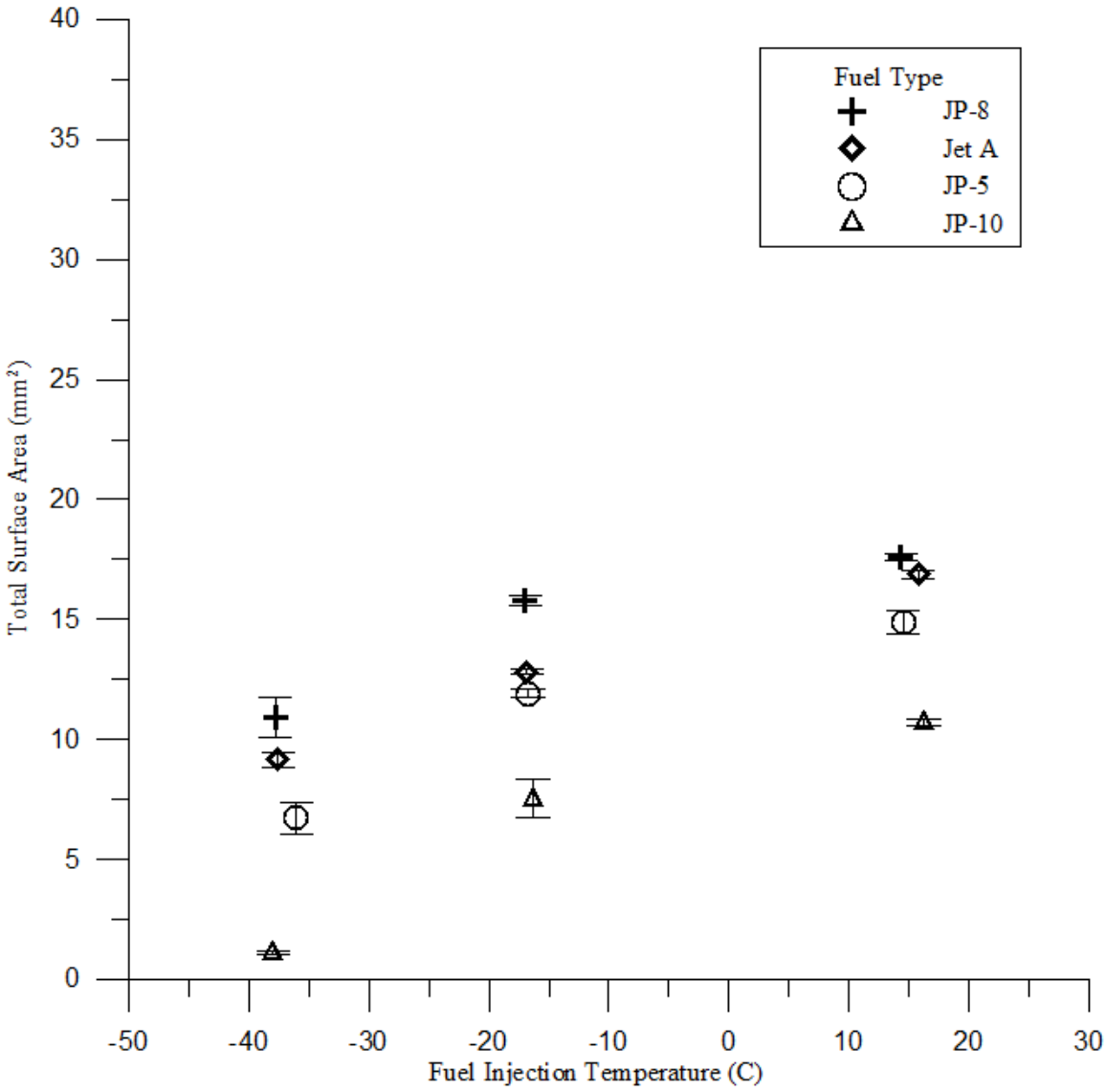

Figure 4.1. Pressure Swirl Atomizer Total Surface Area versus Injection Temperature, 0.345 MPa (50 psi) Injection Pressure.

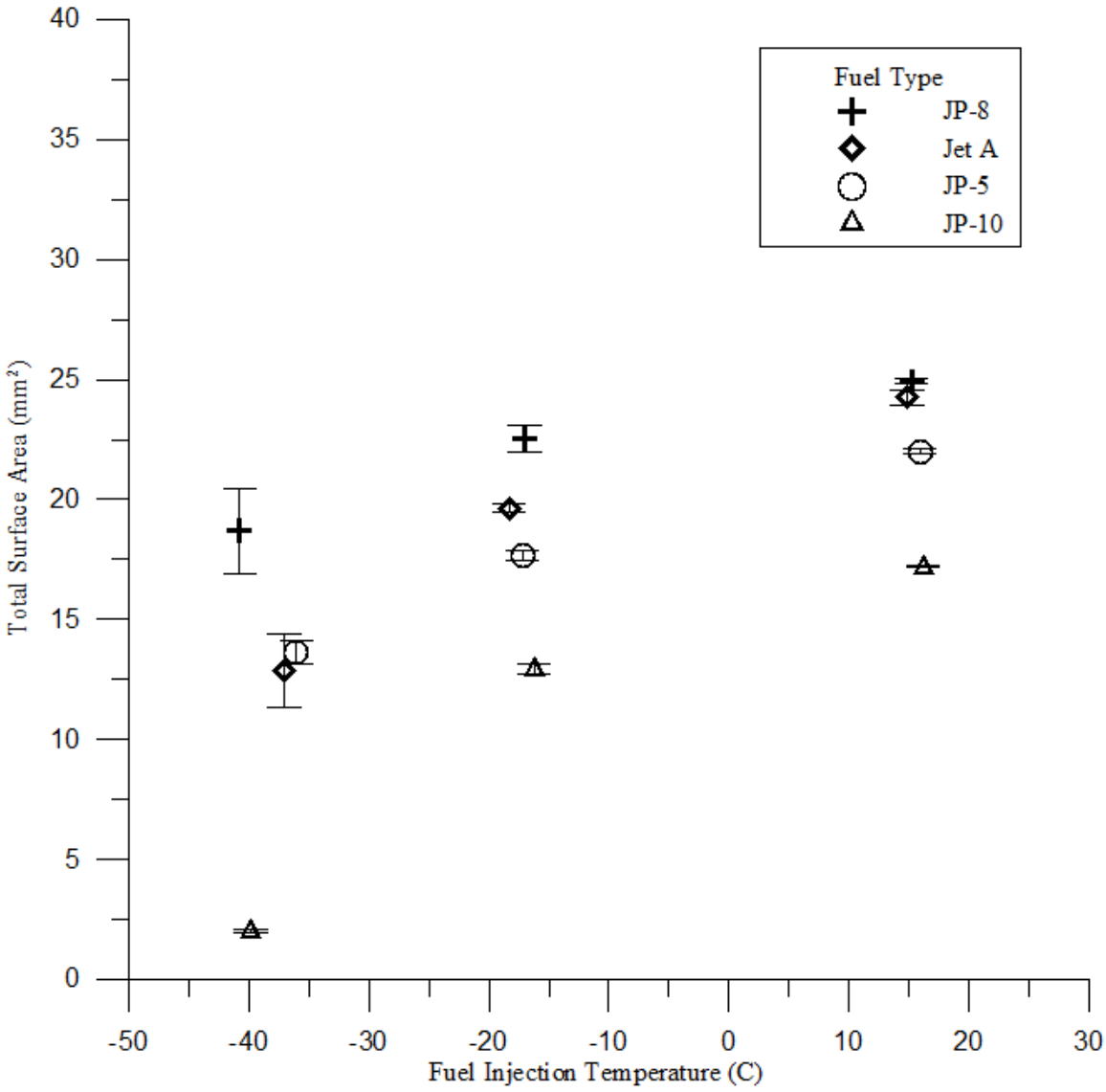

Figure 4.2. Pressure Swirl Atomizer Total Surface Area versus Injection Temperature, 0.689 MPa (100 psi) Injection Pressure.

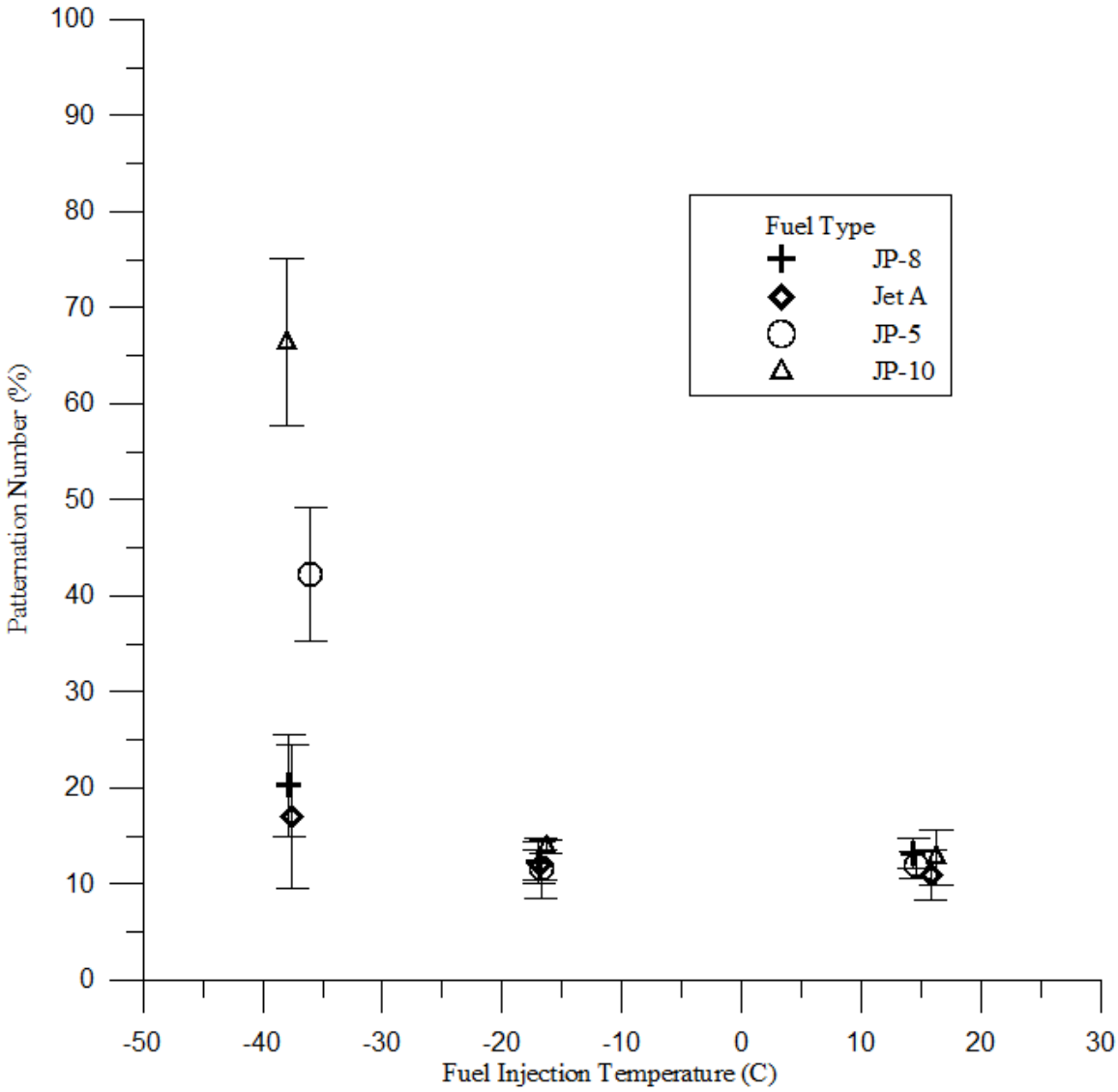

Figure 4.3. Pressure Swirl Atomizer Patternation Number versus Injection Temperature, 0.345 MPa (50 psi) Injection Pressure.

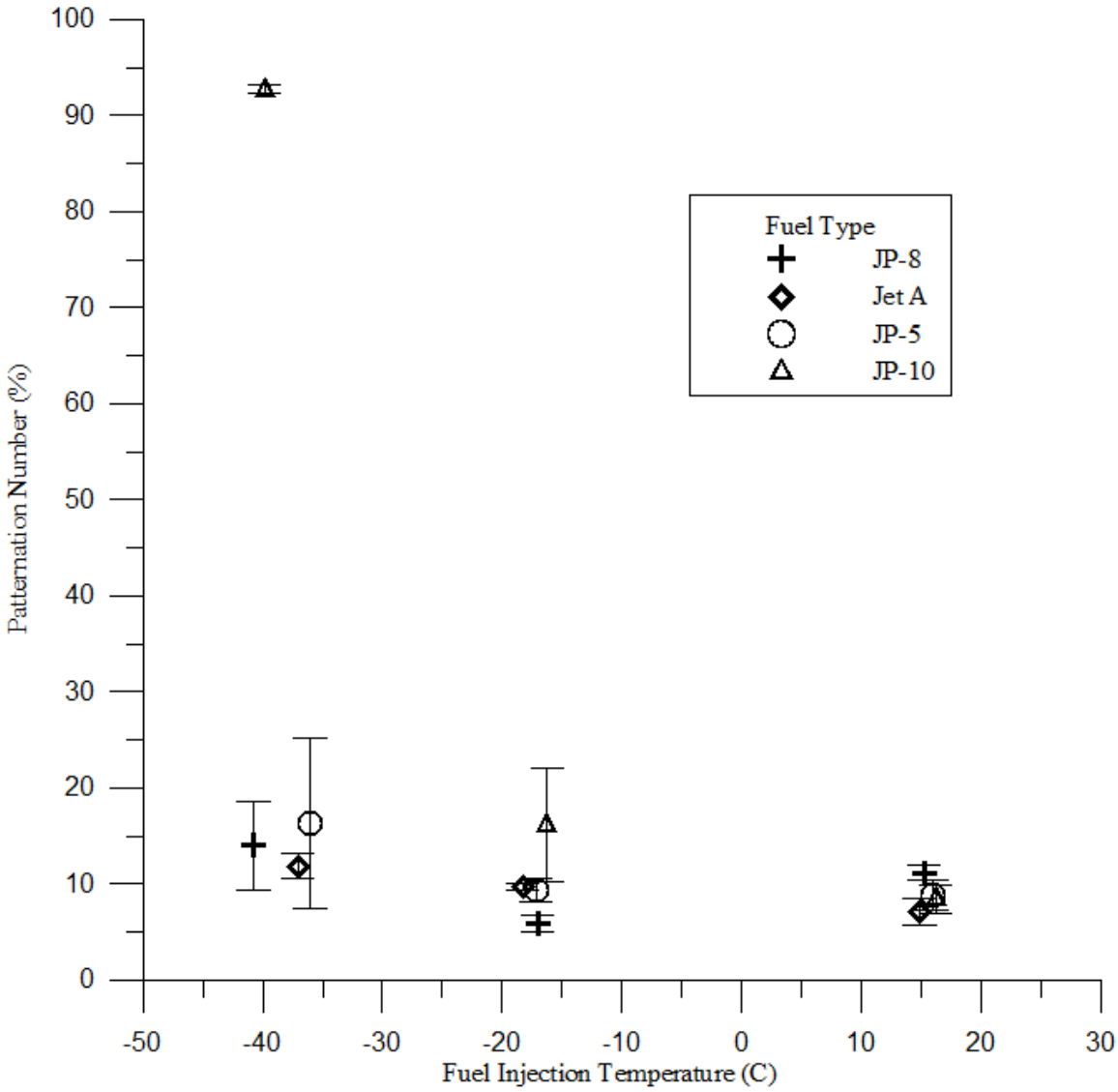

Figure 4.4. Pressure Swirl Atomizer Patternation Number versus Injection Temperature, 0.689 MPa (100 psi) Injection Pressure.

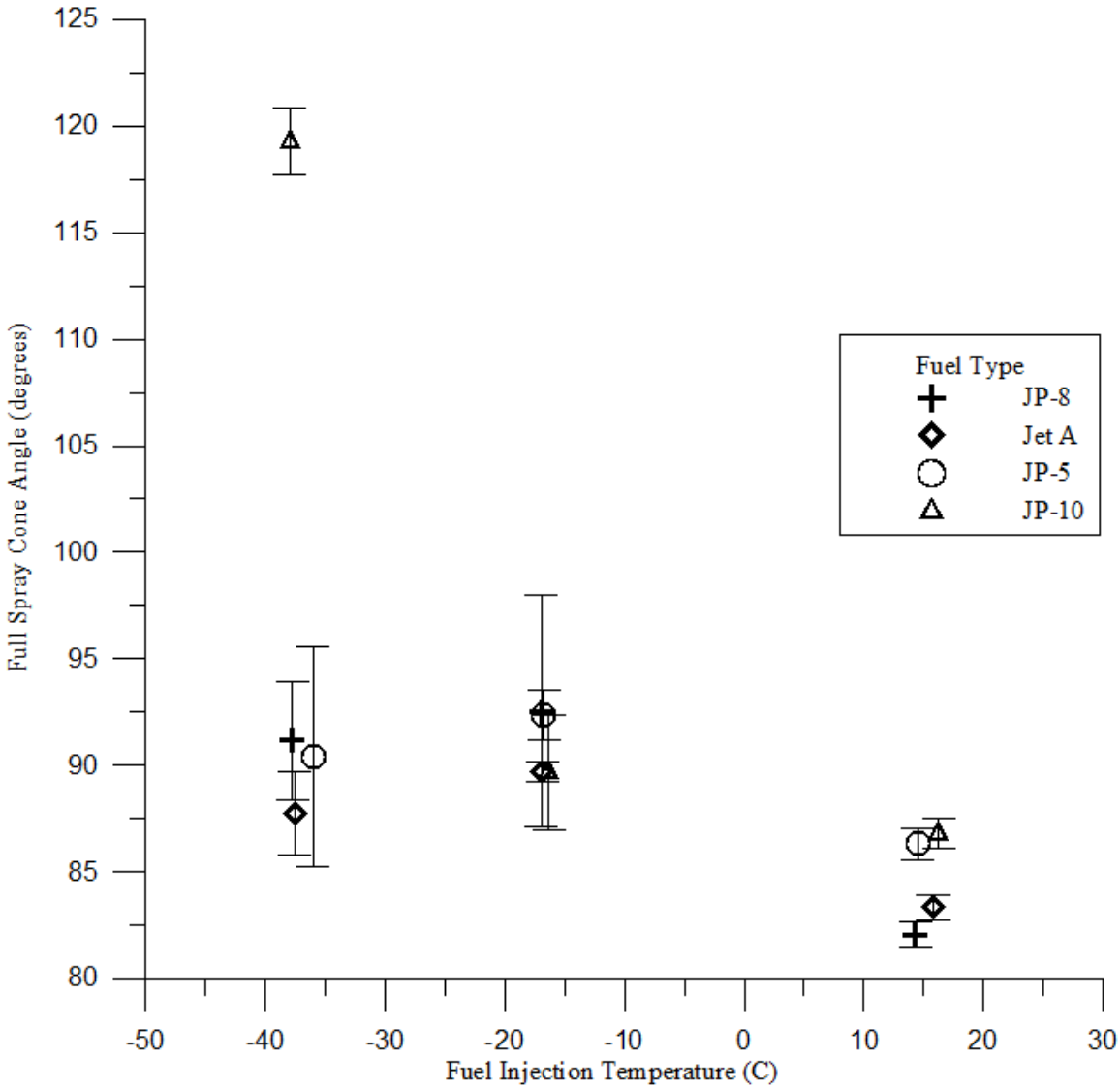

Figure 4.5. Pressure Swirl Atomizer Full Spray Cone Angle versus Injection Temperature, 0.345 MPa (50 psi) Injection Pressure, 38.1 mm (1.5 in) Downstream of Injector.

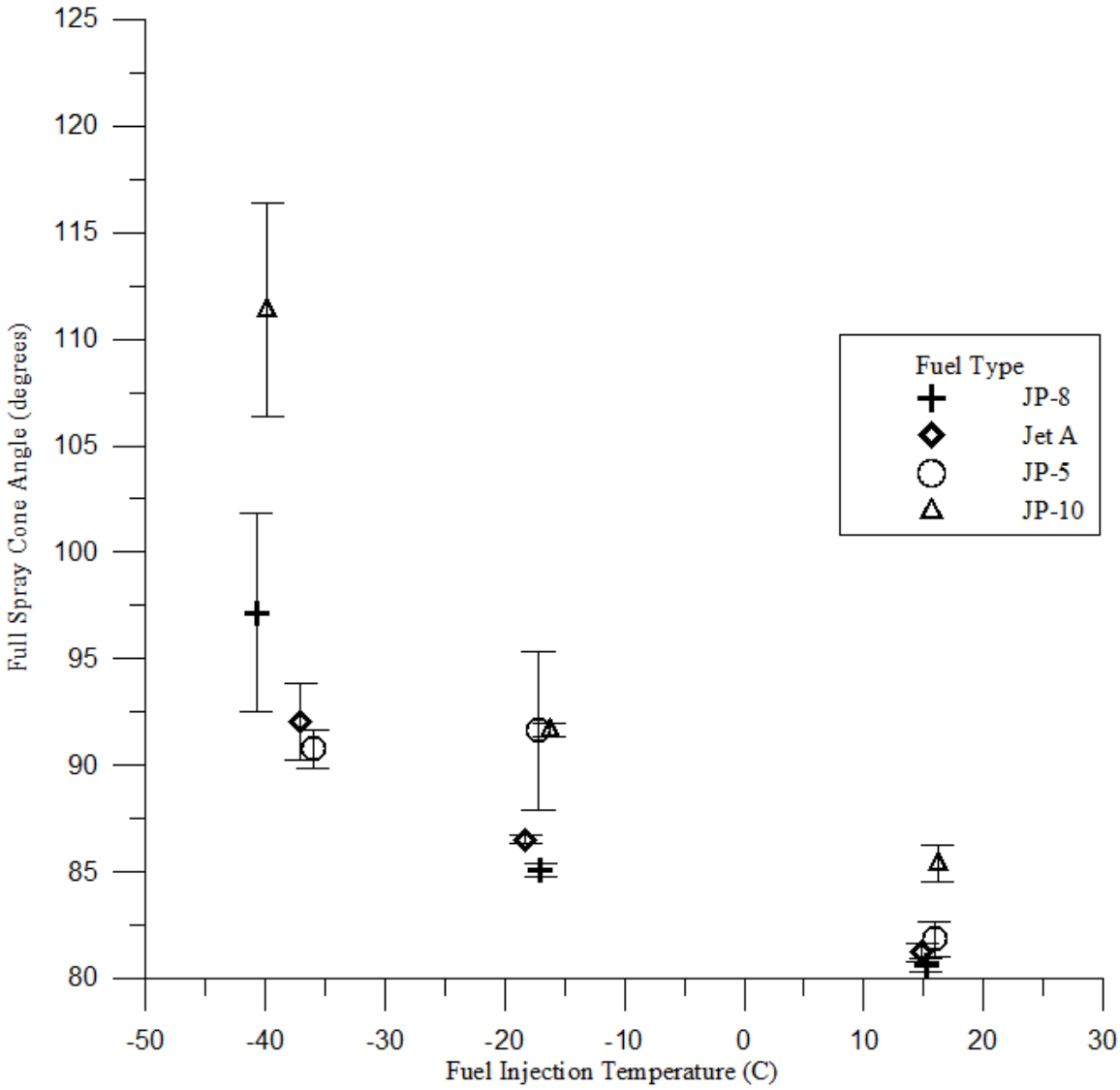

Figure 4.6. Pressure Swirl Atomizer Full Spray Cone Angle versus Injection Temperature, 0.689 MPa (100 psi) Injection Pressure, 38.1 mm (1.5 in) Downstream of Injector.

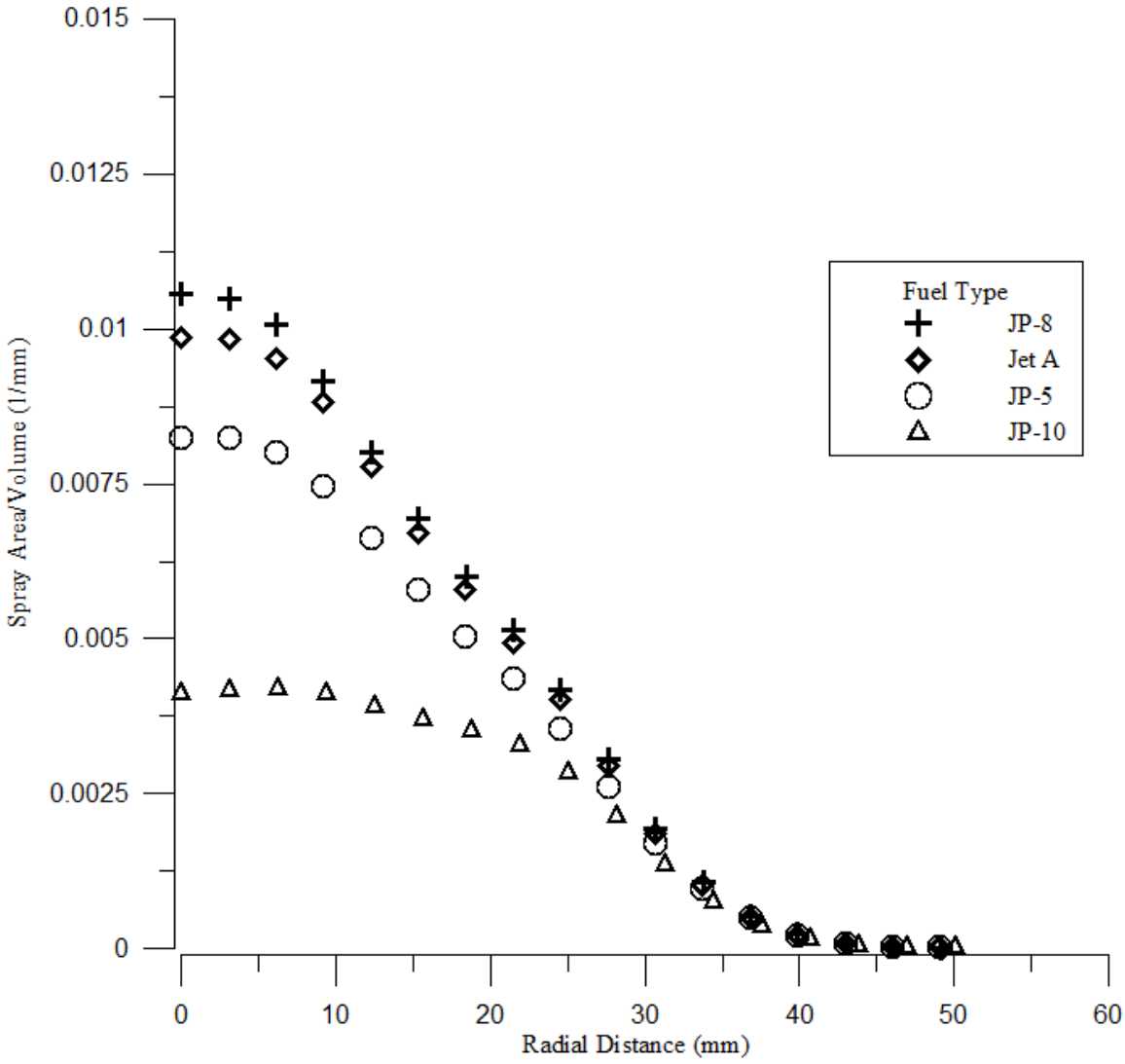

Figure 4.7. Pressure Swirl Atomizer Radial Profile versus Distance from Center of Spray, 15.6 C (60 F) Fuel Injection Temperature, 0.345 MPa (50 psi) Injection Pressure.

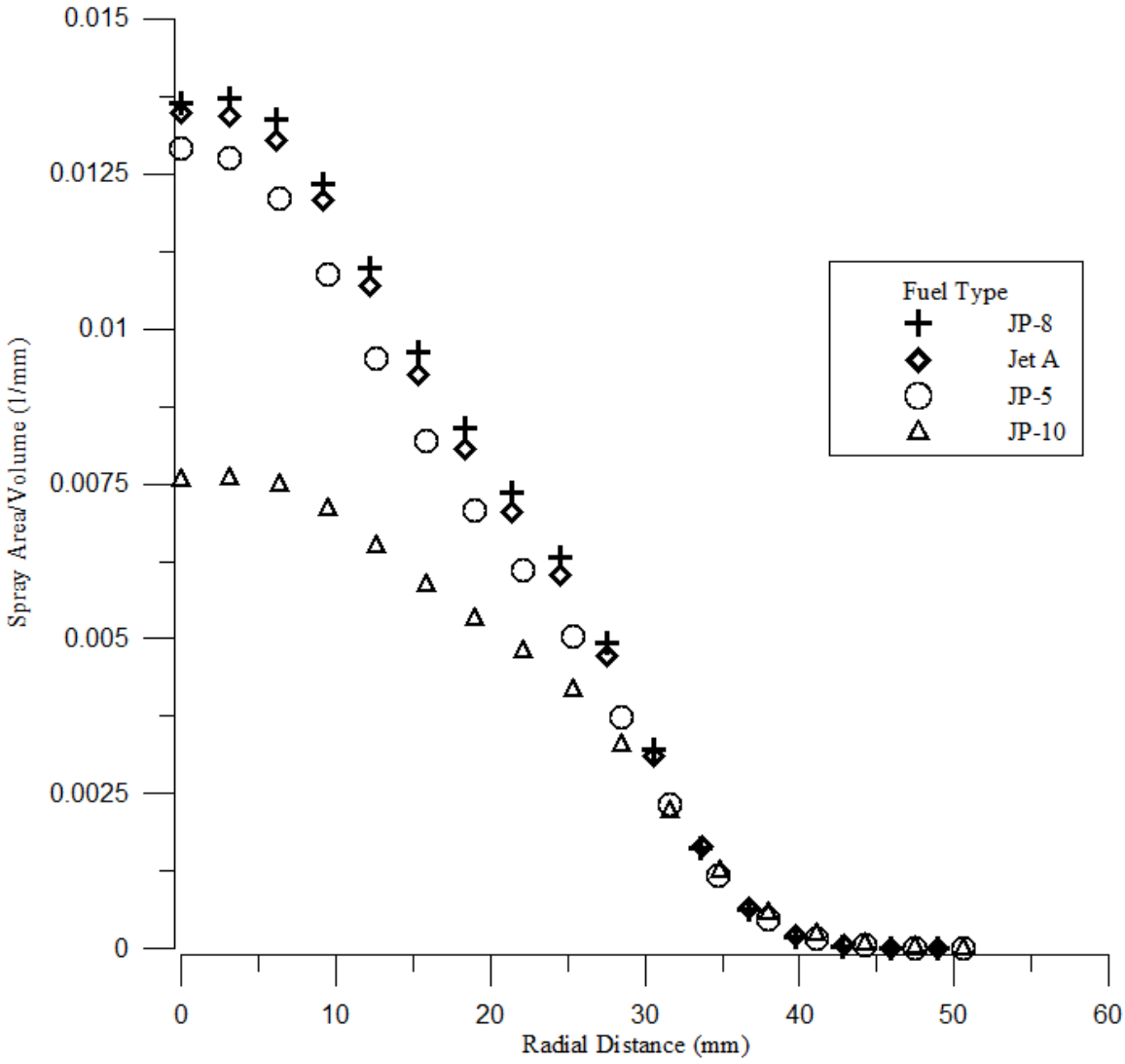

Figure 4.8. Pressure Swirl Atomizer Radial Profile versus Distance from Center of Spray, 15.6 C (60 F) Fuel Injection Temperature, 0.689 MPa (100 psi) Injection Pressure.

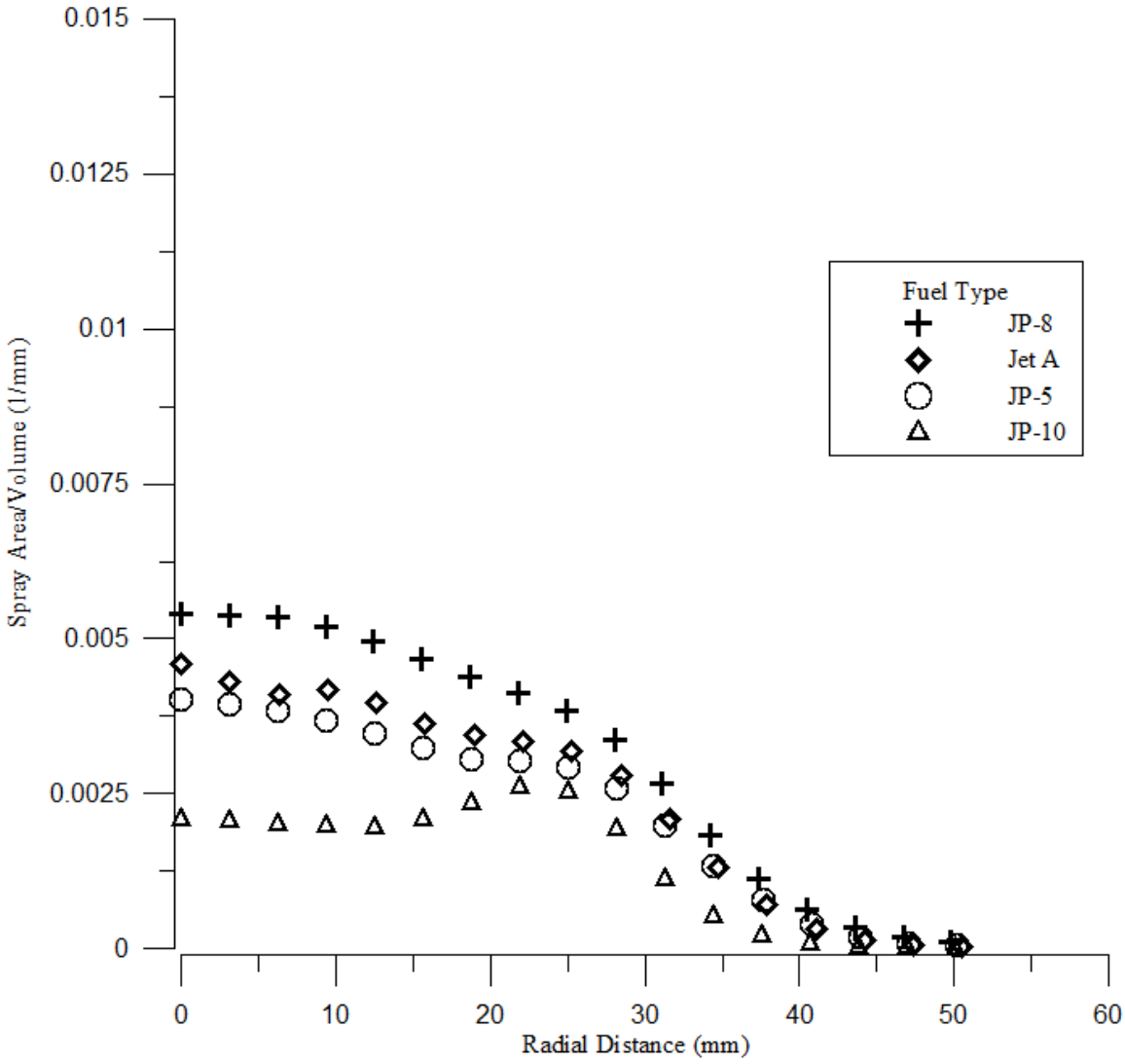

Figure 4.9. Pressure Swirl Atomizer Radial Profile versus Distance from Center of Spray, -17.8 C (0 F) Fuel Injection Temperature, 0.345 MPa (50 psi) Injection Pressure.

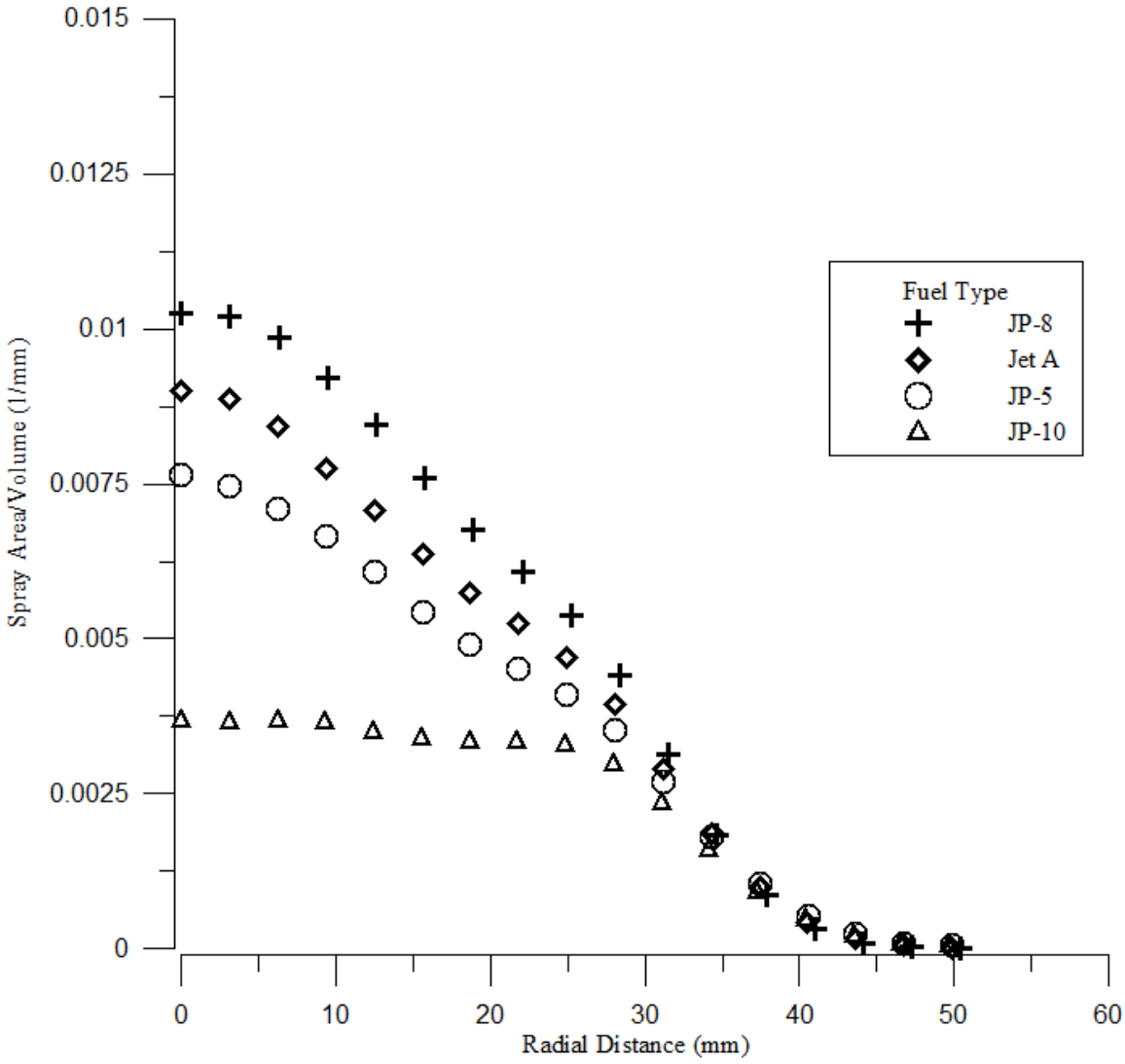

Figure 4.10. Pressure Swirl Atomizer Radial Profile versus Distance from Center of Spray, -17.8 C (0 F) Fuel Injection Temperature, 0.689 MPa (100 psi) Injection Pressure.

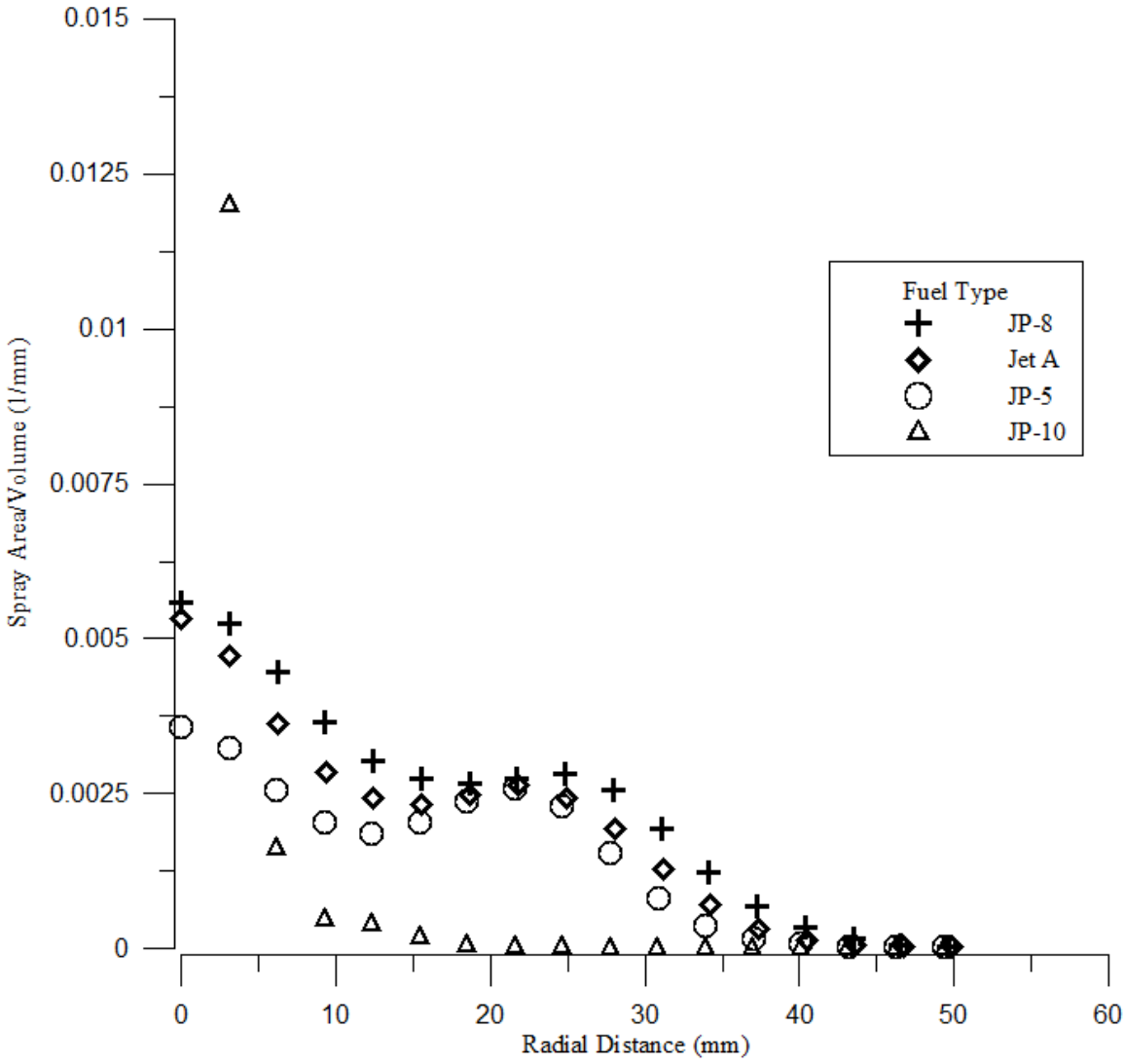

Figure 4.11. Pressure Swirl Atomizer Radial Profile versus Distance from Center of Spray, -40 C (-40 F) Fuel Injection Temperature, 0.345 MPa (50 psi) Injection Pressure.

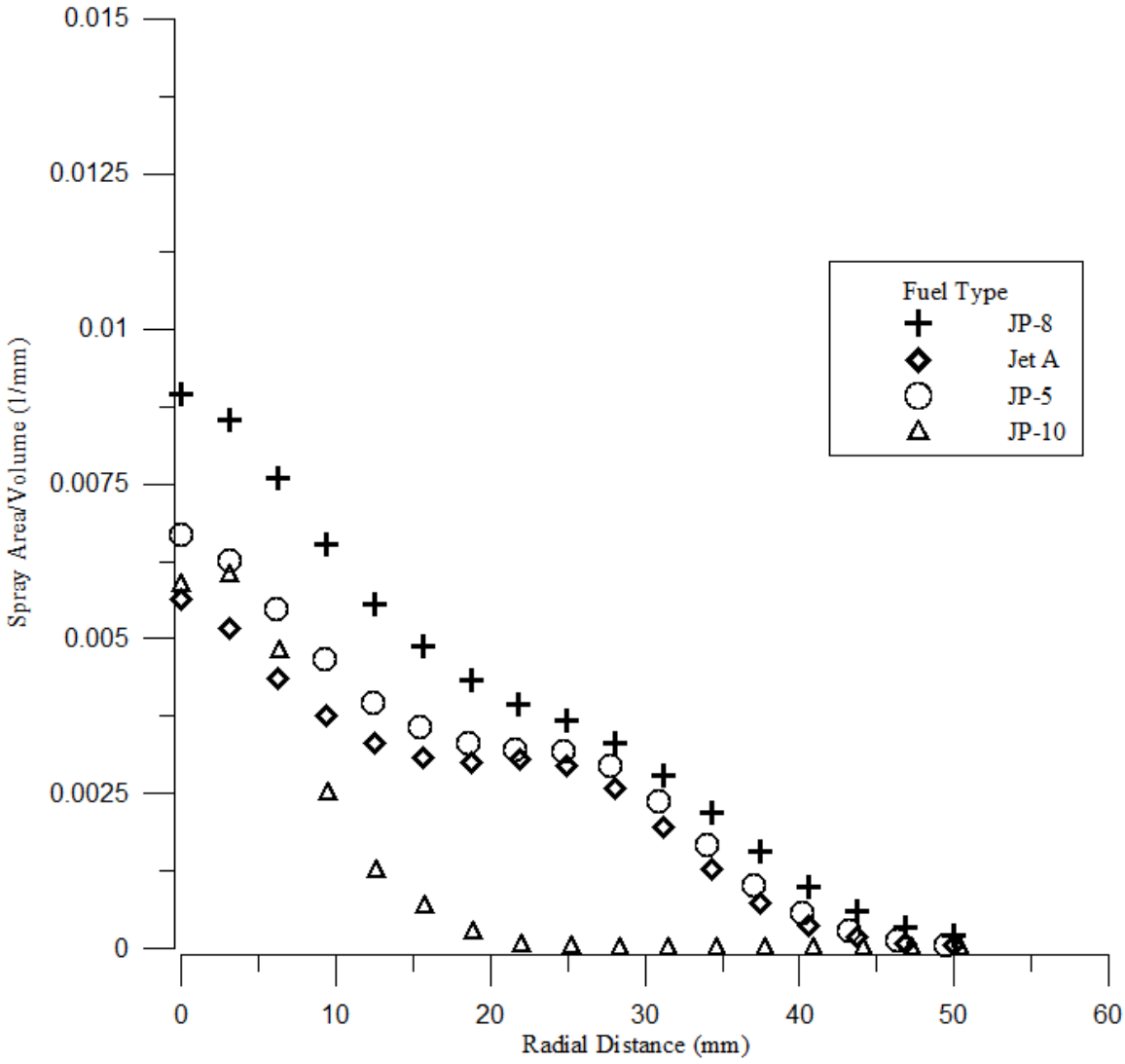

Figure 4.12. Pressure Swirl Atomizer Radial Profile versus Distance from Center of Spray, -40 C (-40 F) Fuel Injection Temperature, 0.689 MPa (100 psi) Injection Pressure.

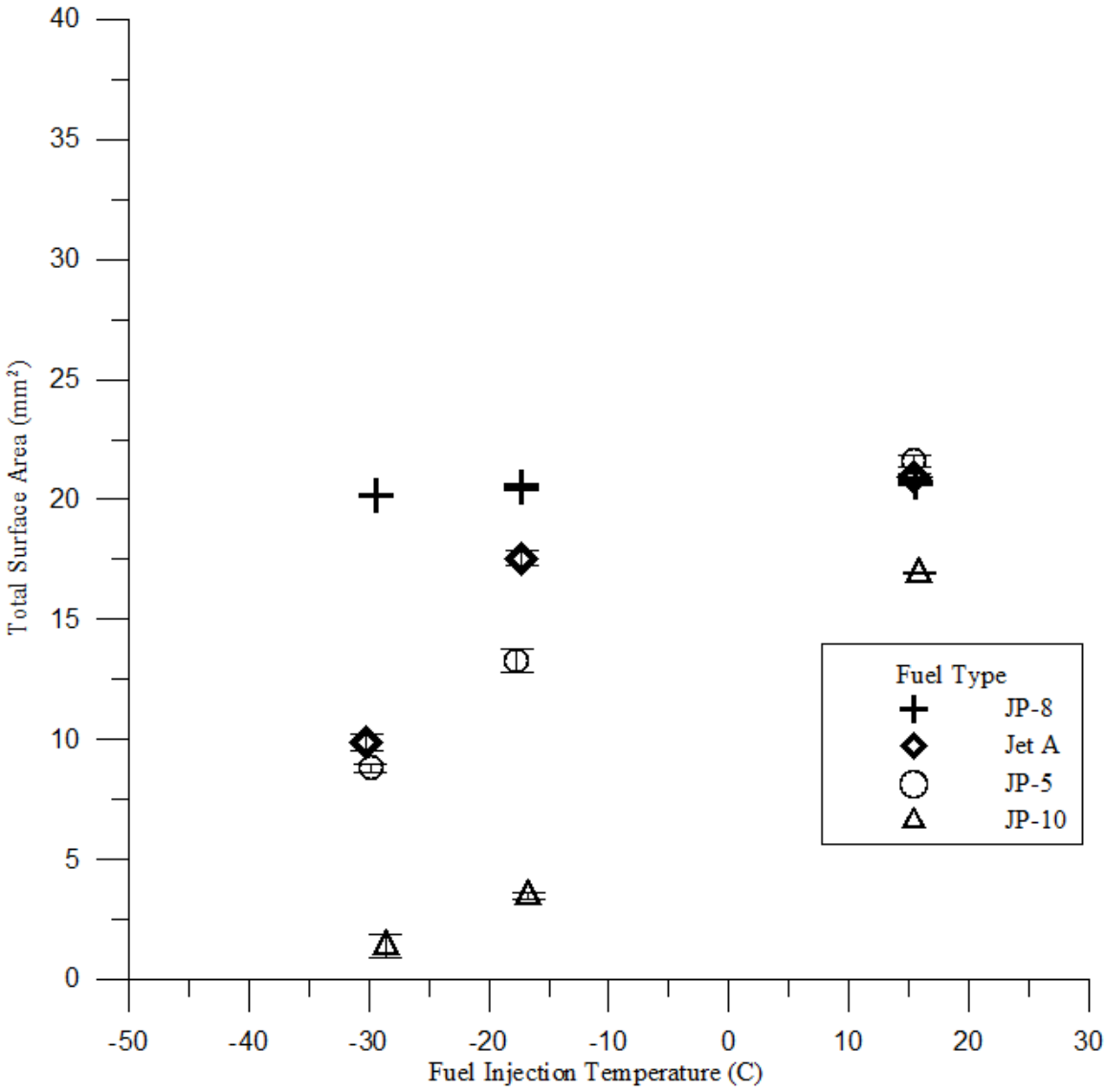

Figure 4.13. Hybrid Air Blast Nozzle Total Surface Area versus Injection Temperature, 0.358 MPa (52 psi) Injection Pressure.

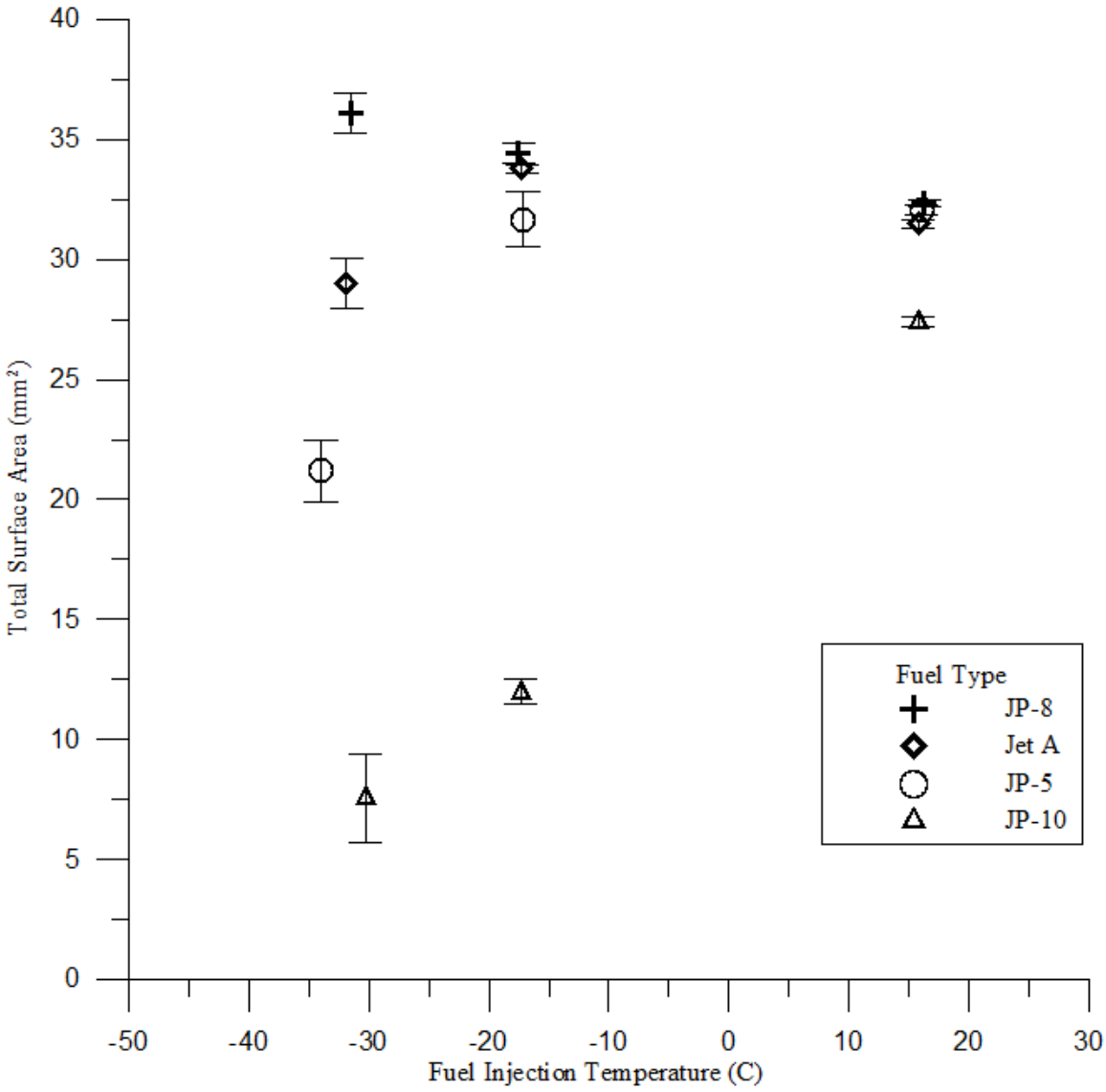

Figure 4.14. Hybrid Air Blast Nozzle Total Surface Area versus Injection Temperature, 0.806 MPa (117 psi) Injection Pressure.

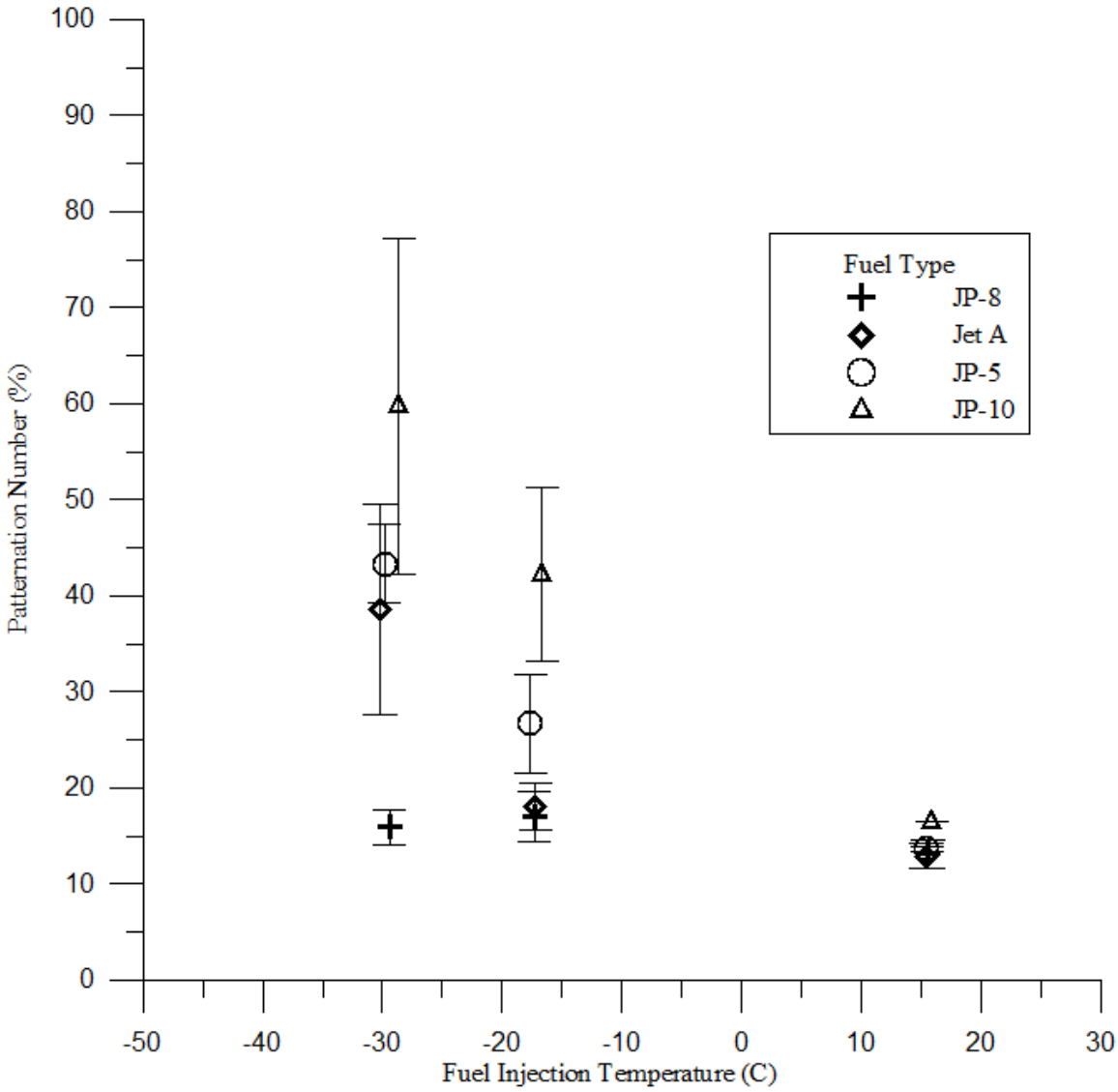

Figure 4.15. Hybrid Air Blast Nozzle Patternation Number versus Injection Temperature, 0.358 MPa (52 psi) Injection Pressure.

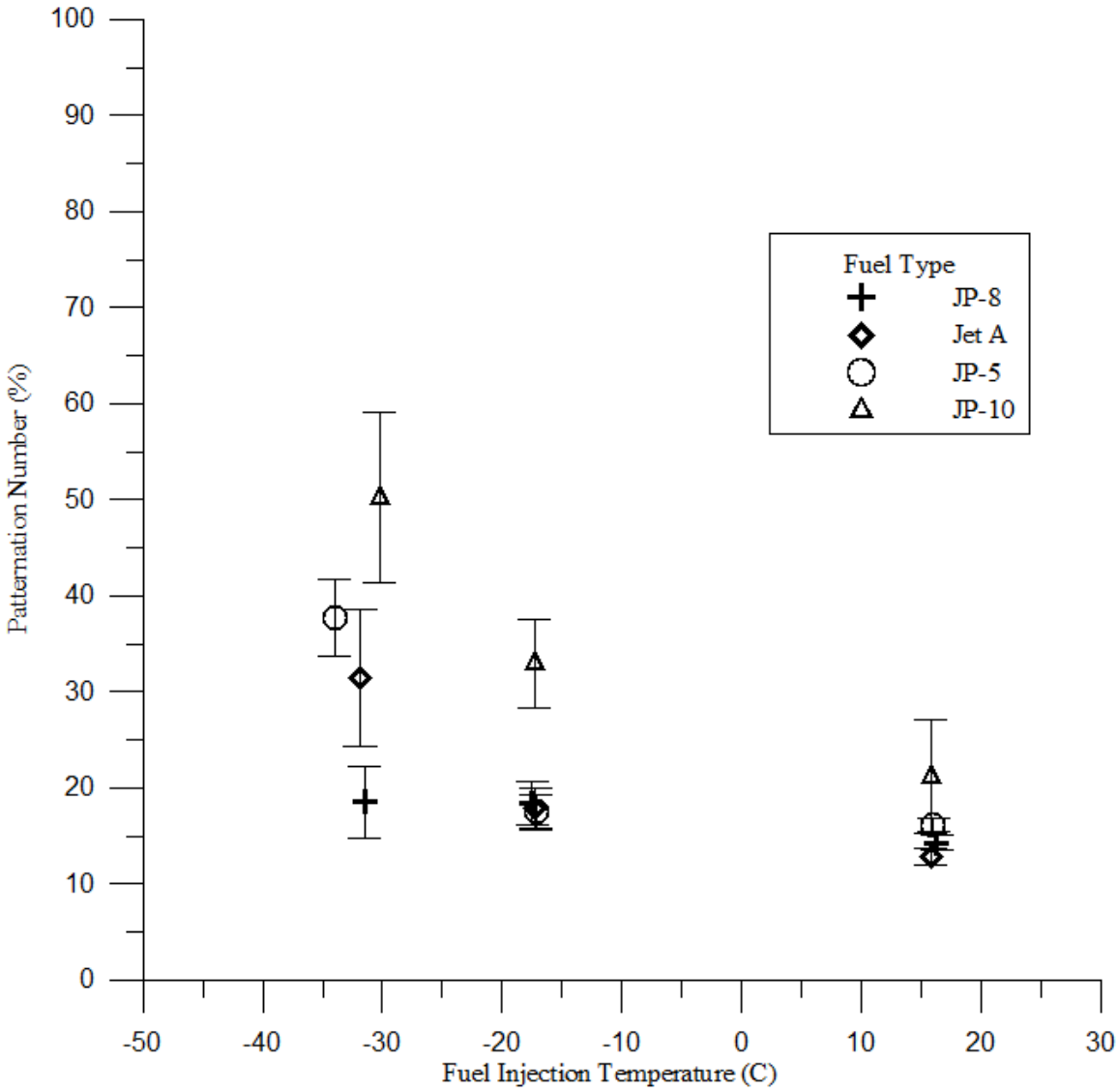

Figure 4.16. Hybrid Air Blast Nozzle Patternation Number versus Injection Temperature, 0.806 MPa (117 psi) Injection Pressure.

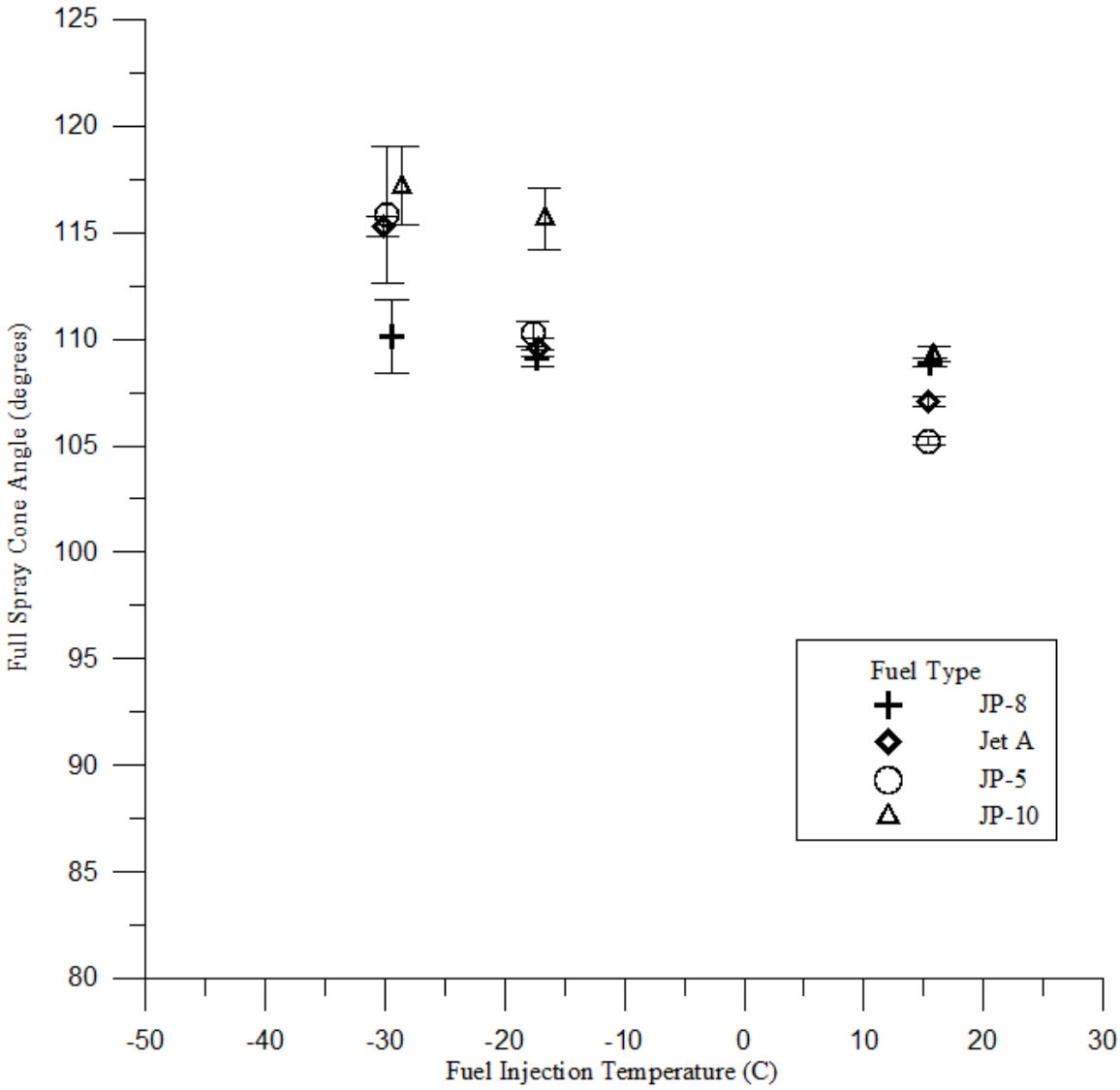

Figure 4.17. Hybrid Air Blast Nozzle Full Spray Cone Angle versus Injection Temperature, 0.358 MPa (52 psi) Injection Pressure, 38.1 mm (1.5 in) Downstream of Injector.

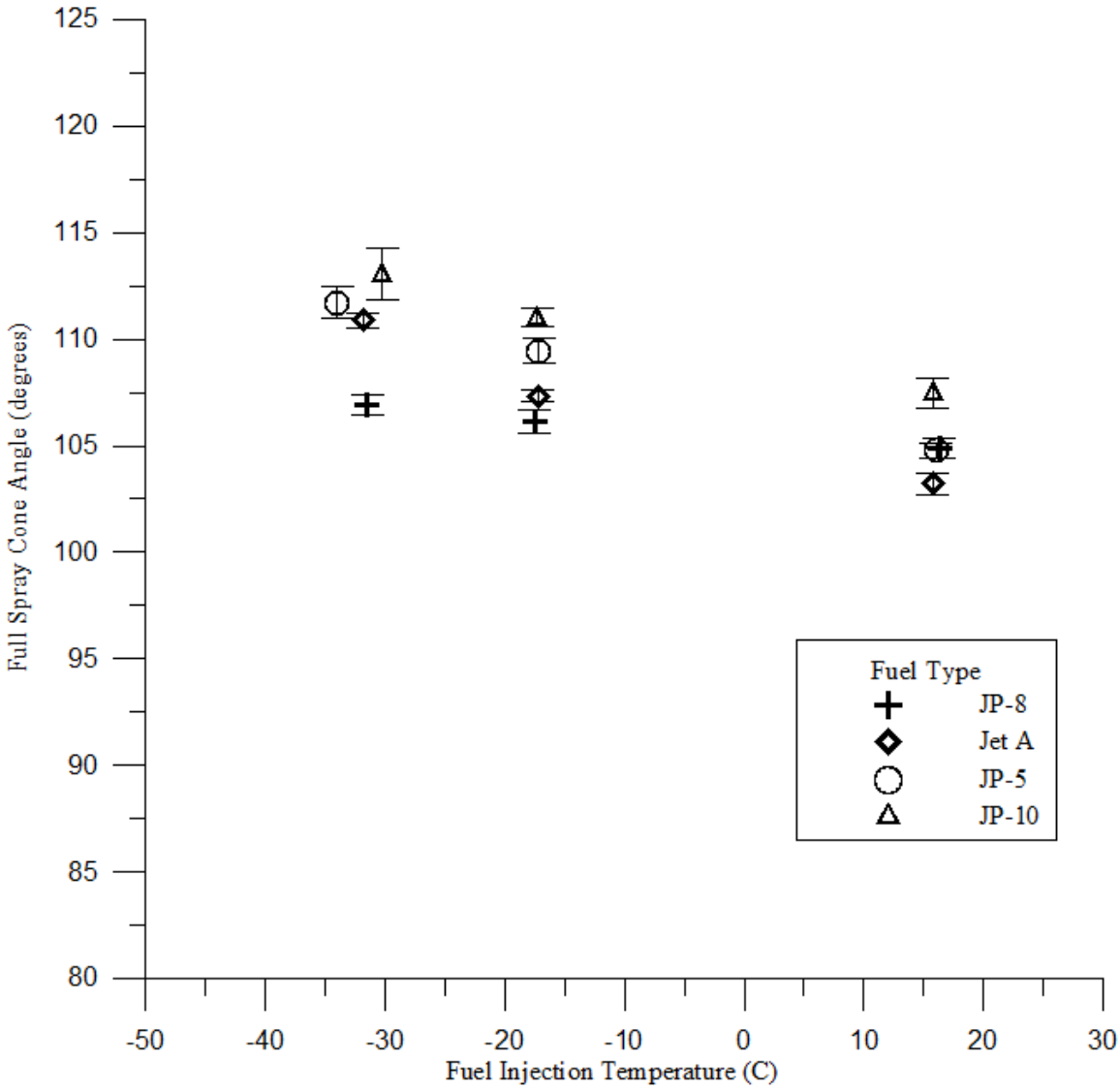

Figure 4.18. Hybrid Air Blast Nozzle Full Spray Cone Angle versus Injection Temperature, 0.806 MPa (117 psi) Injection Pressure, 38.1 mm (1.5 in) Downstream of Injector.

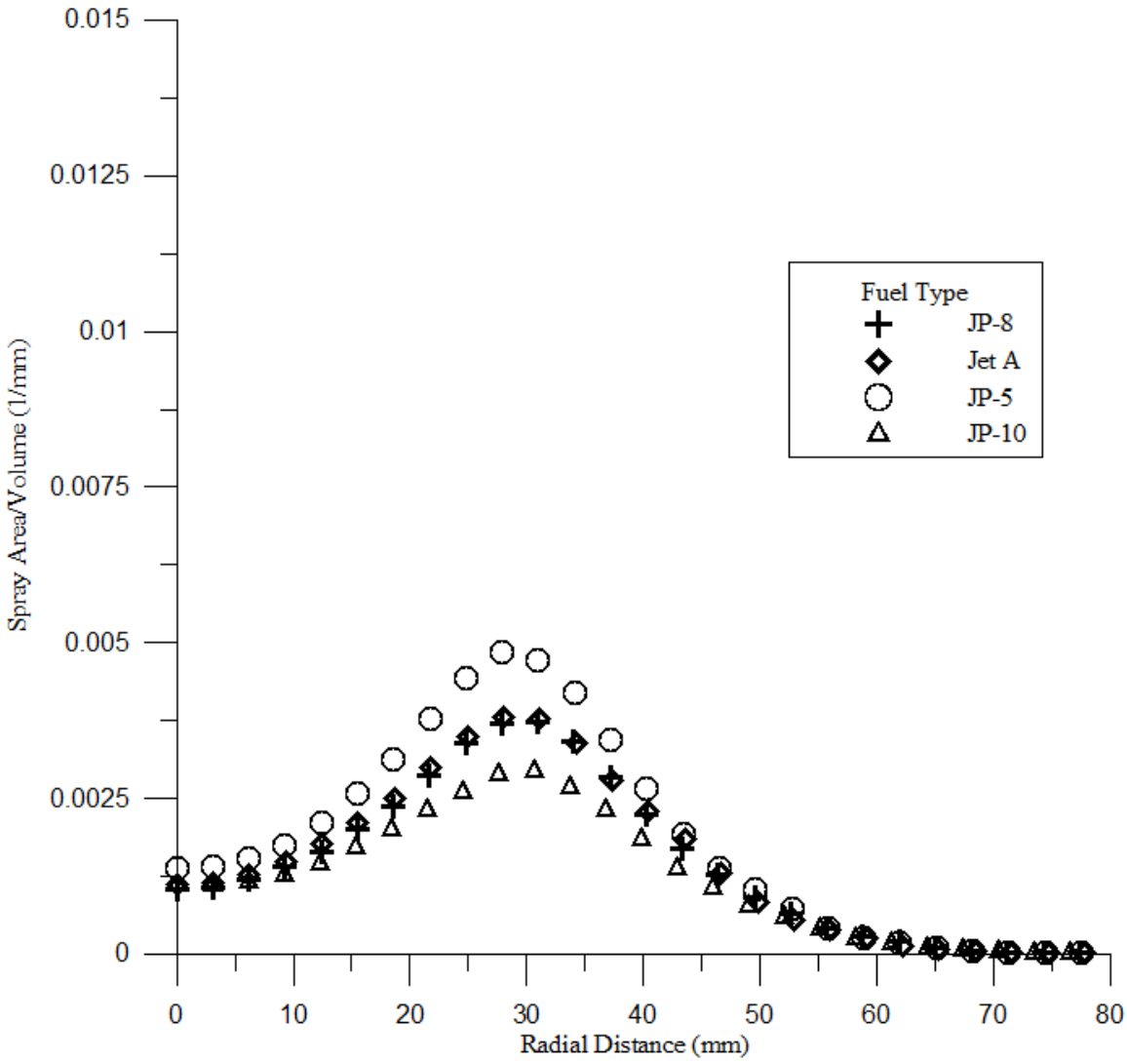

Figure 4.19. Hybrid Air Blast Nozzle Radial Profile versus Distance from Center of Spray, 15.6 C (60 F) Fuel Injection Temperature, 0.358 MPa (52 psi) Injection Pressure.

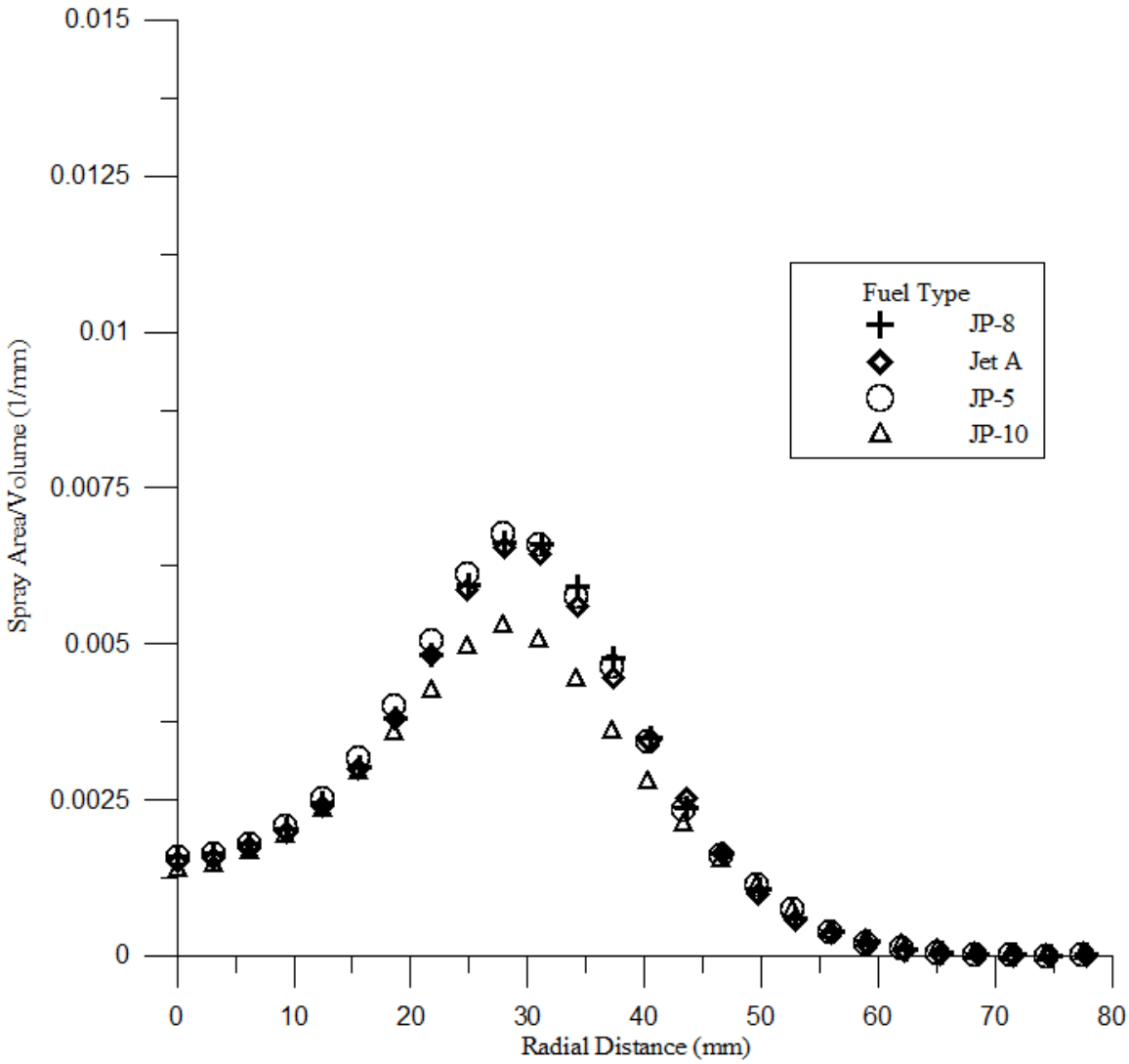

Figure 4.20. Hybrid Air Blast Nozzle Radial Profile versus Distance from Center of Spray, 15.6 C (60 F) Fuel Injection Temperature, 0.806 MPa (117 psi) Injection Pressure.

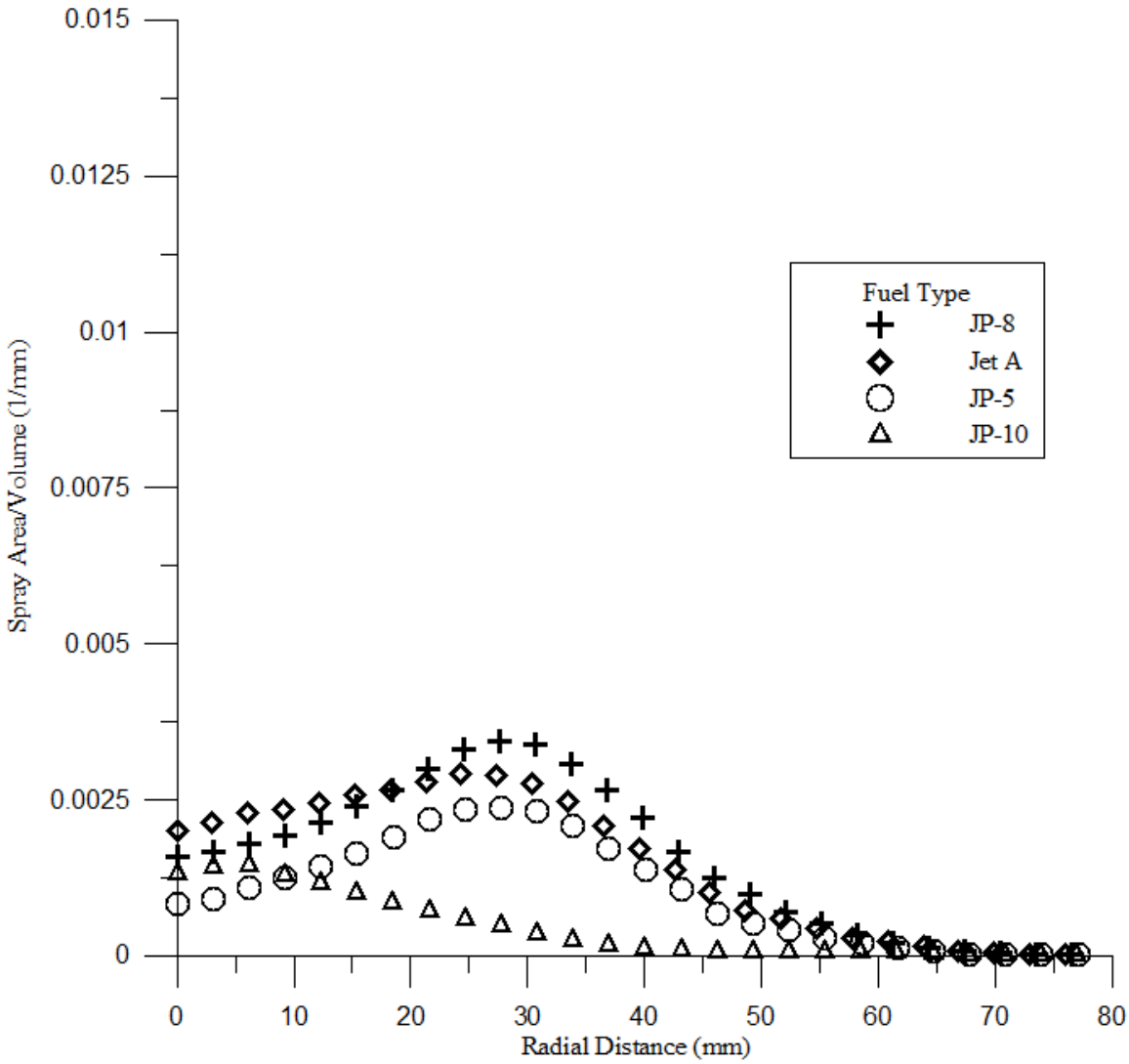

Figure 4.21. Hybrid Air Blast Nozzle Radial Profile versus Distance from Center of Spray, -17.8 C (0 F) Fuel Injection Temperature, 0.358 MPa (52 psi) Injection Pressure.

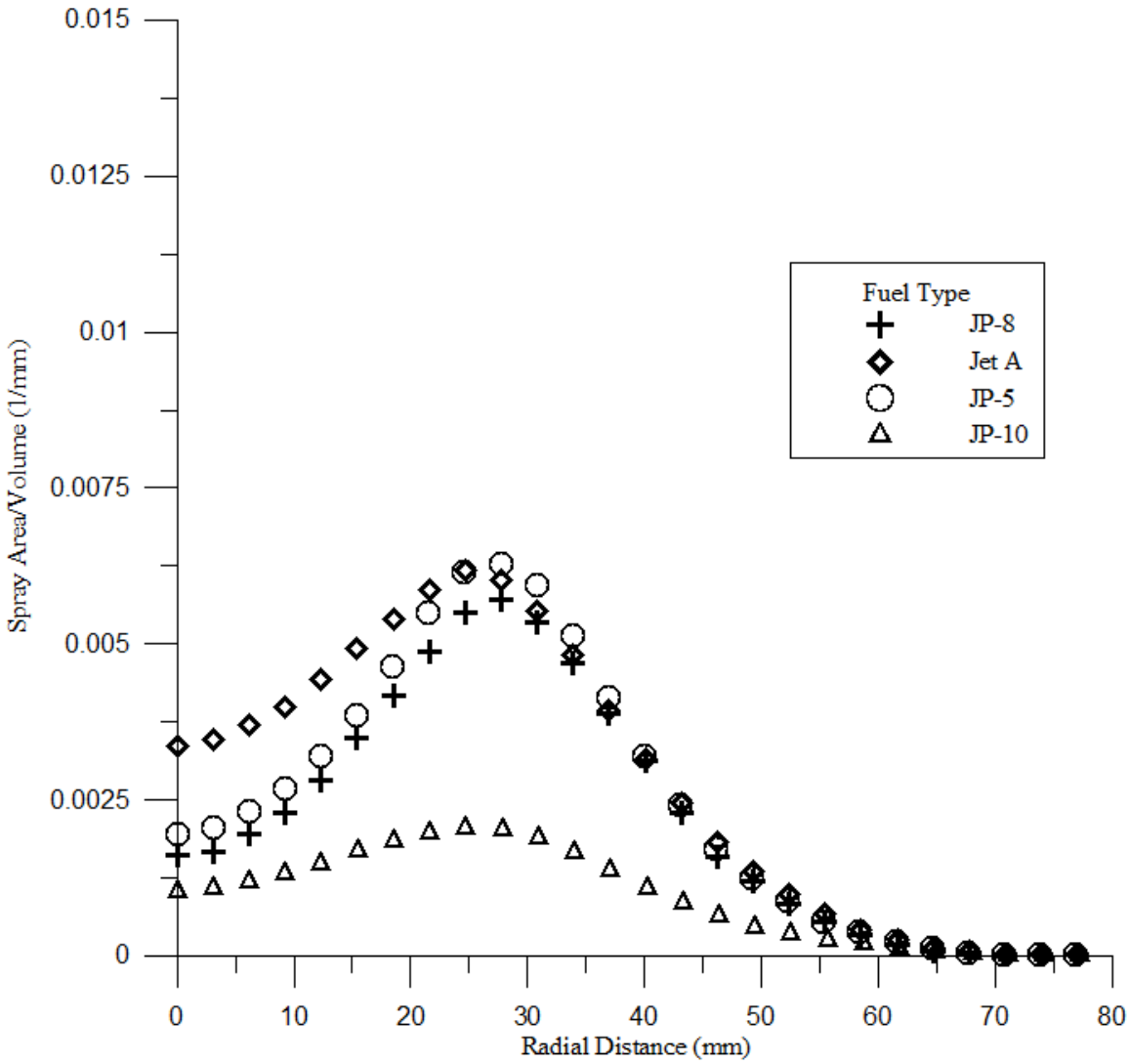

Figure 4.22. Hybrid Air Blast Nozzle Radial Profile versus Distance from Center of Spray, -17.8 C (0 F) Fuel Injection Temperature, 0.806 MPa (117 psi) Injection Pressure.

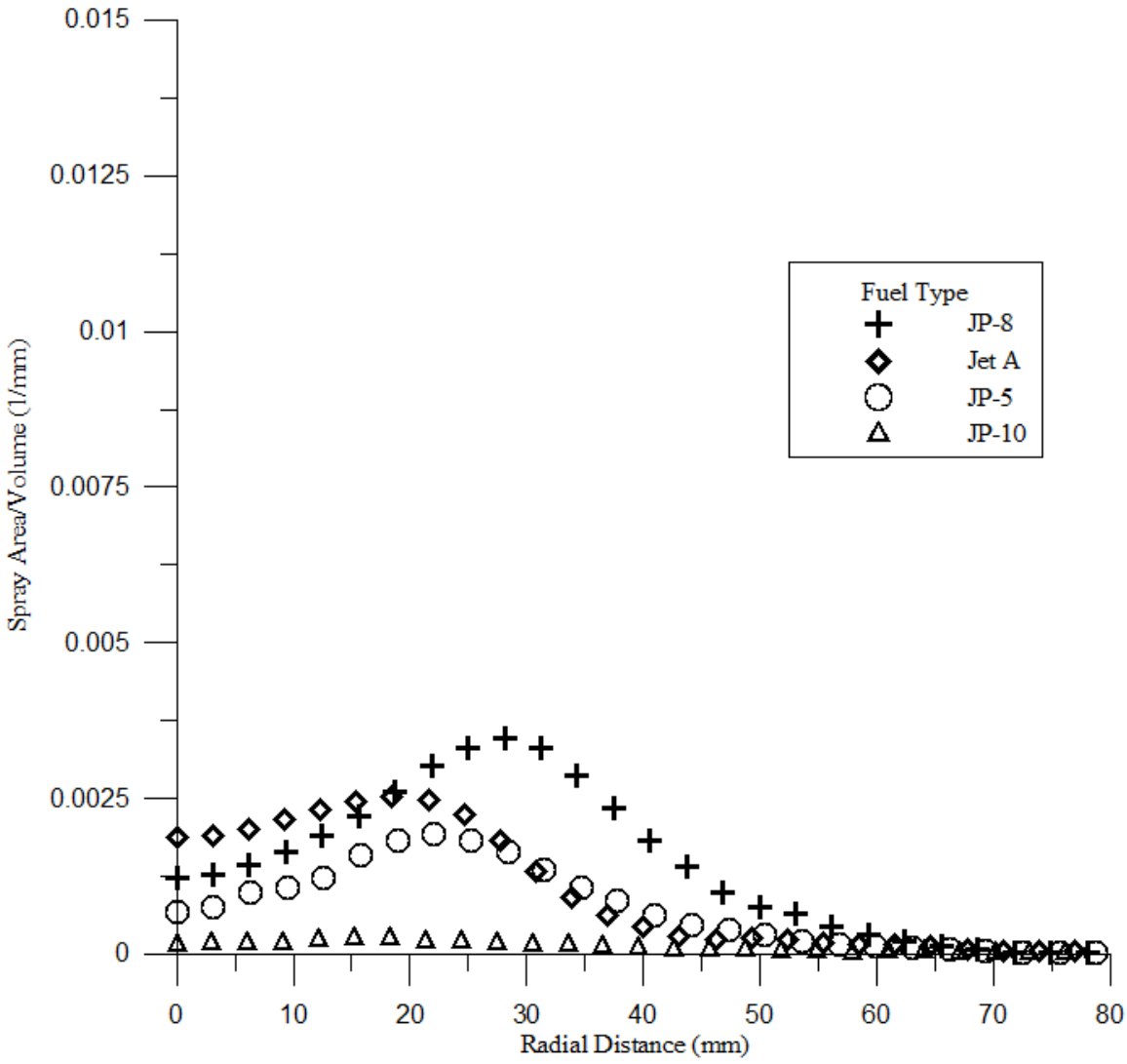

Figure 4.23. Hybrid Air Blast Nozzle Radial Profile versus Distance from Center of Spray, -28.8 C (-20 F)Fuel Injection Temperature, 0.358 MPa (52 psi) Injection Pressure.

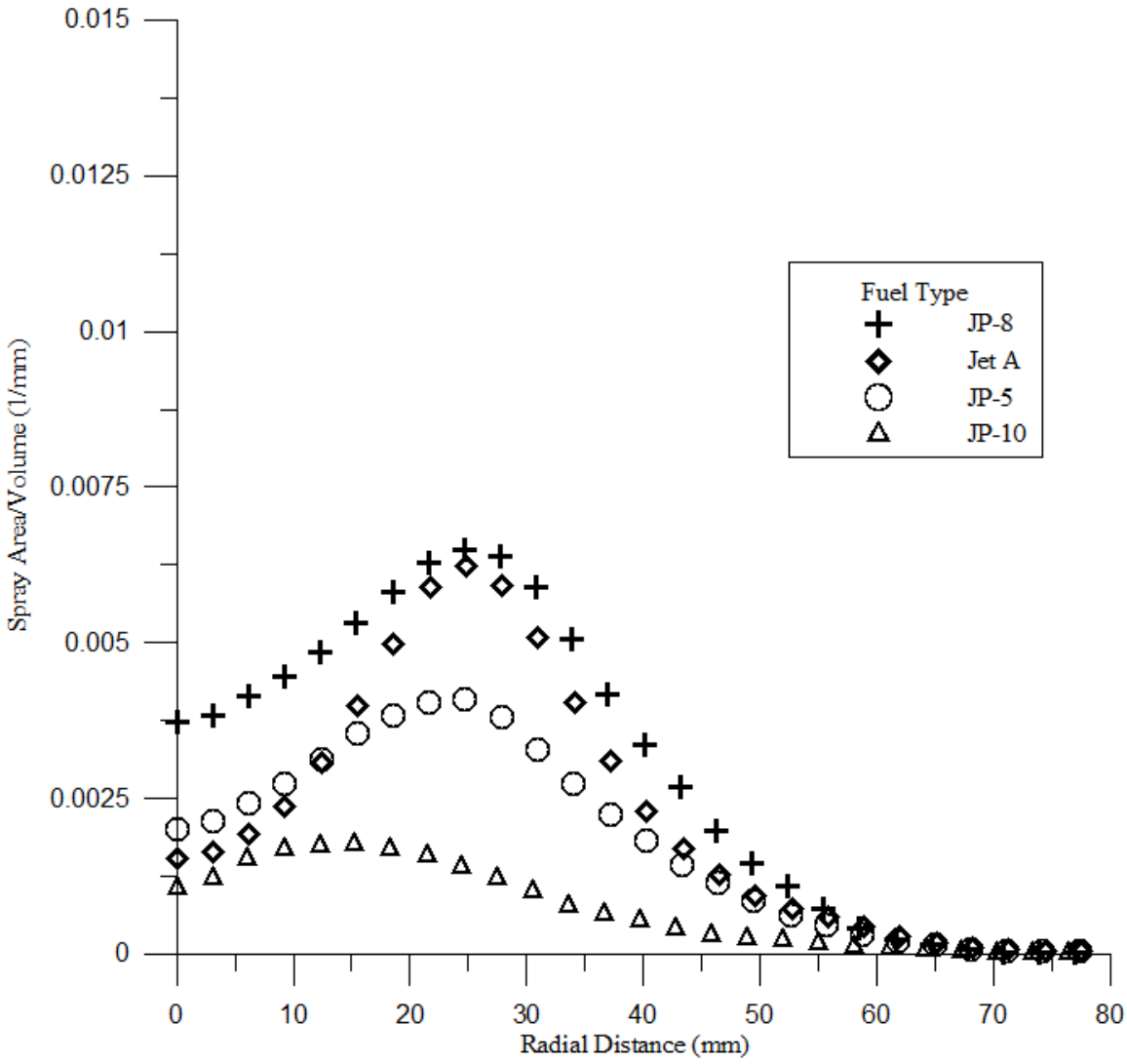

Figure 4.24. Hybrid Air Blast Nozzle Radial Profile versus Distance from Center of Spray, -28.8 C (-20 F) Fuel Injection Temperature, 0.806 MPa (117 psi) Injection Pressure.

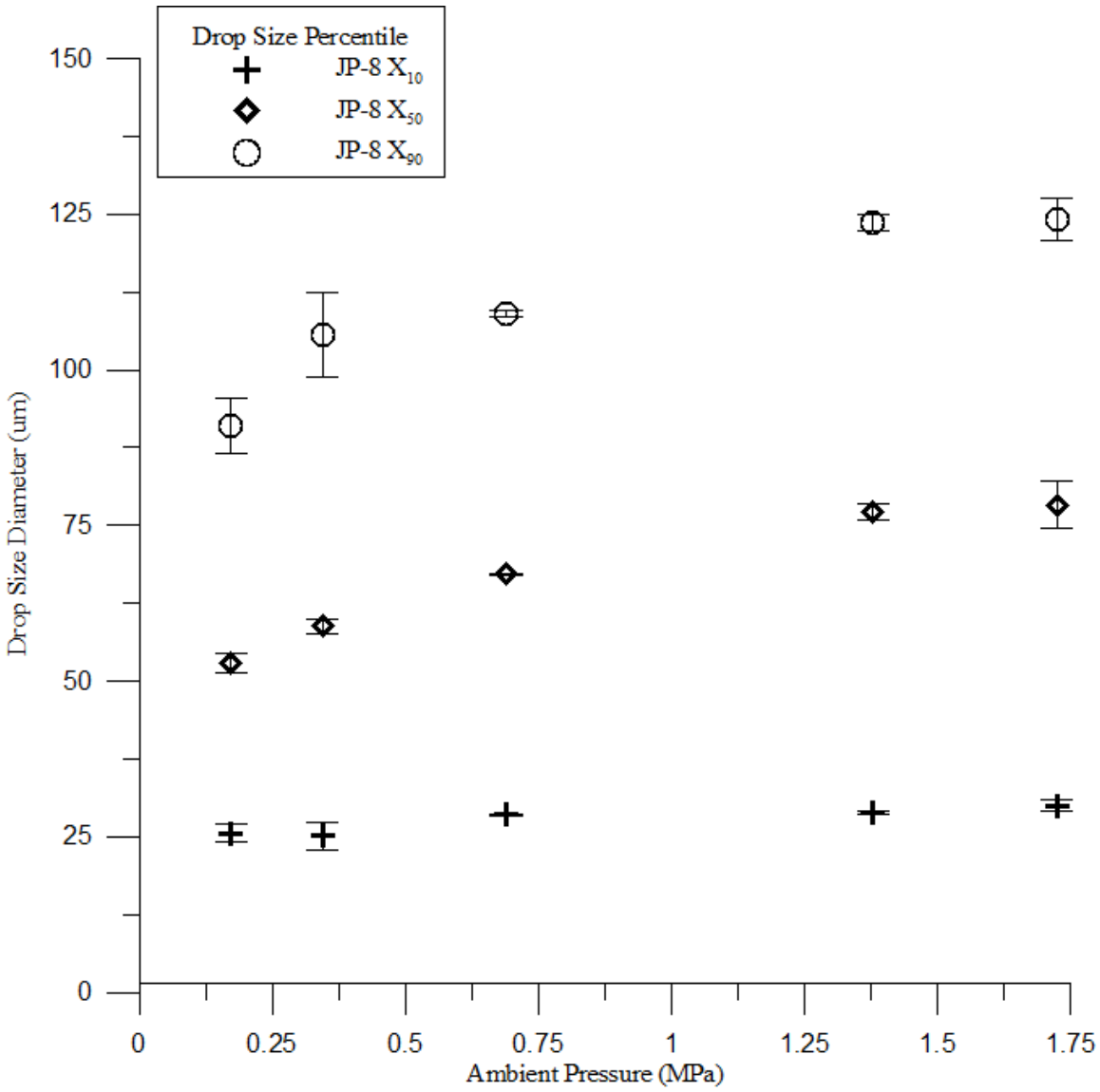

Figure 4.25. Pressure Swirl Atomizer JP-8 Drop Size Percentile versus Ambient Pressure, 15.6 C (60 F) Fuel Injection Temperature, 0.345 MPa (50 psi) Injection Pressure.

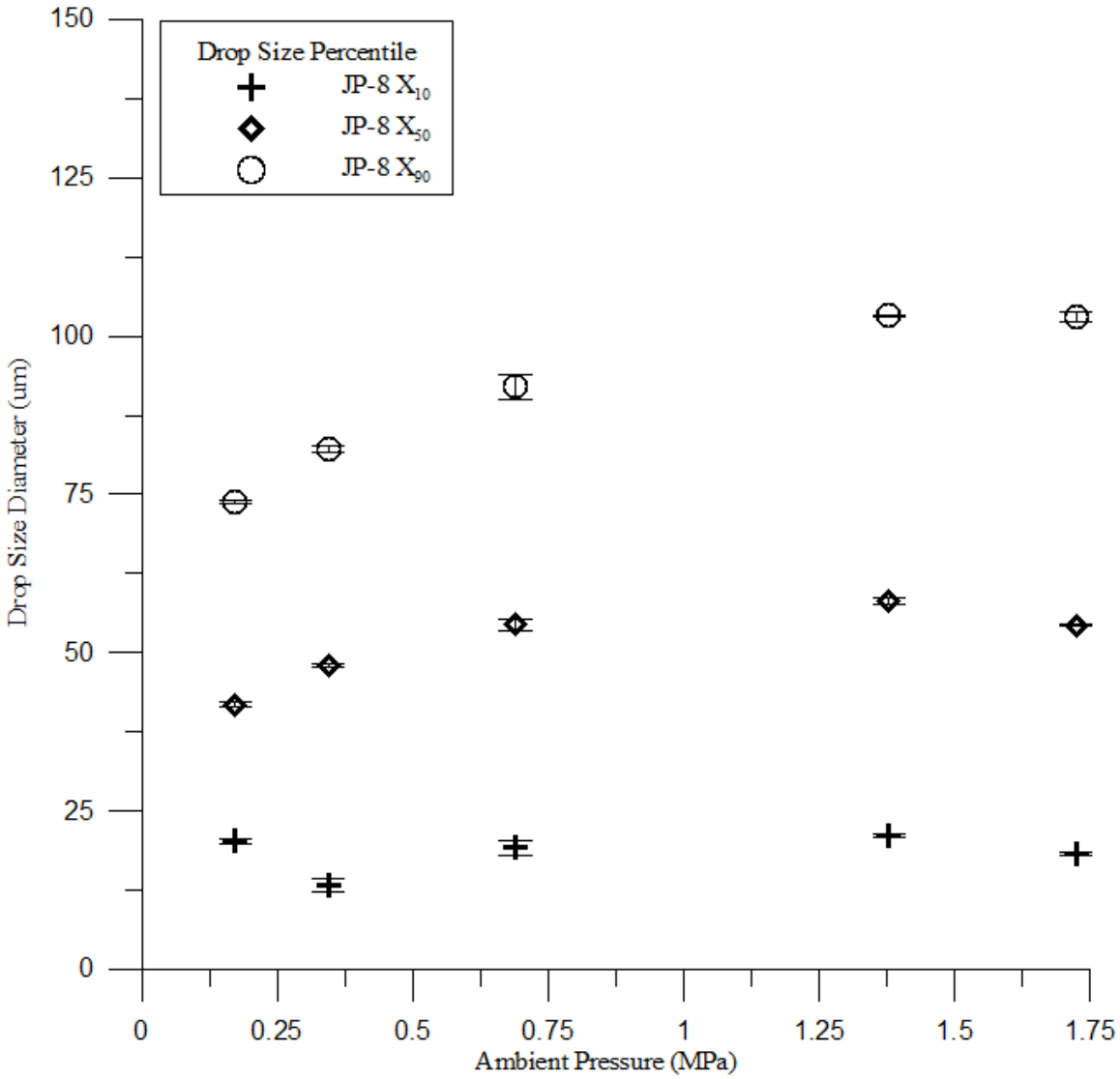

Figure 4.26. Pressure Swirl Atomizer JP-8 Drop Size Percentile versus Ambient Pressure, 15.6 C (60 F) Fuel Injection Temperature, 0.689 MPa (100 psi) Injection Pressure.

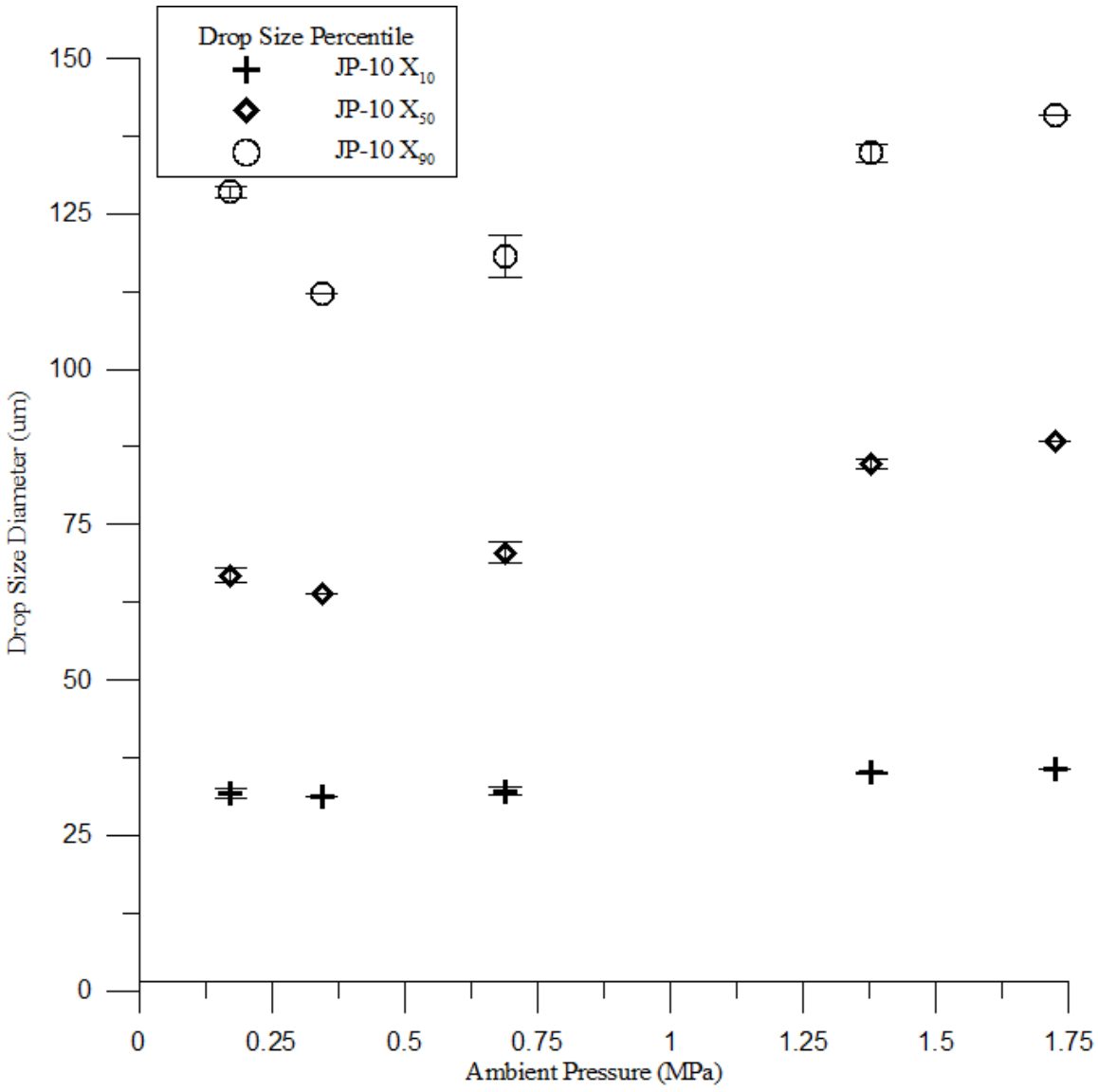

Figure 4.27. Pressure Swirl Atomizer JP-10 Drop Size Percentile versus Ambient Pressure, 15.6 C (60 F) Fuel Injection Temperature, 0.345 MPa (50 psi) Injection Pressure.

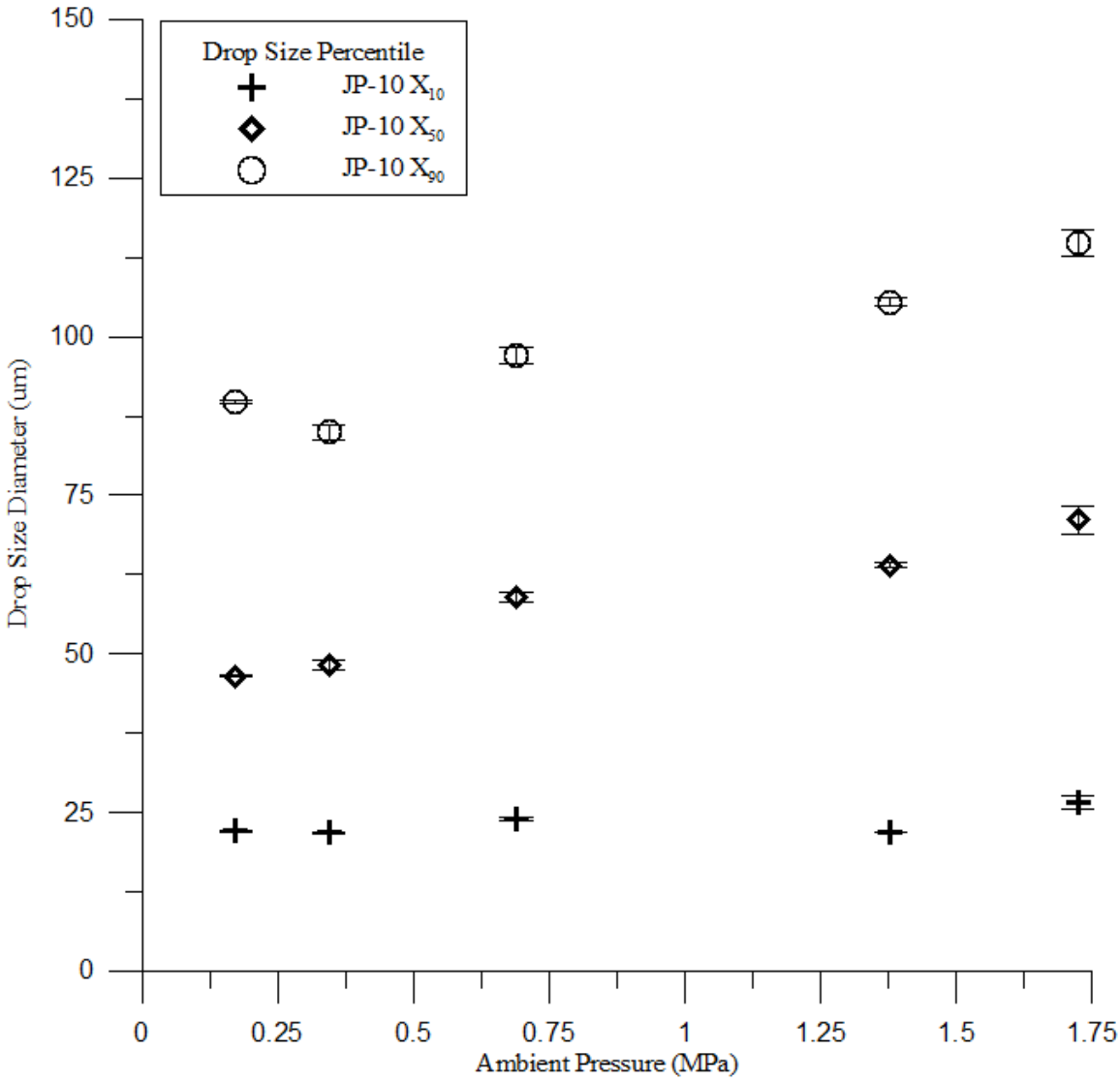

Figure 4.28. Pressure Swirl Atomizer JP-10 Drop Size Percentile versus Ambient Pressure, 15.6 C (60 F) Fuel Injection Temperature, 0.689 MPa (100 psi) Injection Pressure.

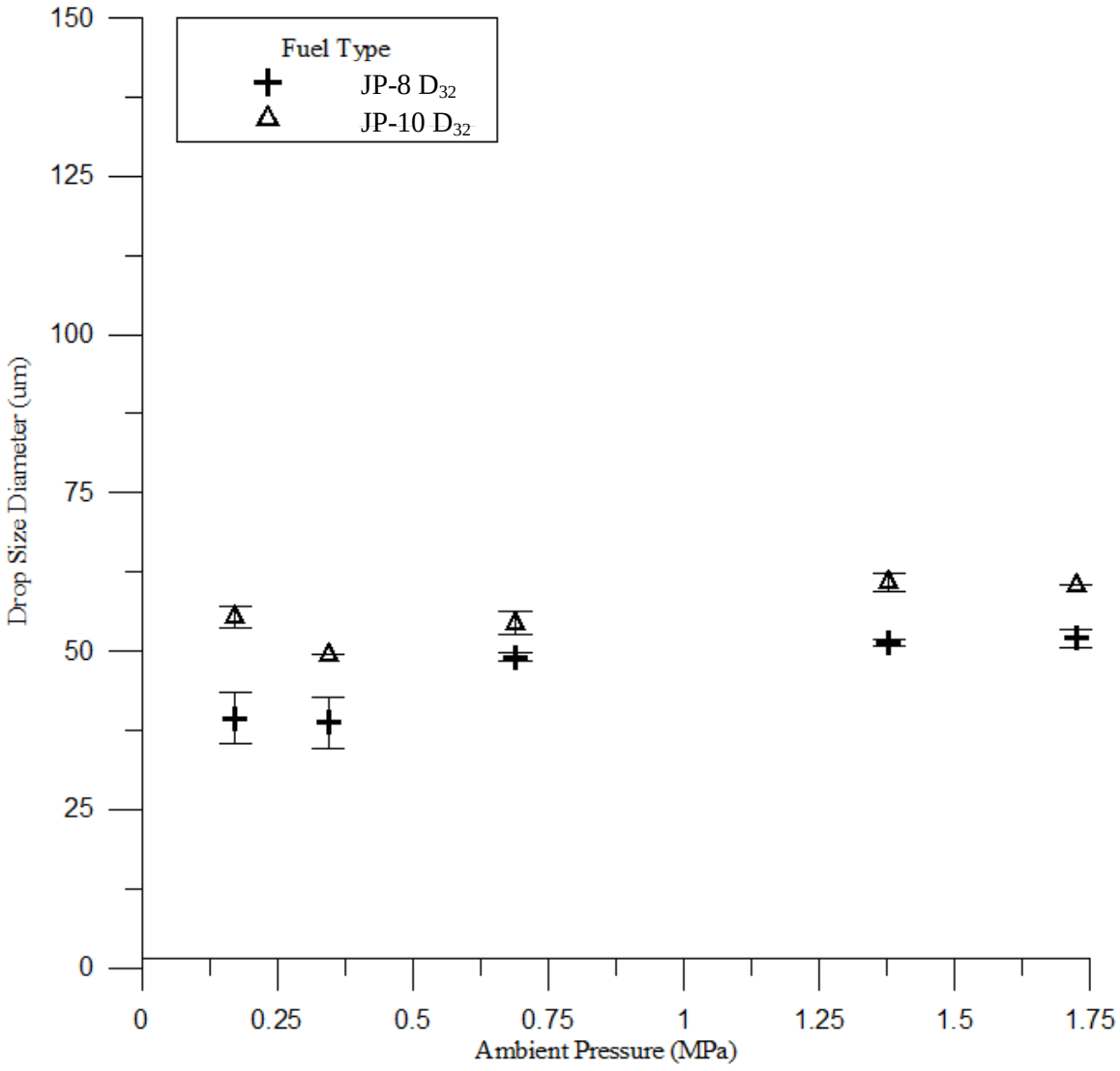

Figure 4.29. Pressure Swirl Atomizer Sauter Mean Diameter versus Ambient Pressure, 15.6 C (60 F) Fuel Injection Temperature, 0.345 MPa (50 psi) Injection Pressure.

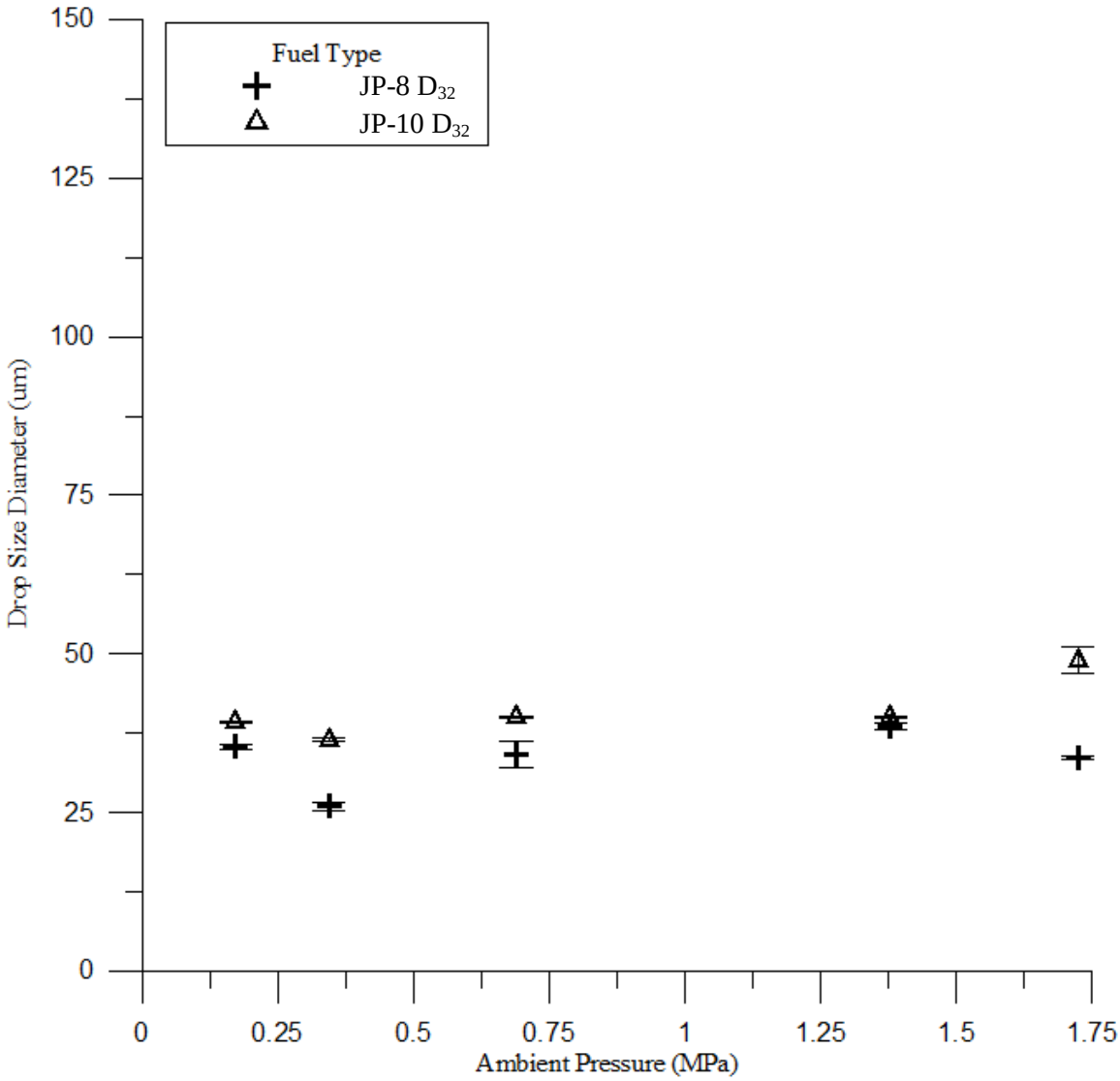

Figure 4.30. Pressure Swirl Atomizer Sauter Mean Diameter versus Ambient Pressure, 15.6 C (60 F) Fuel Injection Temperature, 0.689 MPa (100 psi) Injection Pressure.

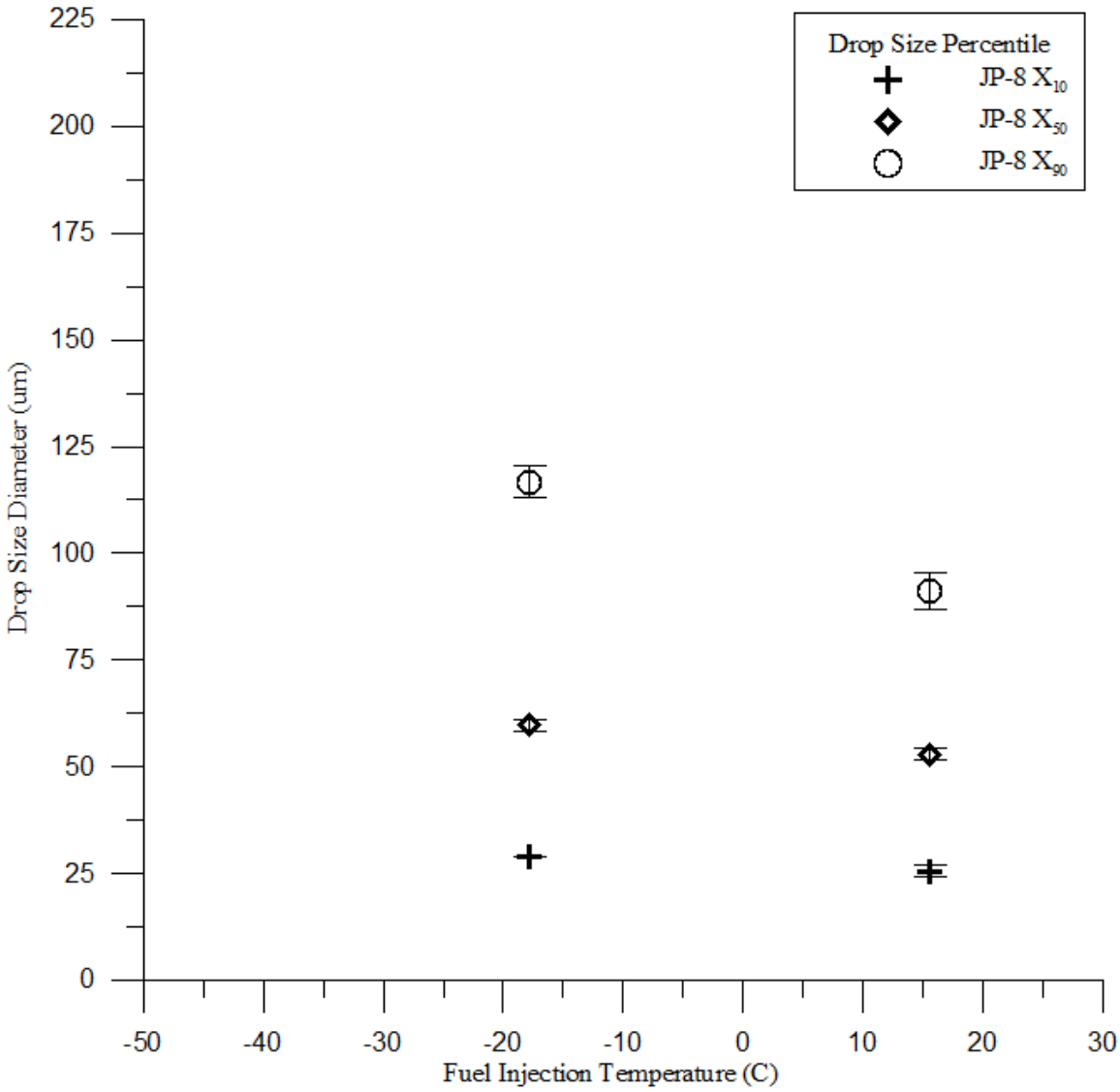

Figure 4.31. Pressure Swirl Atomizer JP-8 Drop Size Percentile versus Fuel Injection Temperature, 0.172 MPa (25 psi) Ambient Pressure, 0.345 MPa (50 psi) Injection Pressure.

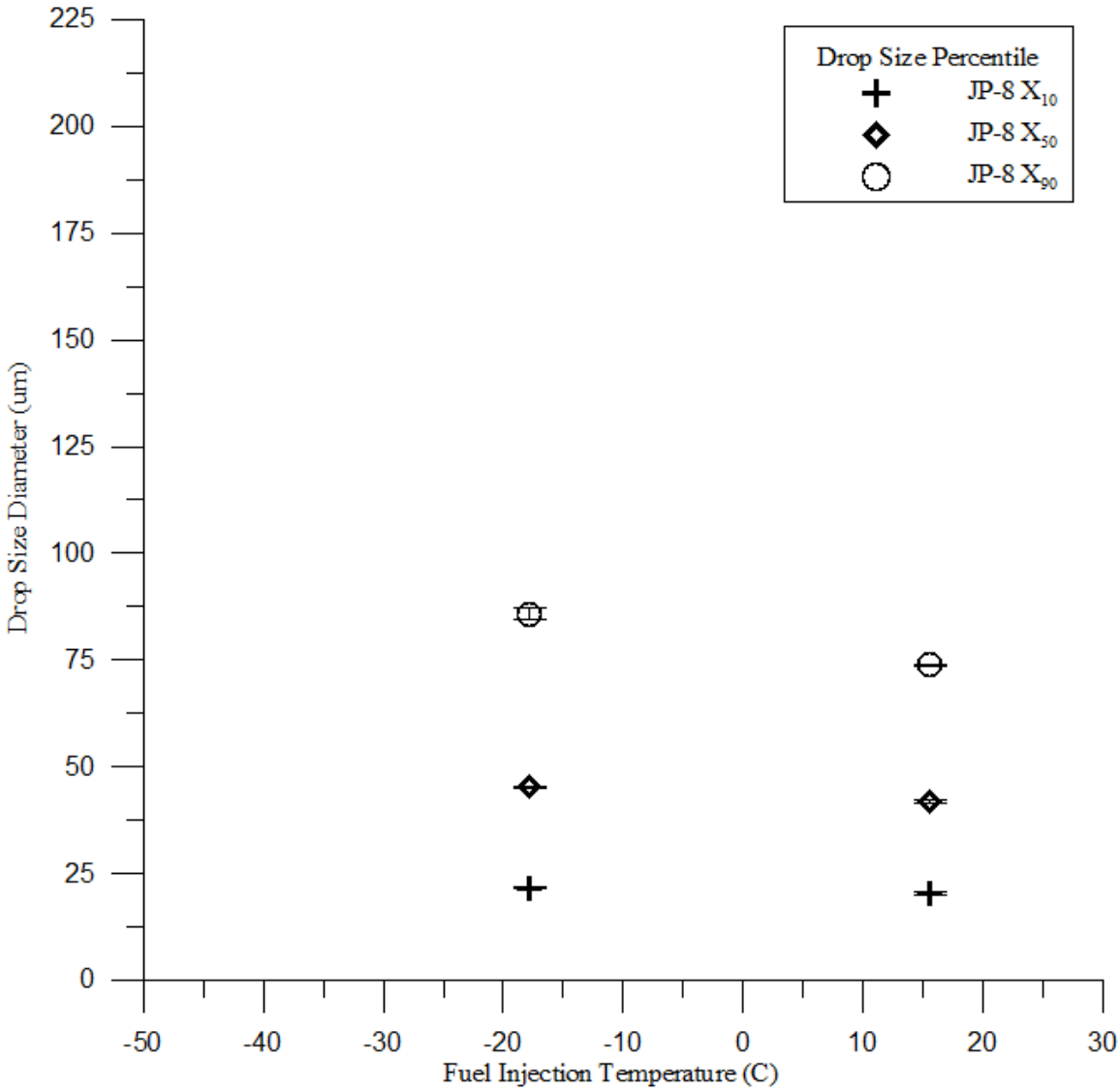

Figure 4.32. Pressure Swirl Atomizer JP-8 Drop Size Percentile versus Fuel Injection Temperature, 0.172 MPa (25 psi) Ambient Pressure, 0.689 MPa (100 psi) Injection Pressure.

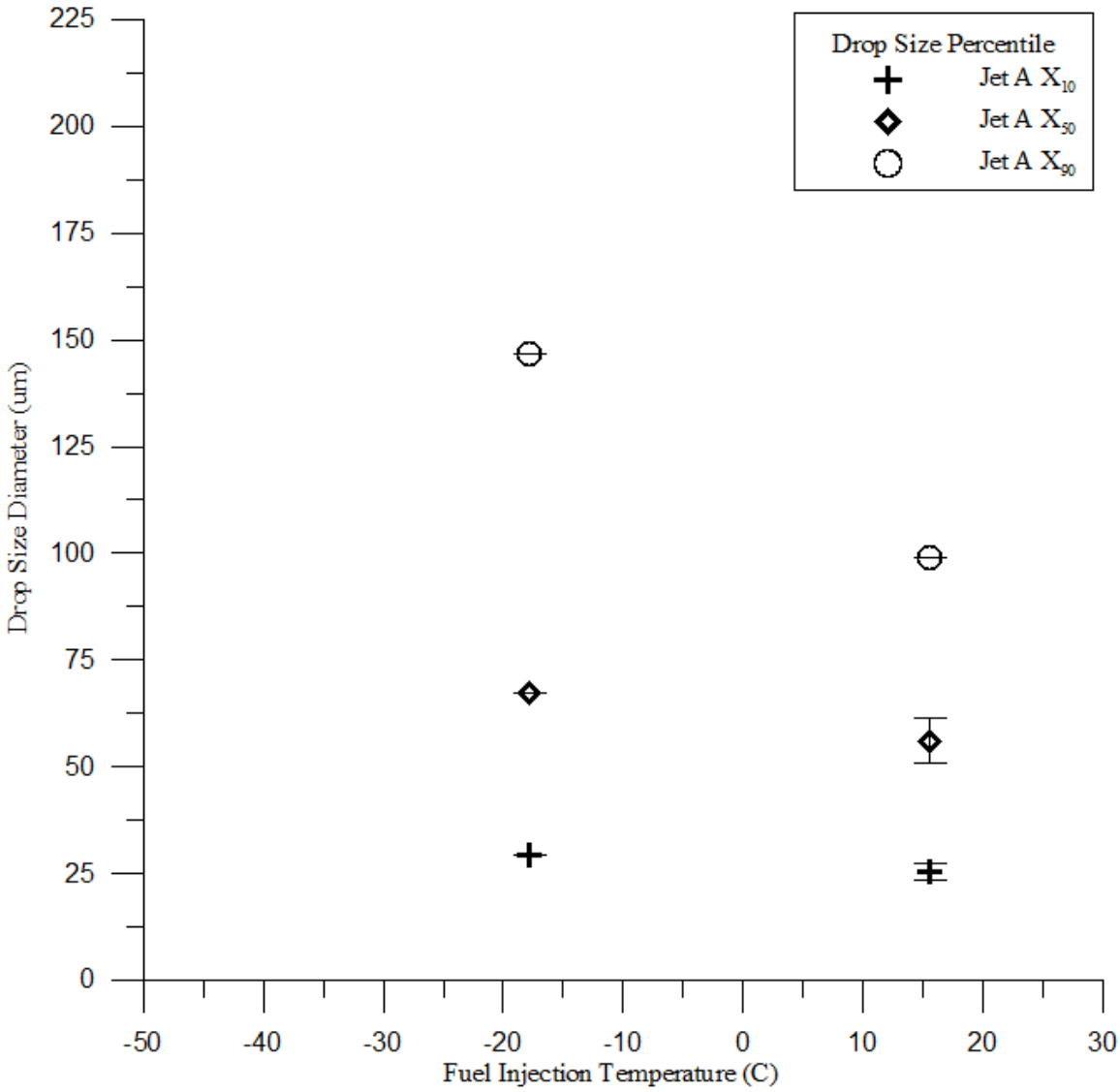

Figure 4.33. Pressure Swirl Atomizer Jet A Drop Size Percentile versus Fuel Injection Temperature, 0.172 MPa (25 psi) Ambient Pressure, 0.345 MPa (50 psi) Injection Pressure.

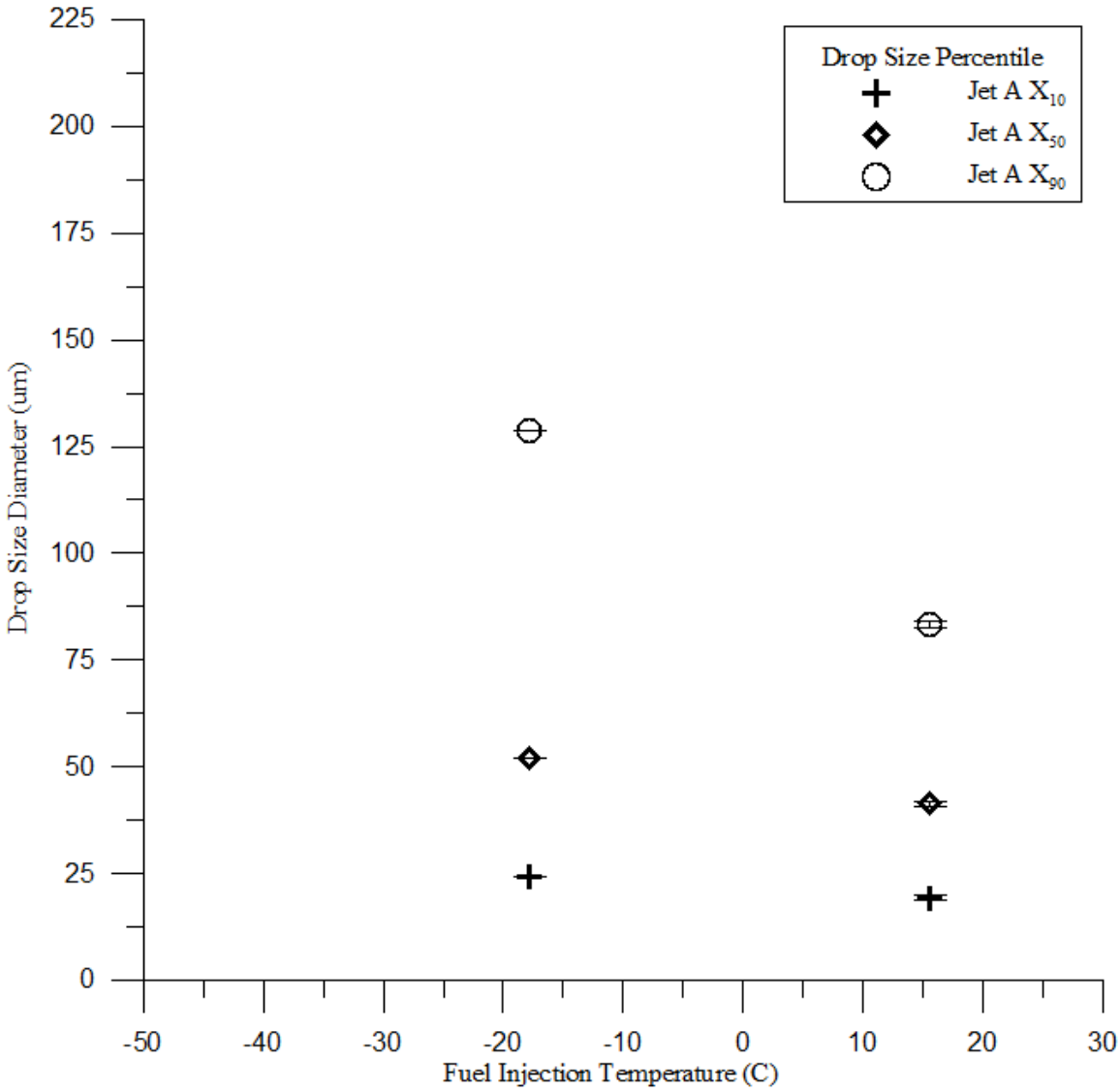

Figure 4.34. Pressure Swirl Atomizer Jet A Drop Size Percentile versus Fuel Injection Temperature, 0.172 MPa (25 psi) Ambient Pressure, 0.689 MPa (100 psi) Injection Pressure.

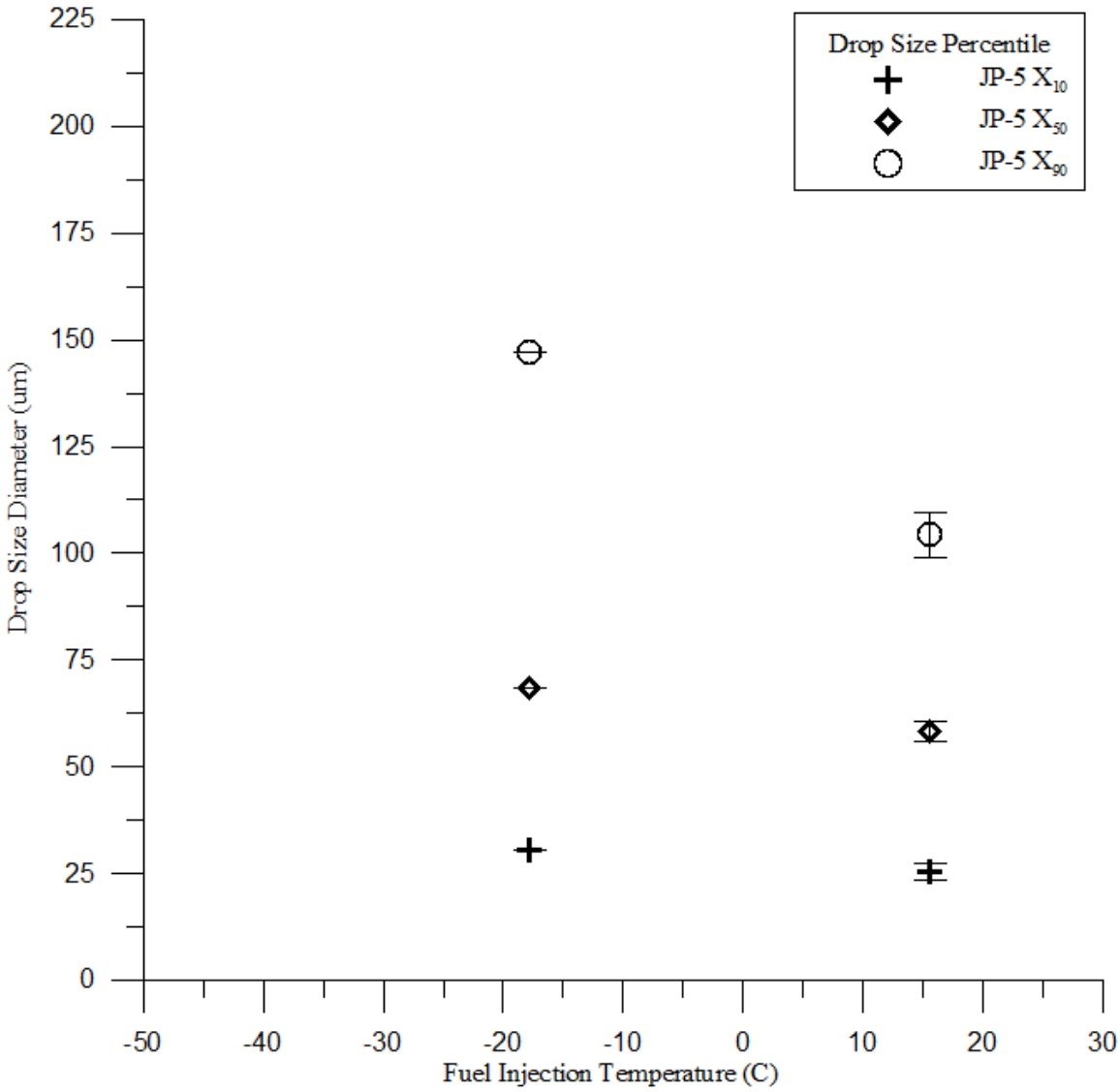

Figure 4.35. Pressure Swirl Atomizer JP-5 Drop Size Percentile versus Fuel Injection Temperature, 0.172 MPa (25 psi) Ambient Pressure, 0.345 MPa (50 psi) Injection Pressure.

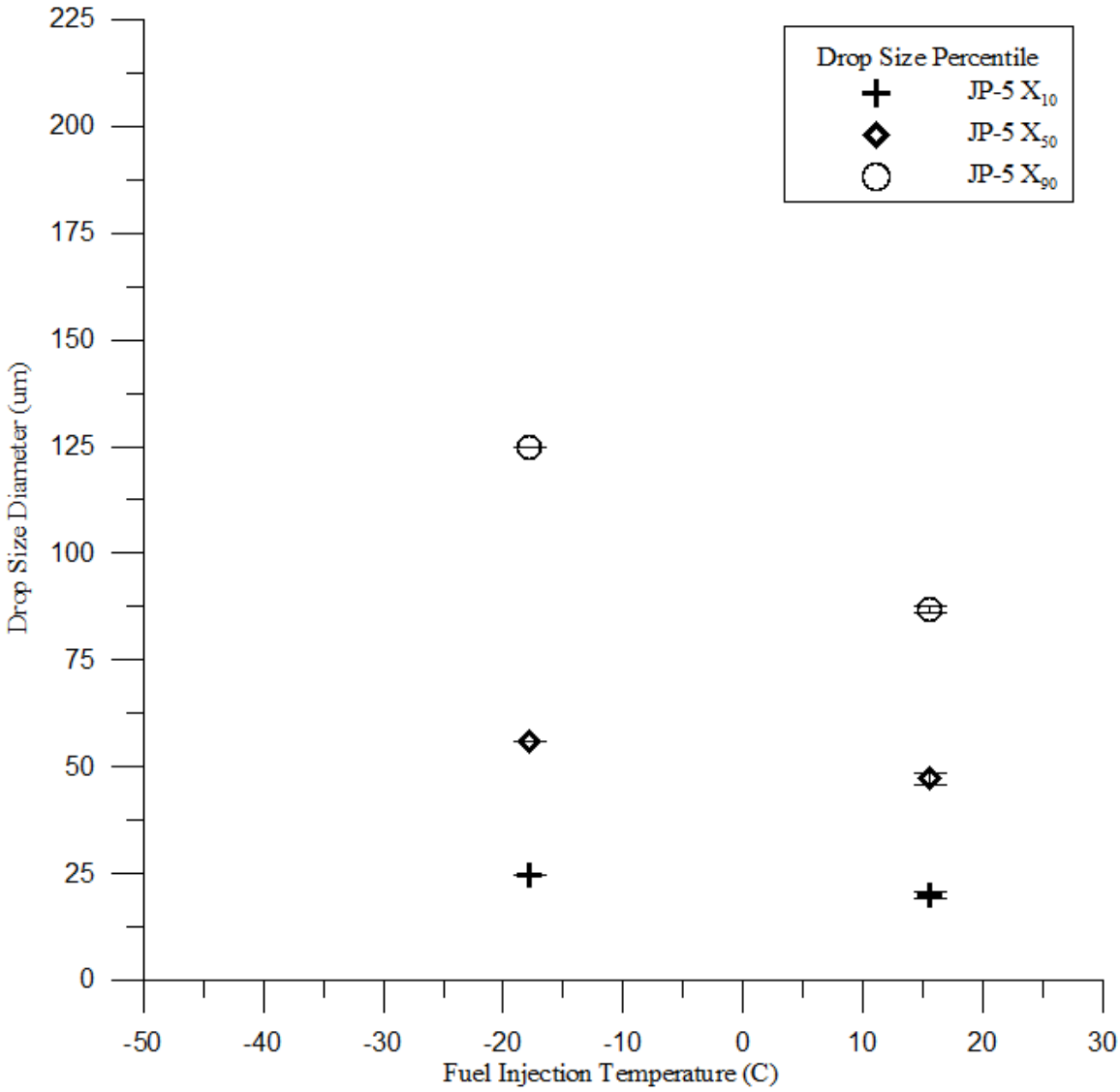

Figure 4.36. Pressure Swirl Atomizer JP-5 Drop Size Percentile versus Fuel Injection Temperature, 0.172 MPa (25 psi) Ambient Pressure, 0.689 MPa (100 psi) Injection Pressure.

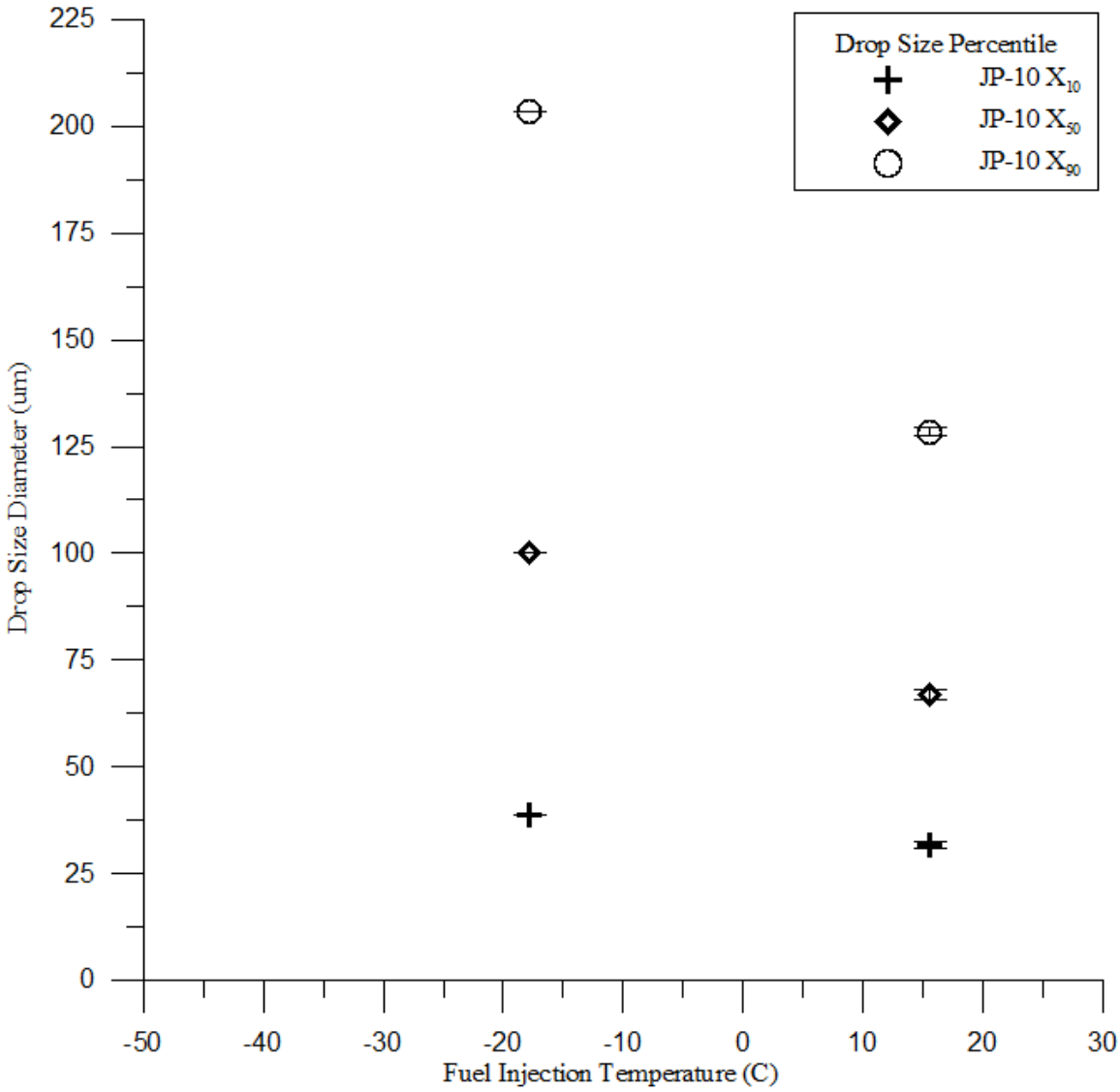

Figure 4.37. Pressure Swirl Atomizer JP-10 Drop Size Percentile versus Fuel Injection Temperature, 0.172 MPa (25 psi) Ambient Pressure, 0.345 MPa (50 psi) Injection Pressure.

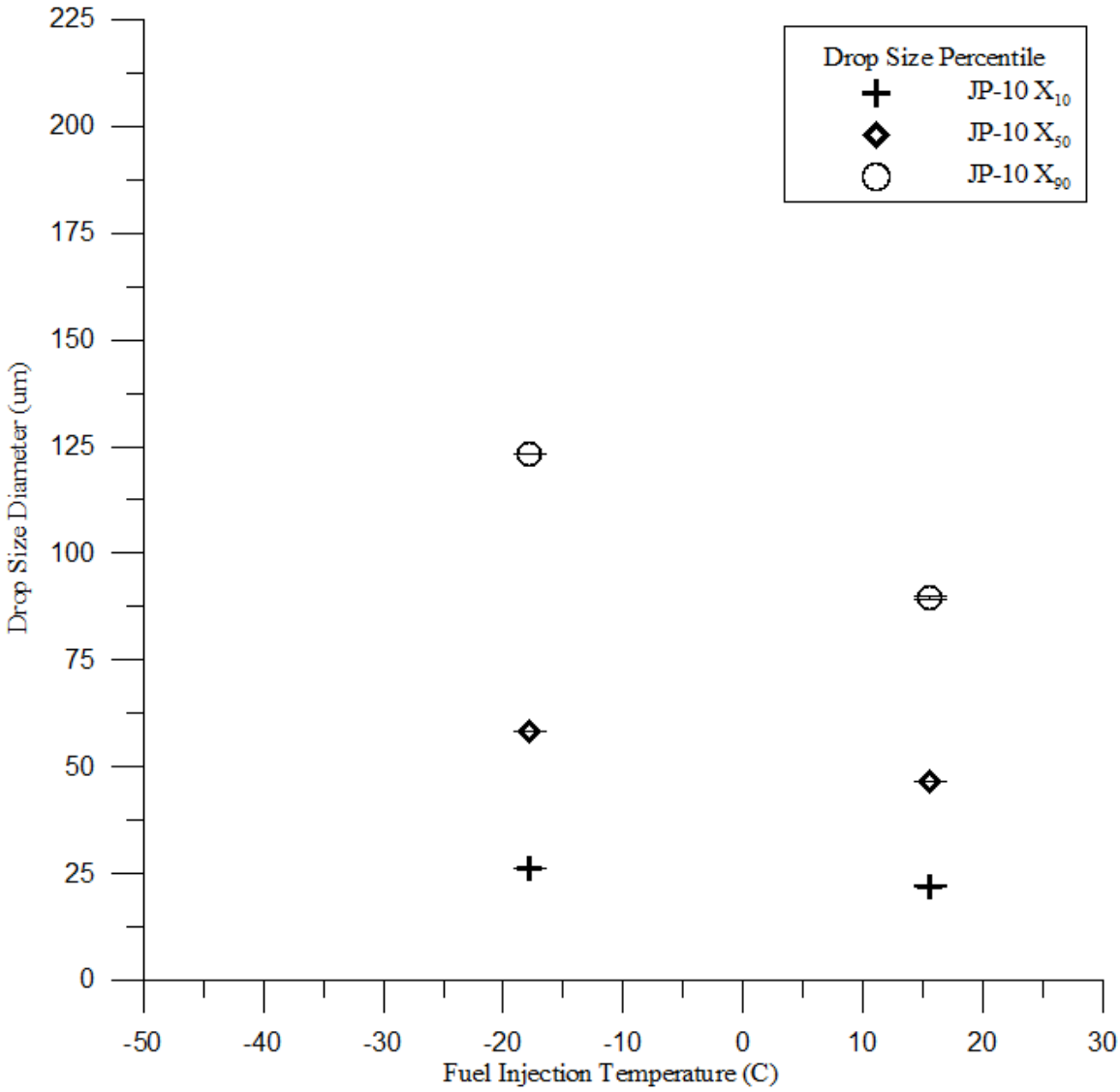

Figure 4.38. Pressure Swirl Atomizer JP-10 Drop Size Percentile versus Fuel Injection Temperature, 0.172 MPa (25 psi) Ambient Pressure, 0.689 MPa (100 psi) Injection Pressure.

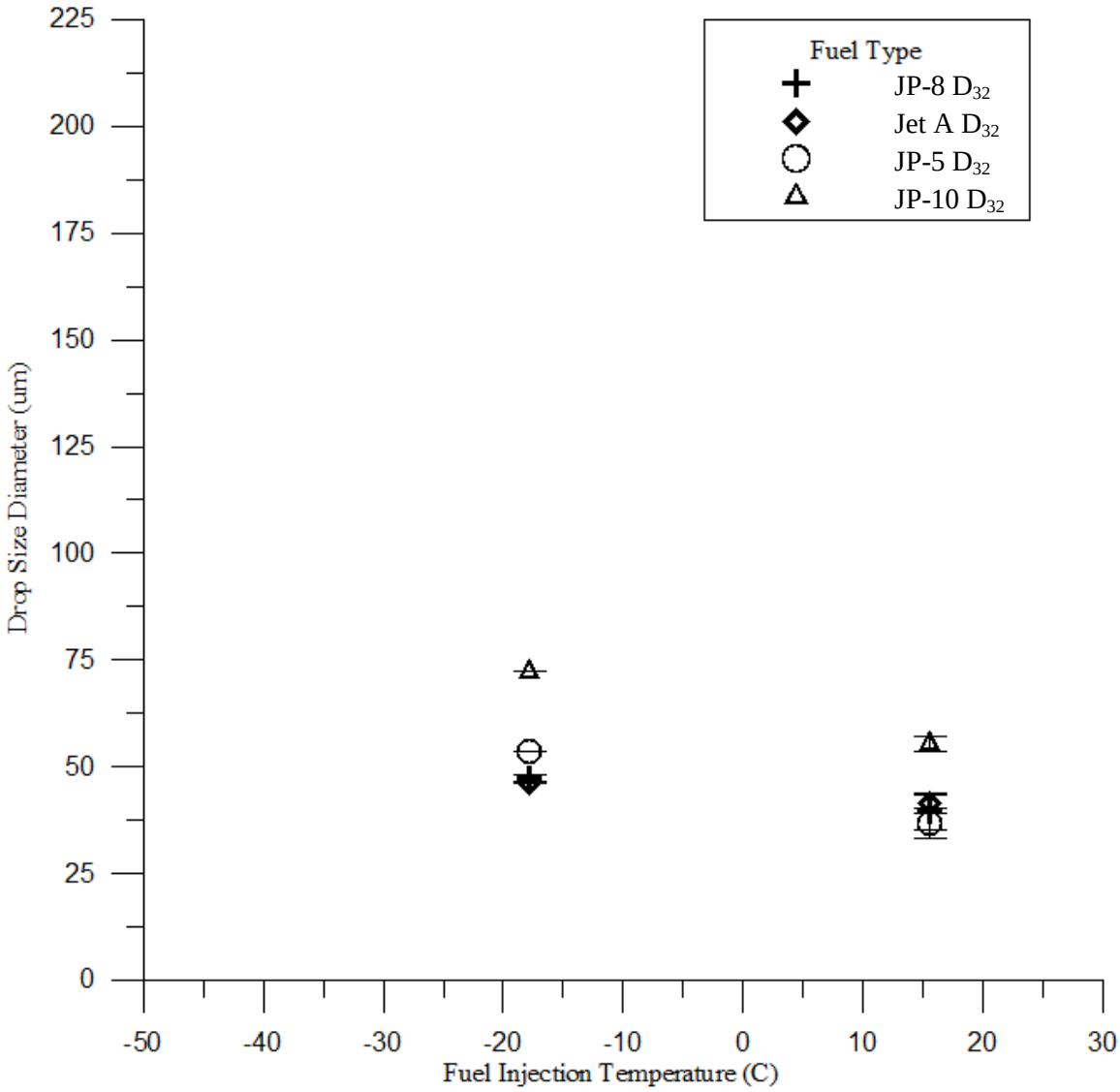

Figure 4.39. Pressure Swirl Atomizer Sauter Mean Diameter versus Fuel Injection Temperature, 0.172 MPa (25 psi) Ambient Pressure, 0.345 MPa (50 psi) Injection Pressure.

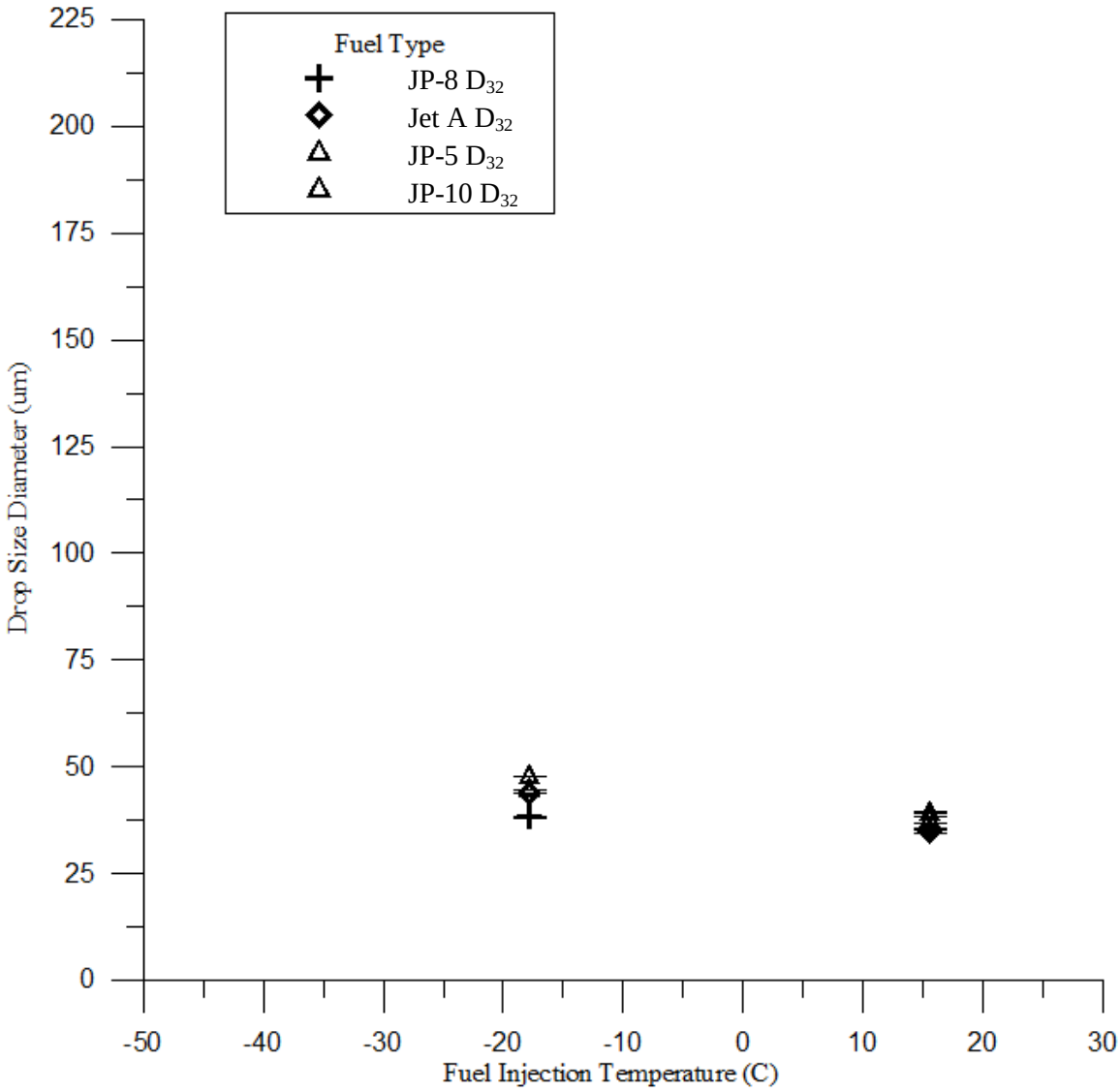

Figure 4.40. Pressure Swirl Atomizer Sauter Mean Diameter versus Fuel Injection Temperature, 0.172 MPa (25 psi) Ambient Pressure, 0.689 MPa (100 psi) Injection Pressure.

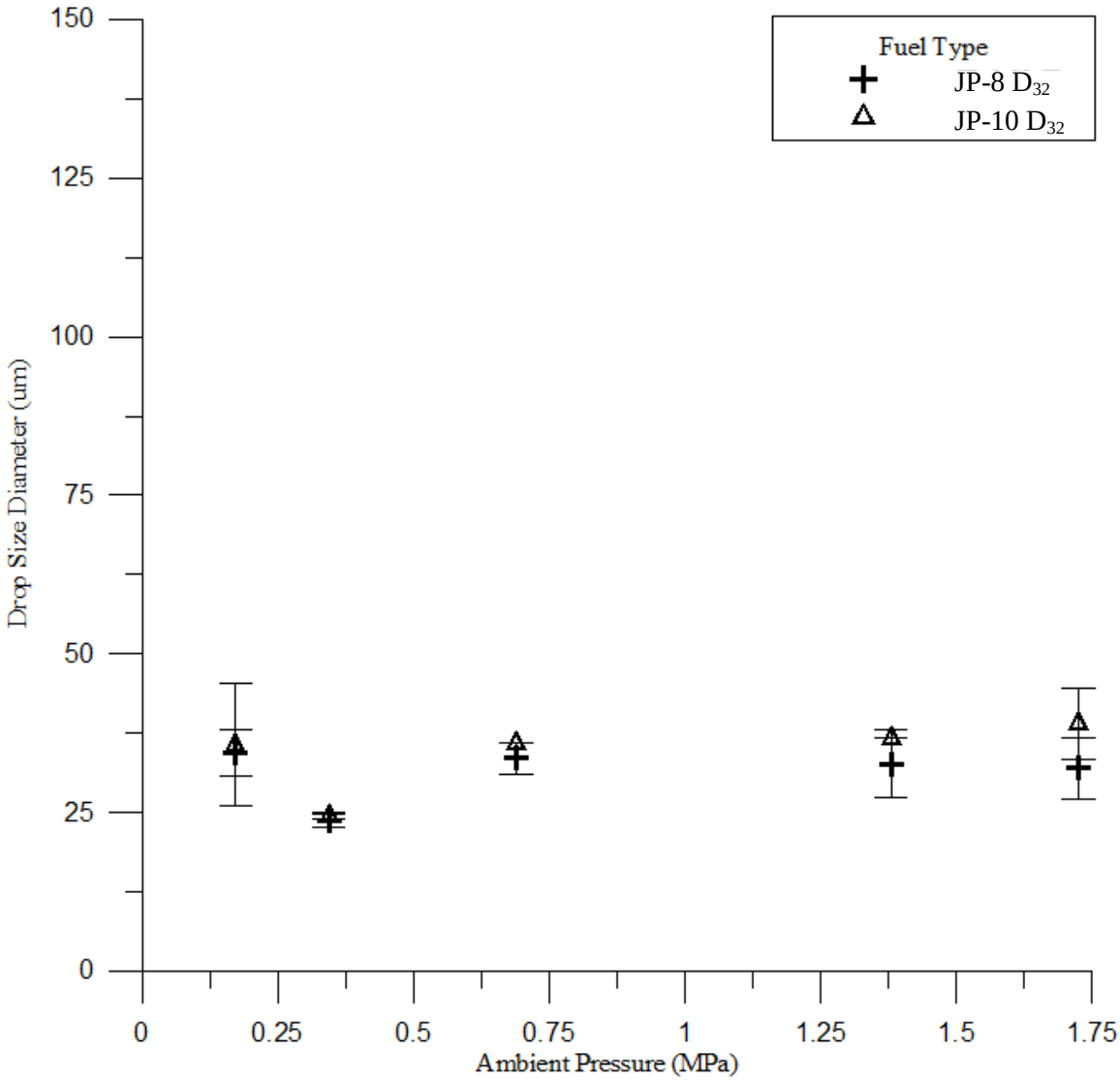

Figure 4.41. Hybrid Air Blast Nozzle Sauter Mean Diameter versus Ambient Pressure, 0.006 Fuel Air Ratio, $\Delta P/P = 0.02$.

CHAPTER 5. SUMMARY AND CONCLUSIONS

5.1 Summary

The effect of aviation fuel type and fuel injection conditions on the spray characteristics of pressure swirl and hybrid air blast fuel injectors was studied. The types of aviation fuel tested were JP-8, Jet A, JP-5, and JP-10. The fuel injection conditions that varied were fuel injection pressure, fuel injection temperature, and ambient pressure. An En'Urga OP-600 SETScan Optical Patternator was used to collect spray data at atmospheric ambient pressure conditions. A Sympatec HELOS laser diffraction device was used to collect spray data at super atmospheric conditions. The changes in spray characteristics for various test matrix set conditions were measured and discussed. The spray atomizer performance of the pressure swirl fuel injector was compared to the hybrid air blast fuel injector.

The differences in liquid properties between types of aviation jet fuel affect the spray atomization performance of the fuel injectors. Dorfner *et al*. (1995) explains how spray drop size depends on liquid viscosity and surface tension. As temperature decreases, drop size becomes a stronger function of increasing viscosity and a weaker function of surface tension. Of the jet fuels tested, JP-8 is the least viscous and the viscosity changes the least over the temperature range that was tested. Jet A is slightly more viscous than

JP-8 for a given temperature. JP-5 is more viscous than Jet A and JP-10 is the most viscous jet fuel tested.

The test matrices for the pressure swirl and hybrid air blast fuel injectors varied injection temperature, injection pressure, and ambient pressure. The purpose of changing set conditions of the atomizer was to obtain optical patternator data that contributes to trends described in the literature for spray drop sizes. Goldsworthy *et al.* (2011) investigated fuels with two different viscosities and the effect of changing injection temperature on drop size. Decreasing temperature tends to increase viscosity. The more viscous fuels sprayed larger drops. Wang *et al.* (1988) discusses how increased injection pressure tends to decrease drop size. De Corso *et al.* (1960) and Guildenbecher *et al.* (2008) explains how increasing ambient pressure tends to promote drop coalescence, resulting in a reduction in spray cone angle and increase in drop size. The experiments provided data using the optical patternator and Sympatec laser diffraction device that contribute to discussion of the importance of set condition on different types of fuel injectors.

Two experimental set ups were used to collect data. Atmospheric ambient pressure testing was conducted at ZL1, Maurice Zucrow Laboratories, Purdue University. The super atmospheric testing was conducted at the High Pressure Laboratory, Maurice Zucrow Laboratories, Purdue University. Both experimental set ups used a fuel cart that was designed to pump, temperature condition, and control the flow rate and injection pressure of the fuel. Pressure, flow rate, and temperature of the experimental set up were monitored with electronic data acquisition. In the atmospheric and super atmospheric

labs the fuel injectors were mounted 38.1 mm (1.5 inches) upstream of the optical measurement plane. The pressure swirl and hybrid air blast fuel injectors were operated at a variety of set conditions. Test matrix set conditions and spray properties were measured and the data was presented in the results chapter of this thesis.

The En'Urga OP-600 SETScan Optical Patternator was used to measure spray properties in the atmospheric tests. Total surface area, patternation number, full spray cone angle, and radial profiles of the spray were reported for these tests. Total surface area is a measure of the atomization quality of the spray. Larger surface area implies that there is better atomization, smaller drop sizes or fewer drops in the spray. Patternation number describes the symmetry of the spray. Lower patternation number describes a more symmetrical spray. Full spray cone angle is calculated by the patternator from the distance of the injector from the measurement plane and the extinction of the spray. Radial profile provides a description of the local droplet surface area divided by volume measurements in the spray. High surface area to volume measurements implies an increase of small droplets in high concentration.

The Sympatec HELOS laser diffraction device finds a probability density function of droplets for the spray. Characteristic diameters X_{10}, X_{50}, X_{90}, and D_{32} can be found from the probability density function. The X_{10}, X_{50}, and X_{90} measurements are drop size percentiles and can describe the size range of drops in a spray. The Sauter mean diameter is a measure of drop diameter that accounts for volume and surface area of drop sizes.

In summary, the experiments provide a review of how fuel injector spray atomization characteristics change with type of fuel injector, fuel type, fuel injection pressure, fuel injection temperature, and ambient pressure. To reiterate the discussion of prior work in Chapter 2, this thesis addresses the following open aspects about fuel injector atomization characteristics.

- Contribute spray patternation measurements to the body of existing drop size data in the literature.
- Discuss the influence of fuel type, ambient pressure and fuel injection temperature and fuel injection pressure on spray atomization quality.
- Compare the performance of a pressure swirl atomizer to a hybrid air blast nozzle at similar set conditions.

5.2 Conclusions

At atmospheric testing conditions, the optical patternator collected total surface area measurements, patternation number measurements, spray angle measurements and radial profile measurements. The bullets below reiterate the findings from Chapter 4 for spray measurements of the pressure swirl and the hybrid air blast fuel injectors.

- Total surface area measurements decreased with decreasing fuel injection temperature and decreasing fuel injection pressure.
- Total surface area measurements depend on fuel type. For the pressure swirl nozzle at 0.345 MPa (50 psi) injection pressure, JP-8 showed a 38% decrease, Jet A showed

a 45% decrease, JP-5 showed a 54% decrease and JP-10 showed a 89% decrease in total surface area from 15.6 to -40 C (60 to -40 F) injection temperature.

- Total surface area measurements were slightly greater for the hybrid air blast nozzle compared to the pressure swirl nozzle at similar conditions
- The fuel type effects on the spray of the hybrid air blast nozzle were similar to the pressure swirl nozzle. For the 0.358 MPa (52 psi) injection pressure case, the total surface area for JP-8 decreased 2%, Jet A decreased 52%, JP-5 decreased 59%, and JP-10 decreased 91% from injection temperature decreasing from 15.6 to -28.8 C (60 to -20 F).
- Patternation number results showed decreasing symmetry in the spray with decreasing fuel injection temperature and decreasing fuel injection pressure.
- The spray angle measurements were independent of fuel type for both fuel injector types. There was a slight increase in spray angle with decreasing temperature for both fuel injectors. Some error in the spray angle measurements occurred at cold injection temperature, resulting in artificially high spray cone angle measurements.
- The radial profile measurements showed decreasing local surface area divided by volume measurements for decreasing fuel injection temperature and decreasing fuel injection pressure.
- The radial profile for the pressure swirl nozzle showed areas of high concentration in the center of the spray. The local surface area to volume of droplets in the spray decreased with decreasing temperature. The difference between fuel types was consistent with the viscosities of the fuel.

- The radial profile for the hybrid air blast nozzle showed an annular ring of high concentration in the spray. The differences between fuel type was less significant compared to the pressure swirl nozzle.

At super atmospheric testing conditions, the Sympatec laser diffraction device collected X_{10}, X_{50}, X_{90}, and D_{32} characteristic diameters. The bullets below summarize the findings for these measurements in the pressure swirl nozzle and the hybrid air blast nozzle.

- The X_{10} measurements did not change significantly with ambient pressure or fuel injection pressure. The X_{10} measurements showed slight increase with decreasing fuel injection temperature for the pressure swirl nozzle. The X_{10} measurements showed slight dependence on fuel type for decreasing fuel injection temperature.
- Especially for the JP-8 results, the X_{50} and X_{90} measurements were shown to increase with increasing ambient pressure and decreasing fuel injection pressure.
- The change in X_{50} and X_{90} measurements depended on the fuel type with changing ambient pressure. The X_{50} showed a 48% increase for the JP-8 fuel and a 10% increase in the JP-10 fuel for 0.345 MPa (50 psi) injection pressure and ambient pressure increasing from 0.172 to 1.723 MPa (25 to 250 psi). X_{90} showed a 32% increase for the JP-8 fuel and a 10% increase in the JP-10 fuel for 0.345 MPa (50 psi) injection pressure and ambient pressure increasing from 0.172 to 1.723 MPa (25 to 250 psi).

- The change in X_{50} and X_{90} measurements depended on fuel type for changing fuel injection temperature. The X_{50} showed a 12% increase for the JP-8 fuel, a 20% increase for the Jet A fuel, a 17% increase for the JP-5 fuel and a 50% increase in the JP-10 fuel for 0.345 MPa (50 psi) injection pressure and fuel injection temperature decreasing from 15.6 to -17.8 C (60 to 0 F). The X_{90} showed a 29% increase for the JP-8 fuel, a 48% increase for the Jet A fuel, a 40% increase for the JP-5 fuel and a 58% increase in the JP-10 fuel for 0.345 MPa (50 psi) injection pressure and fuel injection temperature decreasing from 15.6 to -17.8 C (60 to 0 F).
- The D_{32} for the pressure swirl nozzle was shown to increase slightly with increasing ambient pressure and decreasing fuel injection temperature.
- The D_{32} also depends on fuel type with the most viscous fuel having the greatest D_{32} and the least viscous fuel having the smallest D_{32}.
- The hybrid air blast nozzle did not show significant trends in X_{10}, X_{50}, X_{90}, and D_{32} measurements with ambient pressure or fuel type. One explanation for this is the swirling nitrogen resulted in aerodynamic forces that dominated forces from the set conditions.

5.3 Future Work

There are several areas that the current study did not address. Effect of sub atmospheric pressure on the drop size and spray distribution were not discussed. Spatially resolved drop size and drop velocity measurements at super atmospheric pressures were not addressed. Finally, the effect of increasing nitrogen entrainment through the swirler on the hybrid air blast fuel injector on spray atomization was not investigated.

First, the effect of sub atmospheric pressure on drop sizes was not discussed in this thesis. Guildenbecher *et al.* (2008) observes that the spray cone angle tends to increase with decreasing ambient pressure. However, the relative importance of fuel properties on spray atomization at sub atmospheric pressures is not investigated. The tests at sub atmospheric pressures could provide insight into the effect of surrounding gas entrainment on the flow.

For the set conditions discussed in this thesis at super atmospheric pressures, there is no data for spatially resolved drop velocity and drop size measurements. Phase Doppler Anemometry techniques are required in order to find local drop velocity and drop size in the spray. Drop velocity would provide insight into the extent of spray penetration. Taking measurements at distances farther downstream from the fuel injector would also provide more information about spray penetration.

Studying the effect of increasing nitrogen through swirler on hybrid air blast nozzle would provide insight into how the aerodynamic forces from the nitrogen affects droplet break up in the spray. By increasing the amount of nitrogen flow in the swirler, the droplet break up could be driven by secondary atomization effects. Increases in secondary atomization could affect the distribution of droplets in a spray.

LIST OF REFERENCES

LIST OF REFERENCES

Atkins, D. L., Ervin, J. S., & Shafer, L. (2005). Experimental studies of jet fuel viscosity at low temperatures, using a rotational viscometer and an optical cell. *Energy & Fuels*, *19*(5), 1935–1947.

Benjamin, M. A. (2000). Fuel atomization for next-generation gas turbine combustors. *Atomization and Sprays*, *10*(3-5).

Cha, C. M., Jaing, Rizk, Anand. (2005). A comprehensive liquid fuel injection model for CFD simulations of gas turbine combustors. *43rd AIAA Aerospace Sciences Meeting and Exhibit*, Reno, Nevada, January 10-13.

Coordinating Research Council, Inc. (2004). Handbook of aviation fuel properties. *Society of Automotive Engineers.*

DeCorso, S. M. (1960). Effect of ambient and fuel pressure on spray drop size. *Journal for Engineering for Power*, *82*(1), 10–18.

Dorfner, V., Domnick, J., Durst, F., & Kohler, R. (1995). Viscosity and surface tension effects in pressure swirl atomization. *Atomization and Sprays*, *5*(3).

Frame, E. A. (1981). Behavior of fuels at low temperatures. *Interim Report, U.S. Army Fuels and Lubricants Research Laboratory, Southwest Research Institute*, San Antonio, Texas, June 17.

Goldsworthy, L., Bong, C., & Brandner, P. A. (2011). Measurements of diesel spray dynamics and the influence of fuel viscosity using PIV and shadowgraphy. *Atomization and Sprays*, *21*(2), 167–178.

Guildenbecher, D. R., Rachedi, R. R., & Sojka, P. E. (2008). Pressure-scaling of pressure-swirl atomizer cone angles. *Journal of Engineering for Gas Turbines and Power*, *130*(6), 061501–061501.

Jasuja, A. K. (2006). Some developments in gas turbine fuel injector design. *2006 Japan-China Seminar on Preparation and Utilization of Clean Fuels and their Control of Combustion and Emissions,* Kiryu, Japan, August 21-22.

Li, Z., Wu, Y., Yang, H., Cai, C., Zhang, H., Hashiguchi, K., … Lu, J. (2013). Effect of liquid viscosity on atomization in an internal-mixing twin-fluid atomizer. *Fuel*, *103*, 486–494.

Lim, Sivanthanu. (2005). Optical patternation of a multi-orifice spray nozzle. *Atomization and Sprays*, *15*(6), 687-698.

Lim, Sivathanu, Narayanan, Chang. (2003). Optical patternation of a water spray using statistical extinction tomography. *Atomization and Sprays, 13*(1), 27-43.

Moon, S., Bae, C., Abo-Serie, E. F., & Choi, J. (2007). Internal and near-nozzle flow of a pressure-swirl atomizer under varied fuel temperature. *Atomization and Sprays*, *17*(6), 529–550.

Park, B. S., Kim, H. Y., Kim, Y., & Chung, J. T. (2004). An experimental study on the spray characteristics of a dual-orifice type swirl injector at low fuel temperatures. *Ksme International Journal*, *18*(7), 1187–1195.

Park, B.-S., Kim, H. Y., & Yoon, S. S. (2007). Transitional instability of a pressure-swirl atomizer due to air-core eruption at low temperature. *Atomization and Sprays*, *17*(6), 551–568.

Rizk, N. K., Chin, J. S., & Razdan, M. K. (1997). Modeling of gas turbine fuel nozzle spray. *Journal of Engineering for Gas Turbines and Power*, *119*(1), 34–44.

Rizk, N. K. (2004). AIAA 2004-3540 fuel atomization effects on combustor performance. *40th AIAA/ASME/ASEE Joint Propulsion Conference and Exhibit,* Fort Lauderdale, Florida, July 11-14.

Rizk, N. K., Lefebvre, A. H. (1984). Internal flow characteristics of simplex swirl atomizers. *AIAA, Aerospace Sciences Meeting* (Vol. -1).

Shanshan Yao, J. Z. (2012). Effect of viscosities on structure and instability of sprays from a swirl atomizer. *Experimental Thermal and Fluid Science*, *39*, 158–166.

Wang, X. F., & Lefebvre, A. H. (1987). Influence of fuel temperature on atomization performance of pressure-swirl atomizers. *8th International Symposium on Air Breathing Engines* (Vol. -1, pp. 193–199).

APPENDIX

APPENDIX. TEST PROCEDURES

Test Procedures for Atmospheric Testing

A. PRELIMINARY SET UP

1. SAFETY

Record ambient temperature on TOR (www.weather.com -zip code 47907)
Record ambient pressure on TOR (www.weather.com -zip code 47907)14.7psi
Turn on all video cameras, verify views, verify sound, and ensure video system is configured

2. FUEL CART/INJECTOR SYSTEM SET UP

INSPECT all connections on cart and make necessary plumbing connections for fuel lines, chiller lines and water coolant lines.
CONNECT lines that make loop with cooling coil and water lines
CONNECT nitrogen line from wall panel to fuel cart
CONNECT lines to main and pilot line
VERIFY that air box lines are fully connected
PLUG IN electrical connections for chiller, pump, electrical box and flow meters
CHECK to see that all valves and regulators are closed
BRING UP pressure on fuel cart regulators
ADJUST pneumatic valve regulator to 80psi
VERIFY that there is sufficient coolant liquid in the chiller reservoir

3. DATA AQUISITION SYSTEM SET UP

START labVIEW VI on fuel cart laptop
CONNECT fuel cart USB cable to laptop
RUN VI to see if sensors update in real time
VERIFY that test files can be created and saved

4. PATTERNATOR SYSTEM SET UP

TURN ON optical patternator, allow it to warm up for at least 1HOUR
MEASURE distance between fuel injector tip and laser sheet with tape measure
VERIFY that distance matches requirements on test matrix

B. SYSTEM CHECKS

1. DATA AQUISITION SYSTEM CHECKS

VERIFY that pressure transducers read around atmospheric pressure with pump off. (14.7psi)
VERIFY that thermocouples read around room temperature, approximately 70 degrees F
OPEN and CLOSE pneumatic valves
ACTUATE needle valves on cart

2. FUEL CART SYSTEM CHECKS
Turn ON pump
VERIFY that pump is operating normally
Turn OFF pump
Turn ON chiller
VERIFY that chiller is operating normally
Turn OFF chiller

3. PATTERNATOR SYSTEM CHECKS
Turn OFF lights
Take REFERENCE on optical patternator
Take SCAN with no spray going through the measurement plane
VERIFY that signal to noise plot stays above 400
If system is too noisy, allow for more time for patternator to warm up, repeat for desired result

C. TEST MATRIX FUEL CONDITIONING AND MEASUREMENTS
1. FUEL CART START UP AND FUEL CONDITIONING
Turn ON chiller
ADJUST set point (40F, -40F, -80F)
ALLOW for chiller to reach the set point
Turn ON cooling water
Turn ON pump
VERIFY that pump is pressurizing the fuel recirculation loop to 800psi
OPEN pneumatic valve for pilot line
ACTUATE needle valve to be 60% open for high flow rate
ALLOW fuel temperature to come within 10 degrees of the set point
CLOSE heat exchanger valves so all heat exchanger fluid is diverted to the jacketed fuel line
ALLOW fuel temperature to arrive at the set point (+/- 3 degree tolerance)
ACTUATE needle valve to set test condition delta p or flow rate as specified by test matrix

2. PATTERNATOR AND DATA ACQUISITION MEASUREMENTS
Turn OFF lights
RECORD labVIEW system measurements
RECORD measurement with optical patternator (reference was set during system check)
ALLOW patternator file to finish recording
STOP recording labVIEW system measurements

Save patternator file with file designation
Save LabVIEW file with file designation
ADJUST system properties if they changes off of set point
Repeat patternator and data acquisition measurements section for multiple measurements at test condition
Turn ON lights
CLOSE pneumatic valve
Turn OFF pump

D. SHUT DOWN
CLOSE pneumatic valves
ACTUATE needle valves to closed positions
Turn OFF pump
Turn OFF chiller
CLOSE lab view VI
Turn OFF electrical box
UNPLUG all electrical connections
Turn OFF cooling water
CLOSE facility nitrogen valve
PURGE nitrogen off of line on cart
CLOSE valves and regulators
Turn OFF patternator

E. Changing Fuel Types
Use Stoddard solvent between other fuels

Test Procedure for Super Atmospheric Testing at High Pressure Lab

A. PRELIMINARY SET UP

1. SAFETY

Verify there is no lightning within 10 miles of the test facility
Record ambient temperature on TOR (www.weather.com -zip code 47907)
Record ambient pressure on TOR (www.weather.com -zip code 47907)
Turn on all video cameras, verify views, verify sound, and ensure video system is configured
Verify that test cell containment gates are closed and locked
Verify Test Article is installed per test plan
Verify gN2 supply valve MV-N2-201 is CLOSED (1/2" line on cable tray outside)
Verify gN2 supply valve MV-N2-03 is OPEN (Outside HPL between LN2 tank & tube trailer)
Verify gN2 supply valve MV-N2-04 is CLOSED (1" line)
Turn on Data/Control system and set active configuration in MAX
Start LABVIEW control program
Toggle AI power switches ON on new AI power boards
Verify all data channels are reading properly
Set valve power toggle switch in control room to ON
Set safety light panel to yellow for rooms 133A, 127A, and LOX VENT
Set safety light in Stand B to yellow
Verify that all valves are in their default/de-energized positions
With Rules and Tools VI on, bring up facility nitrogen
Bring up 100psi control pressure

B. TESTING PROCEDURE

MAKE WARNING ANNOUNCEMENT TO ALL PERSONNEL THAT VALVES ARE ABOUT TO BE TESTED

1. PRE TEST CHECKS

Turn on sympatec device, allow to warm up for 30 minutes
Open MV-N2-70 for fuel cart nitrogen
Set control regulator to provide flow to optical windows
Make fuel line connections to fuel and waste drum
Turn on fuel cart laptop
Record ip address 10.184.77.28
Turn on fuel cart power
Set pressure to pneumatic valves and robo valve
Run fuel cart vi
Actuate pneumatic valves
Turn on pump, allow it to pressurize fuel recirculation loop
Check pressure and temperature transducers
Plug in all electrical connections
Verify that optics are aligned
Turn on chiller, set to test condition

Make sure that Facility VI and Fuel Cart VI are remote conndcted to control room computer
Set cameras on test article
Actuate valve on fuel cart
Actuate BP control valve, set to 40% open
Actuate PV-N2-08
Actuate PV N2-15
Take sympatec reference directly before testing begins

2. TESTING PROCEDURE
Open CV-BP-01, 40% open
Check to make sure CR-FU-01 is fully closed
Open PV-N2-02
Open PV-N2-08
Bring regulator set pressure just above fail safe (for low pressure conditions, disable the failsafe)
Verify that nitrogen is flowing and vessel pressure is stabilized
Turn on pump to fuel cart
Verify that CV-FC-01 is fully closed
Open PV-FC-02
Set CV-FC-01 to 20% open
Wait for visual confirmation that fuel is spraying
Check for anomolies with any of the labview numbers

3. DURING THE TEST
Set vessel pressure to the test matrix requirement
Set fuel injector pressure to test matrix requirement (pilot: CV-FU-01, main: CV-FU-02)
If using air box flow, open PV-N2-15
If using air box flow, set $\Delta p/p$ using CR-N2-02
Close CV-BP-01 until spray cone angle is visually unaffected by nitrogen flow
Check to see if temperature is in range
Verify that optical windows look clear
Aquire data on fuel cart
Aquire data with facility vi
Take Sympatec scan
Save Sympatec data
Turn off fuel cart data aquisition
Turn off facility data aquisition
Verify that Sympatec data has no anomalies
Take 2 measurements at every test matrix set point
To set new condition, repeat.

C. SHUT DOWN
Close CR-N2-02

Close CV-N2-15
Close PV-FU-01 and PV-FU-02
Close CV-FU-01 and CV-FU-02
Turn off fuel cart pump
Allow sweeping nitrogen flow to continue for 2 minutes to clear all fuel droplets from the system
Close CR-FU-01
Close PV-N2-08
Open CV-BP-01 100% open
Turn lights in 133A to yellow
Turn off power to chiller
Turn off 3 phase power
Disconnect fuel drum and waste fuel drum from lines.
Turn off Sympatec
Close MV-N2-70
Vent pressure to fuel cart, optical windows, and robo valve
Close manual regulators on fuel cart
Unplug CV-BP-01 so that it remains 100% open
Turn off power to fuel cart DAQ
Bring down 100psi pilot pressure
Turn off facility valve and instrumentation power
Turn off Fuel cart VI
Turn off Facility VI
Set all lights to green.